SATIF-15:
15th Workshop on Shielding aspects of Accelerators, Targets, and Irradiation Facilities

Facility for Rare Isotope Beams (FRIB) at Michigan State University
East Lansing, Michigan USA
20-23 September 2022.

Sessions 2 &3: Code Status, Advances, & Model Converters

Table of contents

1. MARS15 Code Status and Path Forward

Nikolai Mokhov, Igor Tropin, Igor Rakhno, Dali Georgobiani*

Fermi National Accelerator Laboratory, Batavia, Illinois 60510, USA
*georgob@fnal.gov

The MARS15 multi-purpose Monte-Carlo code is Fermilab's particle-matter interaction code that supports the lab's projects along with numerous accelerator facilities in the country and abroad at all stages, from planning and design to operations and decommissioning. The MARS group is involved in the design and upgrades of the high-power targets, beamlines, collimators, absorbers, and experimental flagship facilities at Fermilab, such as LBNF, PIP-II, and mu2e, as well as MI-8, Delivery Ring, and Booster upgrades, along with detailed modelling of the crucial aspects of future projects such as a Muon Collider. Besides all of these applications, the group's activities are currently focused on the code developments in the following areas: (1) increased physics output by maximizing useful particle yields from target systems and minimizing backgrounds in detectors; (2) modelling of 3D distributions of particle flux, energy deposition density, prompt and residual doses, nuclide production, radiation damage, and spectra generated by primary and secondary beams in complex accelerator and detector configurations; (3) optimized performance of predictive particle accelerators and experimental setups (e.g., MARSLBNF); (4) safe designs and operations of accelerator systems and experiments; (5) making MARS even more capable, trustable and usable in practically arbitrary parameter phase space; (6) further development of the SRF modules including detailed underlying physics; (7) creation of the CAD → MARS_ROOT → CAD user-friendly geometry converters compatible with strict requirements for particle-matter simulation in a challenging accelerator environment.

MARS provides several options for geometry descriptions. During the last several years, ROOT TGeo package has been actively used in MARS code for implementation of parametric models for complex setups. It provides good performance and bilateral geometry model exchange with Geant4 by means of direct usage of GDML format. Also, features of this package were used for implementation of an integrated code system MARS-MADX-PTC which becomes highly effective for the class of problems where radiation effects are induced by beam losses along beamlines with electromagnetic fields.

*Further near-term plans include: (1) implementation of modern code management techniques; (2) perfection of codebase (Fortran, C++, VTK, ROOT visualization etc.); (3) improving scalability to prepare for the **e**xascale (10^{18} fpo/s) computing era.*

1.1. Introduction

The consequences of controlled and uncontrolled impacts of particle beams and products of beam-beam collisions on detector and accelerator components can range from minor to catastrophic, with the hottest critical systems and components being high-intensity and/or high-power and/or high-energy beams and interaction regions at colliders, target stations, beam collimators, absorbers, detectors, shielding, and environment. Strong, weak, electromagnetic, and gravitational forces govern high-energy beam interactions with complex components. Therefore, simulations are only possible with a few well-established Monte-Carlo codes. Predictive power and reliability of particle transport simulation tools and physics models in the multi-TeV region need to be well-understood and justified to allow for viable designs of future colliders and experiments with a minimal risk and a reasonable safety margin.

1.1.1. Particle Transport in Matter: Monte-Carlo Method

The Monte-Carlo (random walk) method is the major technique used in particle transport applications. It involves numerical simulations of the interactions and propagation of particles in matter (direct mathematical modelling). All the physics processes are modelled as realistically as possible using realistic geometry and materials, as well as accelerator electromagnetic (EM) fields and experimental setup. Usage of various modifications, so-called variance reduction techniques, helps to simplify the solution in certain cases, yet retaining high accuracy of the result.

The most accurate and efficient method for modelling particle interactions and transport in matter is to use general-purpose Monte-Carlo codes. At present, there are five major Monte-Carlo codes widely used around the globe; these are FLUKA, GEANT4, MARS15, MCNP, and PHITS. Most of these codes allow users to simulate all aspects of a high energy particle cascade in the same run: from the first interaction of a primary beam (of up to multi-TeV energies) over the transport and re-interactions (hadronic and electromagnetic) of the produced secondaries, to detailed nuclear fragmentation, the calculation of radioactive decays, secondary electromagnetic showers, muon and neutrino generation and their interaction with surroundings.

1.2. MARS15 main features

The original MARS code was created in 1974 by Nikolai Mokhov at MEPhi (Moscow), and since then has been under development at IHEP (Protvino), SSCL (Texas) and Fermilab. There are 300 official users and 40 sites worldwide. The code is being constantly developed. The latest updates and new features include improvements in the event generators, materials, low energy neutron treatment, DPA, FTD, transport in electro-magnetic fields, variance reduction, and GUI. Several important features are discussed here in detail.

MARS15 is a collection of Fortran 77 and C++ modules for Monte-Carlo simulations of coupled hadronic and electromagnetic cascades, with heavy ion, muon and neutrino production and interactions in an arbitrary geometry of shielding, accelerator, detector, and spacecraft components. It covers a wide energy range: (i) 1 keV to 100 TeV for muons, hadrons, heavy ions, and electromagnetic showers; (ii) 10^{-5} eV to 100 TeV for neutrons. Nuclear, strong, weak, and electromagnetic interactions, such as electromagnetic showers, hadron-nucleus interactions, decays of unstable particles, emission of synchrotron photons, photo-hadron production and muon pair production, can be simulated exclusively (in a fully or partially analogue mode), inclusively (in a biased mode, with corresponding statistical weights), or in a mixed mode (the mode can be selected via input data). The goal is to maximize computing efficiency in such a way that a resulting RMS error is below 20%. Nuclide production, decay, transmutation, and calculation of the activity distribution is done with the built-in DeTra code. MARS15 uses ENDF/B-VIII.0 (2018) nuclear data to handle interactions of neutrons with energies below 14 MeV and derive the NRT/Stoller/Nordlund DPA cross-sections below 200 MeV. The elemental distributions are automatically unpacked into isotope distributions for both user-defined materials and those from a collection of 172 built-in materials.

1.2.1. Nuclear event generator

A combination of LAQGSM and CEM codes as well as nuclear data libraries TENDL-2019 (TENDL) and ENDF/B-VIII.0 (ENDF) is used as the nuclear event generator (for more details, see Mokhov, 2021). The LAQGSM model reproduces experimental data very well (Figure 1.1). The TENDL-2019 library covers kinetic energy range from 200 MeV

down to 1 MeV for seven projectiles (p, d, t, ^{3}He, ^{4}He, γ and neutron). The ENDF/B-VIII.0 library is used to describe neutron collisions with kinetic energies from 20 MeV down to 10^{-5} eV.

Figure 1.1. Double differential cross-sections of HE protons producing pions and kaons.

Charged pion (left) and kaon (right) production differential cross-sections in interaction of 8 GeV/c and 3.5 GeV protons with tantalum and gold nuclei calculated using LAQGSM vs experimental data (Mokhov, 2014)

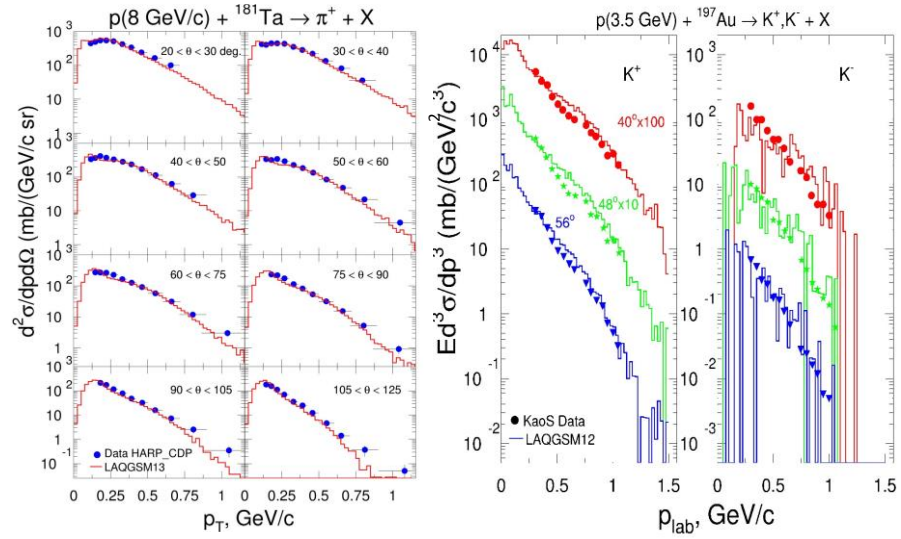

1.2.2. Mean stopping power

Mean stopping power for heavy charged particles in matter is described as -dE/dx = a(E) + b(E) × E, where a(E) is the electronic stopping power, b(E) is due to radiative processes – bremsstrahlung, pair production and photonuclear interactions – and E is particle energy (Groom et al., 2001). Both a(E) and b(E) are slowly varying functions of energy at high energies. The electronic stopping power of charged particles heavier than electrons is given by the Bethe-Bloch expression (Figure 1.2):

$$-\frac{1}{\rho}\frac{dE}{dx} = 4\pi N_A r_e^2 m_e c^2 z^2 \frac{Z}{A}\frac{1}{\beta^2} L(\beta) \qquad (1)$$

where A and Z are the target atomic mass and number, respectively, z is the projectile charge and the other variables have their usual meaning. The ionization logarithm, $L(\beta)$, is presented in the following form:

$$L(\beta) = L_0(\beta) + \sum_i \Delta L_i \qquad (2)$$

$$L_0(\beta) = \ln\left(\frac{2m_e c^2 \beta^2 \gamma^2}{I}\right) - \beta^2 - \frac{\delta}{2} \qquad (3)$$

where I and δ are the mean ionization energy and density correction, respectively. When neglecting all the corrections ΔL_i and dealing only with $L_0(\beta)$, the expression (1) is referred to as the Bethe equation. The corrections ΔL_i take into account deviations from the Bethe theory for heavy ions at both low and high energies (Rakhno et al., 2005): (i) Lindhard-Sørensen correction (exact solution to the Dirac equation; terms higher than z^2); (ii) Barkas correction (target polarization effects due to low-energy distant collisions); and (iii) shell correction. Projectile effective charge z_{eff} instead of z comes separately as a multiplicative factor that takes into account electron capture at low projectile energies.

Figure 1.2. Mean stopping power of projectiles from proton to uranium in silicon.

Lines and symbols represent Eq. 1 and experimental data, respectively (see Rakhno et al., 2005).

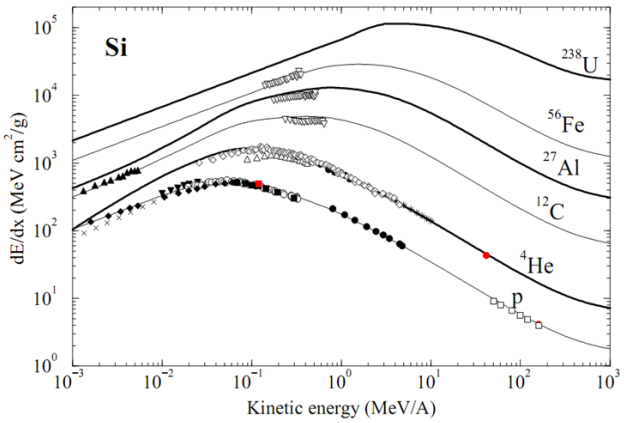

1.2.3. MARS15 Tagging, Variance Reduction, Links to other codes and GUI

Tagging technique used in Monte Carlo codes allows us to tag origin (phase space coordinates) of a given signal (event) for source term or sensitivity analyses. Several variance reduction techniques, such as weight windows, particle splitting, and Russian roulette, are employed in the code. MARS15 is used with ANSYS for iterative studies of thermo-mechanical problems; it can be also linked to a hydrodynamic code to study phase transition phenomena and a so-called “hydrodynamic tunnelling”.

A powerful GUI tool allows us to visualize geometry and plot 2D histograms; 3D visualization is currently possible with ROOT. Advanced built-in version is being developed, and its realization is envisioned within one year.

1.2.4. Electromagnetic Fields and MARS-MADX-PTC Integration

A wide class of problems solved with the MARS code is the assessment of radiation effects on accelerator equipment and environment due to interaction of beam particles with beam pipe aperture during beam transportation along beamline. Tools invented and created in the process of solving such problems are combined in a library and included in the MARS distribution. The library contains functions and C++ classes that provide an interface between MARS15 and MAD-X (MAD) with its PTC (Forest et al., 2002) module.

The tools allow us to create ROOT/TGeo (Bruns & Rademakers, 1997) geometry using input file containing description of a beamline optics in MAD-X format. Alignment of the elements is performed by means of survey table internally calculated by MAD-X. User has a tool to provide specific geometry builder for particular class of elements declared in MAD-X file. This tool is a part of beamline builder component of the library. Among other things, it automatically creates and provides magnetic field objects generated from MAD-X description. The user can associate these field objects with stepper objects of a class provided by the library.

One particular stepper, which becomes especially useful for generation of beam losses during multi-turn transport in circular machines, is the stepper based on MAD-X PTC module. This stepper has been built with a special purpose to provide interaction with

MARS transportation module: (i) if a trajectory being propagated by PTC hits the beam pipe, it will be transferred to MARS for further transport in material of the beam pipe and outside it; (ii) if a charged particle being transported by MARS goes from the beam pipe into the beam pipe aperture, the trajectory will be transferred to PTC for further transport if phase coordinates and particle type are within acceptance of the model. Figure 1.3 shows a consistency check for the MARS15 and MAD-X PTC tracker.

Advantages of the MARS-MADX-PTC code system have been successfully demonstrated in the Fermilab's new PIP-II Booster Collimator design optimisation analysis (see Tropin & Mokhov, 2021). One more stepper class provided by the library makes possible to transport particles in time-dependent EM fields. It was designed to use in simulations which include propagation of particles in SRF cavities and dark current simulations.

Figure 1.3. A consistency check for MARS15 and MADX-PTC module.

Beam orbits in the Fermilab 8-GeV Recycler calculated with MADX-PTC module (blue) and MARS15 helix stepper (red).

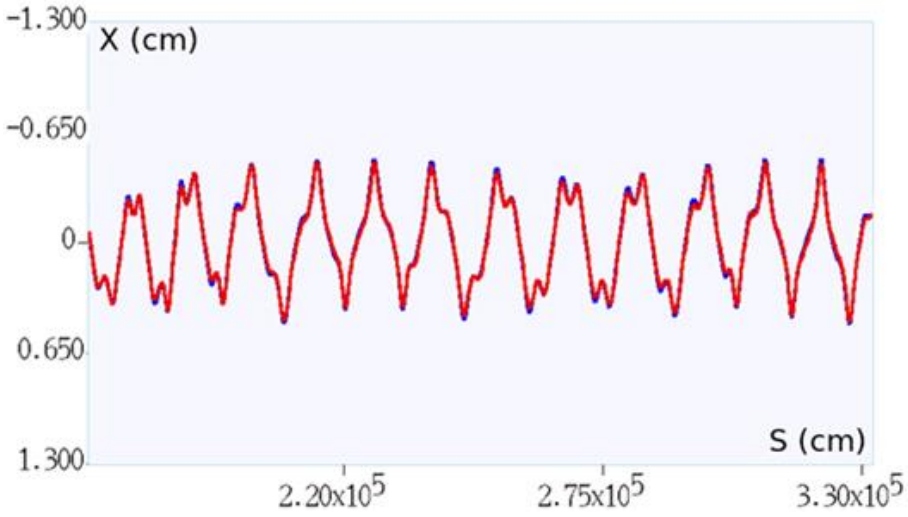

1.2.5. MARS15 Options for Geometry Description with ROOT/TGeo

The ROOT/TGeo package was added to the list of geometry model options in 2011 to support development of a MARS application with included geometry of the CMS detector at the LHC, and then it was used to develop a model of the LBNF facility. Since 2011 the package has been used in MARS-based radiation studies for almost all existing and future components of the Fermilab accelerator complex.

At present, a ROOT/TGeo geometry model in a MARS-based application can be created in the following ways:

- providing a C++ function called from the MARS user subroutine REG1. This is suitable to create parametric geometries;
- importing geometry from a ROOT or GDML file generated by a third-party software, such as a ROOT script or Geant4 application;

- using the ROOT visual geometry editor which is a built-in feature of the package, or the GDML Workbench of the FreeCAD modeler (see FreeCAD GDML Workbench).

One more option would be using CAD-to-GDML converters. However, the latest production version of ROOT (v.6.28.04 at the time of this writing) still does not support navigation queries for volumes bounded by “tessellated” shapes that are used in CAD geometries. The possibility to process the “tessellated” shapes has been introduced only in the development version 6.29.01 when ROOT is compiled with VecGeom support.

Figure 1.4 shows an example of a geometry model in GUI of the FreeCAD GDML Workbench. Figure 1.5 demonstrates parts of the LBNF model in the ROOT OpenGL viewer, and Figure 1.6 shows ROOT-based Beamline Builder models. The target model shown in Figure 4 was used for calculations of the residual dose rates for a comparison between MARS calculations and the benchmark experimental data of the SINBAD database (see SINBAD).

The ROOT/TGeo package demonstrated efficient navigation in complex geometry models. Also, it allows us to import and use a part of or an entire geometry model created by other developers.

An experimental version of a MARS interface library, based on both the ROOT/TGeo and VecGeom software, allows us to perform modelling in a geometry imported from CAD, and this development is currently under testing.

Figure 1.4. A target model used in a MARS simulation of residual dose rates.

MARS simulations were performed to compare predicted residual dose rates with the benchmark experimental data of the SINBAD database (CERF experiment).

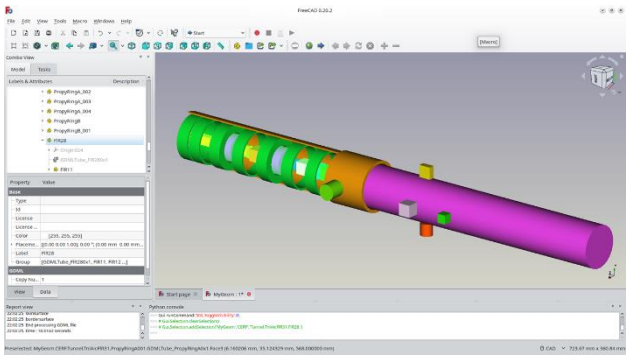

Figure 1.5. Parts of the LBNF model in the ROOT OpenGL viewer.

MARS models of the downstream end of the LBNF Decay Pipe (left) and lower part of the LBNF Absorber Building (right).

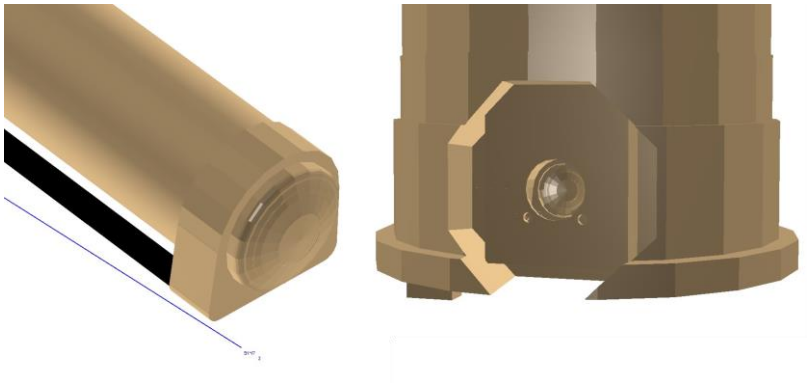

Figure 1.6. MARS15 ROOT-based Beamline Builder models.

MARS models of the Fermilab Booster collimation region (left) and LHC IP5 region (right).

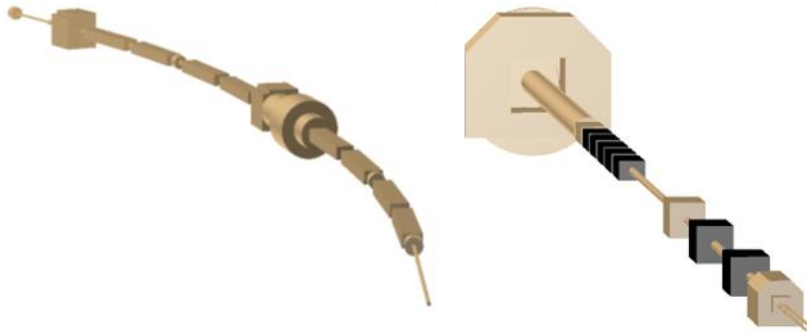

1.3. MARS15 Code Application Examples

A few examples are presented to demonstrate powerful MARS15 analysis methods.

1.3.1. Fermilab LBNF Absorber

As an example of the scoring system/meshing application, a model of the LBNF Absorber is shown in Figure 1.7. The model was used to study the so called "water hammer effect" in the cooling channels. Figure 1.8 shows meshing of the model. The mesh was provided as a file in the CGNS format with about 3.7M mixed 2nd order cells. Figure 1.9 shows calculated energy deposition (EDEP) results on an unstructured ANSYS mesh and corresponding predicted temperature rise in the Absorber core block caused by an accidentally displaced beam pulse. For the visualization, Salome ParaVis module was used. Energy deposition maximum is found to be in the 3rd core block. MARS output data on energy deposition are saved in the CGNS file that can be read as an input by ANSYS code. The data can be used by ANSYS also for further simulation of the pressure spikes induced by several beam pulses.

Figure 1.7. Study of water hammer effect in the cooling channels of the LBNF Absorber.

Proton beam parameters: 120GeV, 2.88 MJ/pulse, 1.2 s between pulses. LBNF Absorber model elevation view is shown along the z coordinate (left) and along the beamline (centre). A 3D view of the 3rd core block is shown as well (right).

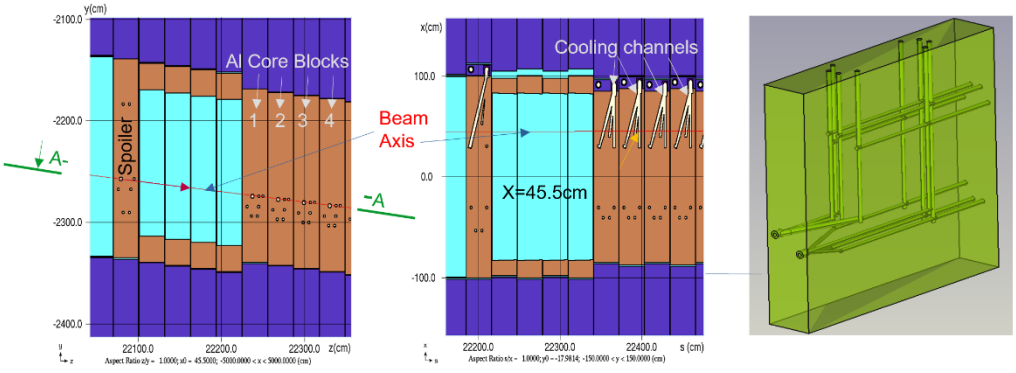

Figure 1.8. A mesh in the 3rd Absorber block generated with ANSYS.

Coarser mesh in the aluminium body (left), region affected by the beam with a refined mesh (centre), and a mesh in the cooling channels (right).

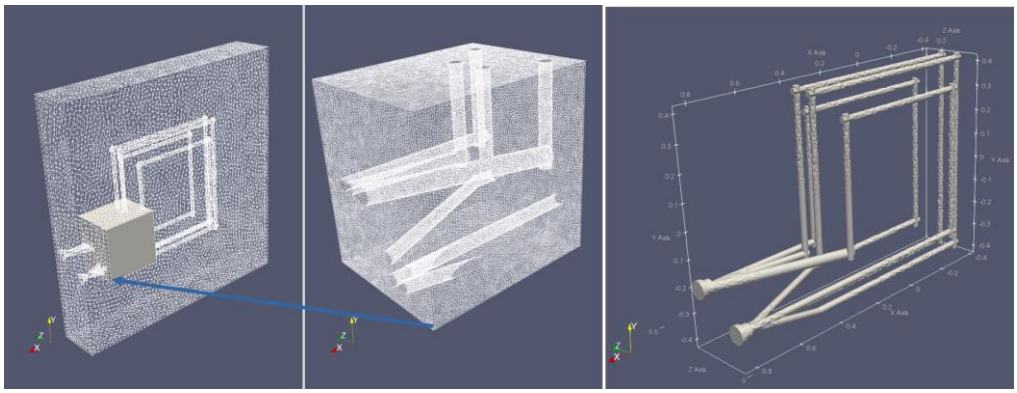

Figure 1.9. MARS EDEP results on an unstructured ANSYS mesh.

EDEP and temperature rise in the Absorber core block caused by an accidentally displaced beam pulse: EDEP in the block, general view (left) as well as detailed distribution along the beam axis of the temperature rise per pulse (centre) and EDEP per pulse (right).

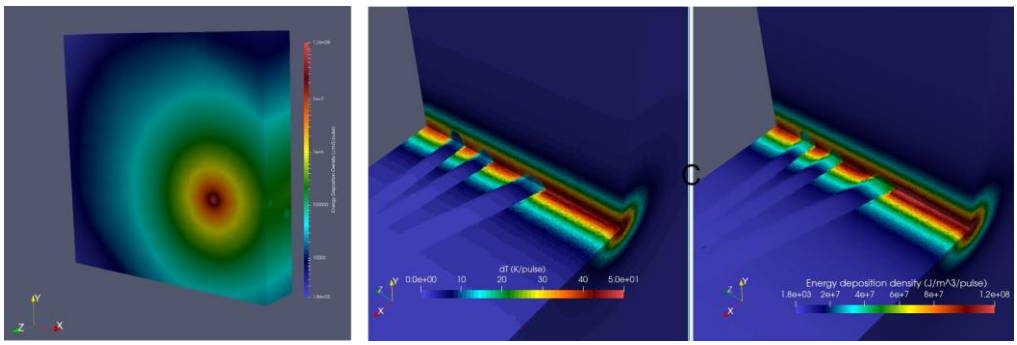

1.3.2. Fermilab Muon Campus Delivery Ring

A MARS model has been created to simulate the beam losses accompanying slow extraction process in the Muon Campus Delivery Ring at Fermilab with an 8 GeV proton beam. The model is shown in Figure 1.10. Beam transport in the apertures of the beam line elements along the ring is performed by the MAD-X PTC module while lost particles are propagated by MARS. Major beam loss in the ring is due to particles interacting with the tungsten strips (foils) in the septum. Using resonant optics, the sample particles are directed into the C-magnet at the beginning of the 1st and 4th turns. The part of the sample that misses the strips is extracted after a passage of three turns in the ring with no losses. The beam protons that passed the strips are the source of the distributed losses in the Delivery Ring elements. Figure 1.11 shows the simulated particle tracks in the injection region.

Figure 1.10. A MARS model of the Muon Campus Delivery Ring.

The model has been built for simulation of the beam losses accompanying the slow extraction process in the Delivery Ring. A general view of the Ring (left) and the extraction region (right) are shown.

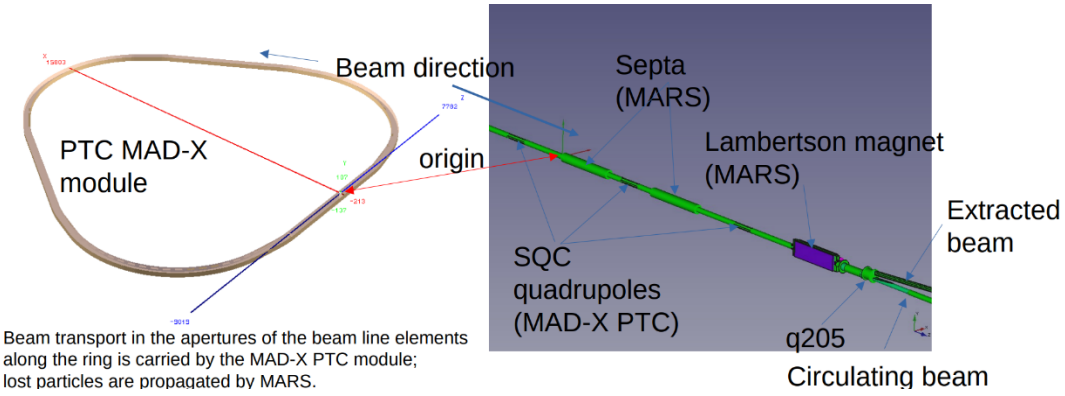

Figure 1.11. Muon Campus Delivery Ring injection region: effect of strips in septa.

Effect of the proton beam propagation through the strips: a thousand of tracks with energy above 0.5 GeV (initial particle energy is 8 GeV) over 5 turns calculated with MARS15-MADX-PTC. Sample particles are directed into the C-magnet at the beginning of the 1st and 4th turns. The numbers shown in red are turn numbers, e – extracted beam, c – circulating beam. Elevation view is shown on the left; plan view is shown on the right.

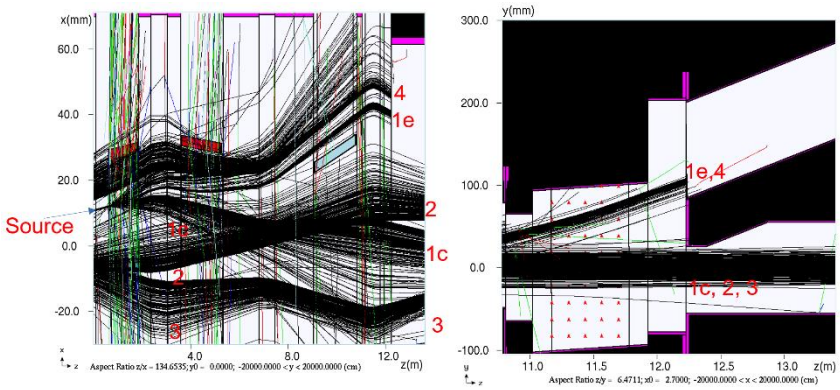

Figure 1.12 shows a calculated beam loss distribution along the Delivery Ring. These results can be used to design a collimation system, select its location and collimator parameters, as well as study the impact of the beam loss on the radiation environment.

Figure 1.12. A calculated beam loss distribution in the Delivery Ring.

The loss point is determined as the location of the particle hitting the beam aperture during 5 turns. This assumes a normalization corresponding to the full beam intensity of 9.0×10^{10} protons. The calculated loss distribution represents basic data for design of the collimation system as well as for selection of its location and collimator parameters.

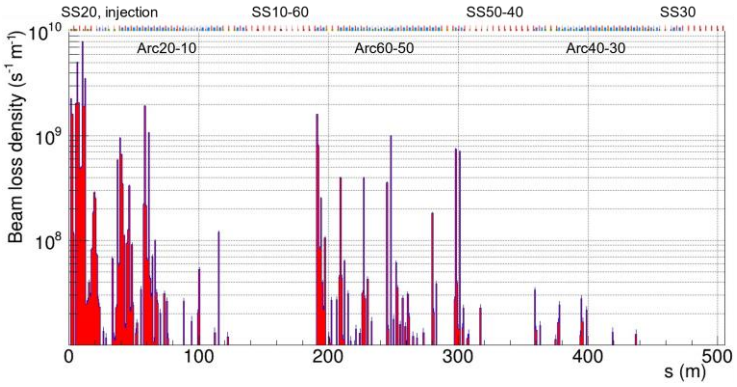

1.4. MARS15 Development Goals and Path Forward

Near- to midterm MARS15 development plans include further improvements, modernization, and fine-tuning of the predictive accelerator and experiment models; further development of the modules for transport in EM fields and underlying physics; development of the CAD → MARS15_ROOT → CAD user-friendly geometry converters compatible with strict requirements for simulation of particle interactions and transport in matter in a challenging accelerator environment; creation of a user-friendly module to calculate 3D residual dose maps around accelerator equipment in accelerator tunnels and other enclosures with ParaView software; a new 3D GUI to display and analyse 3D histograms; update and modernize the MARS15 User's Guide and website; restore the earlier MARS15 practice of regular tutorials.

The plans also include implementation of the modern code-management techniques, namely, improving strategy, implementation, benchmarking and optimization of the Fortran and C++ modules, as well as improving scoring techniques. Message-Passing Interface (MPI) and multiple-core job handling were kept standard for two decades (100-1000 cores routinely, up to 10^5 as needed). Current plan is to improve usability on HTC systems with containers and prepare for the exascale computing era on HPC clusters.

1.5. List of references

R. Brun and F. Rademakers (1997), ROOT – An Object Oriented Data Analysis Framework, Proceedings of AIHENP'96 Workshop, Lausanne, Sep. 1996, Nucl. Inst. & Meth. In Phys. Res. A 389, 81-86.

ENDF – ENDF/B-VIII.0 Evaluated Nuclear Data Library, ENDF/B-VIII.0 Evaluated Nuclear Data Library (bnl.gov)

E. Forest, F. Schmidt, and E. McIntosh (2002), Introduction to the polymorphic tracking code Fibre bundles, polymorphic taylor types and "Exact Tracking" (KEK-2002-3), Japan

FreeCAD GDML Workbench, https://github.com/KeithSloan/GDML

D.E. Groom, N.V. Mokhov, and S.I. Striganov (2001), Muon Stopping-Power and Range Tables: 10 MeV-100 TeV, Atomic Data and Nuclear Data Tables 78, 183-356.

MAD – Methodical Accelerator Design, http://madx.web.cern.ch/madx/

N.V. Mokhov et al. (2014), Prog. Nucl. Sci. Technol., 4, 496-501.

N.V. Mokhov and C.C. James (2018), The MARS Code System User's Guide, Version 15, Fermilab-FN-1058-APC; https://mars.fnal.gov

N.V. Mokhov and I.S. Tropin (2018), MARS15-Based System for Beam Loss and Collimation Studies, Proc of ICFA Mini-Workshop, CERN, Geneva

N.V. Mokhov, Y.I. Eidelman, V.S. Pronskikh, I.L. Rakhno, D. Reitzner, S. I. Striganov, I.S. Tropin (2021), Mars15 code developments and applications to the LBNF/DUNE project, in the Proceedings of the SATIF-14 held in Gyeongju, Korea, October 30 – November 2, 2018

N. V. Mokhov (2022), MARS15 Code Overview, Detector Simulation Working Group Meeting, Fermilab - CERN, https://indico.cern.ch/event/1107097

I.L. Rakhno, N.V. Mokhov, and S.I. Striganov (2005), Modelling Heavy Ion Ionization Loss in the MARS15 Code, Fermilab-Conf-05-019-AD

SINBAD – OECD/NEA Databank, NEA-1552/15, https://www.oecd-nea.org/science/wprs/shielding/sinbad/

TENDL – TALYS-based evaluated nuclear data library, TENDL-2019 nuclear data library (psi.ch)

I.S. Tropin and N.V. Mokhov (2021), MARS15-MADX integration and its application for design of the Fermilab Booster collimation system, in the Proceedings of the SATIF-14 held in Gyeongju, Korea, October 30 – November 2, 2018

Acknowledgements

This work is supported by Fermi Research Alliance, LLC under contract No. DE-AC02-07CH11359 with the U.S. Department of Energy. This research used, in part, ALCC allocations at the Argonne Leadership Computing Facility (ALCF) and at the National Energy Research Scientific Computing Centre (NERSC) which are DOE Office of Science User Facilities supported under Contracts DE-AC02-06CH11357 and DE-AC02-05CH11231, respectively.

List of abbreviations and acronyms

3D	Three-dimensional
ANSYS	ANalysis SYStem (Engineering Simulation Software)
CAD	Computer Aided Design
CEM	Cascade-Exciton Model
CFD	Computational Fluid Dynamics
CGNS	CFD General Notation System
DPA	Displacement Per Atom
EM	Electro Magnetic

fpo	floating point operation
FTD	Flux-To-Dose (conversion coefficients)
GDML	Geometry Description Markup Language
GUI	Graphical User Interface
HPC	High Performance Computing
HTC	High Throughput Computing
LAQGSM	Los Alamos version of the Quark-Gluon String Model
LBNF	Long Baseline Neutrino Facility
LHC	The Large Hadron Collider at CERN
MAD-X	Methodical Accelerator Design
MI-8	Main Injector at FNAL
PIP-II	Proton Improvement Plan at FNAL
PTC	Polymorphic Tracking Code
ROOT	An object-oriented computer program at CERN
SRF	Superconducting Radio Frequency
VTK	The Visualization Toolkit

2. The FLUKA group- and point-wise neutron treatment

Giuseppe Battistoni[1], Giuseppina Bisogni[2,3], Mauro Campanella[1], Mario Pietro Carante[4,5], Pavel Degtiarenko[6], Ricardo dos Santos Augusto[7], Alberto Fassò[8], Alfredo Ferrari[9], Anna Ferrari[10], Giorgi Kharashvili[11], Aafke Kraan[2], Mario Nicola Mazziotta[12], Maria Cristina Morone[13,14], Silvia Muraro[1], Stefan E. Mueller[10], Vincenzo Patera[15,16], Lawrence S. Pinsky[17], Reuven Rachamin[10], Sofia Rollet[18], Paola Sala[19*], Mario Santana Leitner[20], Lucia Sarchiapone[21], Thomas Tessonnier[22], Lorenzo Zana[23]

[1]INFN sezione di Milano, Milano, Italy
[2]INFN sezione di Pisa, Pisa, Italy
[3]Dipartimento di Fisica, Università di Pisa, Italy
[4]INFN sezione di Pavia, Pavia, Italy
[5]University of Pavia, Pavia, Italy
[6]Jefferson Lab, Newport News, VA, USA
[7]TRIUMF, 4004 Wesbrook Mall, Vancouver, BC V6T 2A3, Canada
[8]Retired, Eysins, Switzerland
[9]Thoiry, France
[10]Helmholtz-Zentrum Dresden-Rossendorf, Dresden, Germany
[11]Brugg, Switzerland
[12]INFN sezione di Bari, Bari, Italy
[13]Università di Roma Tor Vergata, Roma, Italy
[14]INFN sezione di Roma Tor Vergata, Roma, Italy
[15]S.B.A.I. Department, Sapienza Università di Roma, Roma, Italy
[16]INFN sezione di Roma1, Roma, Italy
[17]Physics Department University of Houston, Houston, Texas, USA
[18]Retired, Vienna, Austria
[19]On leave of absence from INFN Milano
[20]SLAC National Accelerator Laboratory, Menlo Park, California, USA
[21]INFN, Legnaro National Laboratory, Legnaro, Italy
[22]Heidelberger Ionenstrahl-Therapiezentrum (HIT) Heidelberg, Germany

[*]paola.sala@mi.infn.it

The low energy neutron treatment in the FLUKA code has been greatly expanded over the last couple of years.

Until recently, the treatment of neutrons below 20 MeV was based on a 260-group library built with NJOY99 (plus ad-hoc extensions) and to various degrees based on ENDF/B-VIR8, ENDF/B-VIIR0, ENDF/B-VIIR1, and JEFF-3.2. New evaluations are now available which contain more isotopes, more accurate information, and with new formats (eg for unresolved resonances) which are incompatible with older NJOY versions. Consequently, the entire processing chain is now built on NJOY16 and a vast majority of the isotopes are now processed out of the most recent evaluations, mostly ENDF/B-VIIIR0. At the same time, the library, besides the residual nuclei cross sections, now contains also the probability of producing isomers with cross sections derived from EAF-10.

Fully correlated point-wise treatment for some isotopes (^{1}H, ^{2}H, ^{3}He, ^{4}He) was available also in previous FLUKA versions. However no general point-wise treatment was possible, unless in a few exceptional cases (eg ^{40}Ar, ^{208}Pb) which were not generally distributed because of several limitations. Now, a novel point-wise based alternative is provided in FLUKA for all stable isotopes. This approach, using as much as possible the evaluated data file information, which is strictly inclusive, complemented with physics modelling and

some reasonable assumptions, is now able to produce event-by-event, exclusive, fully correlated neutron interactions in the 10^{-5} eV - 20 MeV energy range. The point-wise library is based on ENDF/B-VIIIR0 and TENDL-2019, and it is built with a combination of PREPRO19, NJOY16 (both somewhat modified), and an extensive in-house developed code.

Examples proving the neutronics performances of the pointwise libraries against the group-wise library will be presented. Applications that could not be possible without the fully correlated point-wise treatment will also be presented.

During the development of the point-wise libraries, several issues denoting inconsistencies or outright errors in the evaluated data files emerged. Moreover, some problematic tendencies in the way new evaluated data files are produced were also noted. It is important for our community to be aware of those issues, and possibly exert pressure on the evaluator community to take into account our concerns.

2.1. Introduction

FLUKA (Ferrari et al. 2005; Böhlen et al. 2014; Ferrari et al. 2022) is a general-purpose tool for calculations of particle transport and interactions with matter.

Neutrons represent a very important radiation component in most of the FLUKA applications. A faithful simulation of neutron transport and interaction is evidently essential for all shielding and activation calculations, even those related to electron/photon radiation sources. Besides, in hadron therapy, neutrons are the only source of radiation hazard far from the tumour area. Despite the enormous energies of primary particles, low energy neutrons are one of the handles helping to fully characterize cosmic rays showers (Engel et al. 2021) and albedo neutrons from cosmic ray showers feed the radiation belts when decaying. Every time a particle detector is immersed in a radiation field, its response depends on the associated neutron field, often difficult to measure. Even in deep underground particle detector experiments, neutrons are a dangerous source of background.

For neutron energies above 20 MeV, FLUKA treats neutron interactions, as for all other hadronic interactions, with microscopic models, driven and benchmarked by experimental data (Ferrari et al. 2014 and references therein). Below this threshold, the complexity of nuclear physics calls for specialized algorithms.

The standard method for low energy neutron transport in FLUKA is a multigroup algorithm based on publicly available evaluated nuclear data files. The FLUKA “group-wise” neutron library allows for simulations at different temperatures, different self-shielding conditions and different atomic bindings. It has been recently synchronized with the latest ENDF/B-VII (Brown et al. 2018) data.

Multi-group transport is a perfect tool for many applications, being fast and reliable. However, it requires a guess spectrum for group averaging the cross sections and does not allow, by definition, for a direct connection between the exact neutron energy and the corresponding cross section/reaction products. Moreover, due to the inclusive distribution provided by datasets, energy conservation is ensured only on average, not at each interaction.

A major step forward has been realized in FLUKA and made public with the FLUKA2021 version: point-wise fully correlated neutron transport.

As will be discussed in the following, not only the evaluated data are associated with the exact neutron energy at every step, in a “point-wise” way, but the energy and directions of

reaction products, including nuclear recoils, are correlated among themselves so that energy-momentum conservation is ensured in an event-by-event basis.

The two neutron transport algorithms, as implemented in FLUKA, are described and compared in sections 2 to 4 below. Section 5 and 6 contain examples of applications where point-wise correlated treatment is essential for reproducing experimental results.

2.2. Group-wise neutron transport

The multi-group technique, widely used in low-energy neutron transport programs, consists in dividing the energy range of interest into a given number of intervals ("energy groups"). Elastic and inelastic reactions are simulated not as exclusive processes, but by group-to-group transfer probabilities forming a so-called "downscattering matrix" (upscatterings are also possible in the thermal energy range).

In the FLUKA neutron cross section library, the energy range up to 20 MeV is divided into 260 energy groups of approximately equal logarithmic width, 31 of which are thermal.

The angular probabilities for neutron scattering are obtained by a discretisation of a P5 Legendre polynomial expansion of the actual scattering distribution which preserves its first 6 moments.

The production of secondary neutrons via (n,xn) reactions is taken into account implicitly by the so-called "non-absorption probability", a group-dependent factor by which the weight of a neutron is multiplied after exiting a collision. Fission neutrons, however, are treated separately and created explicitly using a group-dependent fission probability.

Gamma generation by low energy neutrons (but not gamma transport) is treated in the frame of a multigroup scheme too. The FLUKA library contains 42 gamma energy groups, covering the range from 1 keV to 50 MeV. With the exception of a few important gamma lines, such as the 2.2 MeV capture transition of Deuterium and the 478 keV photon from $^{10}B(n,\alpha)$ reaction, the actual energy of the generated photon is sampled randomly in the energy interval corresponding to its group. These photons are further transported in the same way as all other photons in FLUKA, using continuous cross sections and an explicit and detailed description of all their interactions with matter, allowing for the generation of electrons, positrons, and even secondary particles from photonuclear reactions.

Recoil protons from interactions on Hydrogen and protons from the $^{14}N(n,p)$ reaction are produced and transported explicitly. No other charged secondaries, including fission fragments, are transported but their kinetic energy is deposited at the point of interaction (kerma approximation).

For most materials, group-dependent information on the residual nuclei produced by low-energy neutron interactions is available in the FLUKA libraries and can be used for activation studies.

The default FLUKA neutron cross section library contains more than 250 different materials (natural elements or single isotopes), selected for their interest in physics, dosimetry, and accelerator engineering.

The preparation of the library involves the use of the NJOY code (MacFarlane 2010) and several ad-hoc programs written to adjust the output to the particular FLUKA structure (Cuccoli 1991).

Hydrogen and carbon cross sections, which have particular importance in neutron slowing-down, are available also for different types of molecular binding: free, H_2O, CH_2, for hydrogen, free gas and graphite for carbon.

Cross section sets with different degrees of self-shielding have been included in the FLUKA libraries for a few important elements (Al, Fe, Cu, Au, Pb, Bi).

Some cross sections are available in the library at two or three different temperatures, mainly in view of simulations of calorimeters containing cryogenic media.

Doppler broadening is taken into account.

Even before 2021, point-wise transport was, and still is, available as user option for a few isotopes, due to their relevance: ^{1}H, ^{2}H, ^{3}He, ^{4}He, and ^{12}C. For the reactions ^{10}B (n,α)^{7}Li and ^{14}N(n,p)^{14}C, the α, and proton respectively are explicitly generated.

Starting with FLUKA2020, neutron cross sections for several isotopes have been updated with more recent evaluations, mostly ENDFB-VIIIR0 (Brown et al 2018), and more isotopes have been included in the FLUKA library (for instance tellurium, ^{13}C, ^{17}O, and ^{18}O).

At the same time, fission fragment yields by low energy neutrons have been updated with the most recent evaluations, ENDFB-VIIIR0 (Brown et al 2018) , JEFF-3.3 (Plompen et al. 2020), and JENDL-4.0 (Shibata et al. 2011).

Updates are in continuous progress, and will soon take into account the recent release of the JENDL-5 (Iwamoto et al. 2020) evaluation.

Neutron cross sections now contain the information for the production of isomers, out of the European Activation File (EAF) (Sublet 2010). Therefore, isomer versus ground state production by low energy neutrons is calculated according to evaluated data when available.

2.3. Point-wise cross sections

The FLUKA point-wise library is built by processing evaluated data with the PREPRO19 (Cullen 2019) and NJOY2016 (MacFarlane et al. 2016) codes, supplemented by FLUKA-specific code that converts to FLUKA format and takes care of correlations as will be discussed in the next section.

The FLUKA library includes all stable isotopes, a few important unstable ones (e.g. ^{135}Xe) and the most important transuranic ones, pre-processed at different temperatures: 4, 87, 296, 430, and 686 K. Most isotopes are processed from ENDF/B-VIIIR0, a few from TENDL-19 (Koning et al. 2019).

The use of NJOY allows accounting correctly for unresolved resonances in the cross sections. The unresolved resonances region (URR) typically covers an important energy window, in between ~1 keV and ~1 MeV. These resonances are not resolved experimentally but the induced fluctuations in the neutron cross section affect neutron transport. NJOY can compute the probability distribution of the cross section and store them in probability tables, to be further employed by the transport codes. An example of the importance of URR is shown in Figure 2.1. The spectra presented in Figure 2.1 are produced in a simple validation geometry in which point-wise transport has been compared to group-wise for each and every isotope included in the FLUKA library. It consists of three concentric spheres, two made of the material under consideration, and the third, in the middle, made of water. 20 MeV neutrons are injected at the centre of the spheres, and their spectra are collected at all boundaries.

It is evident in Figure 2.1 that the new point-wise cross sections are consistent with the standard group-wise ones if and only if the URR treatment is enabled.

Figure 2.1. Comparison among neutron lethargy spectra obtained from FLUKA with group-wise and point-wise transport, in a spherical gold-water geometry (see text) . Left: with careful URR treatment. Right: without URR treatment.

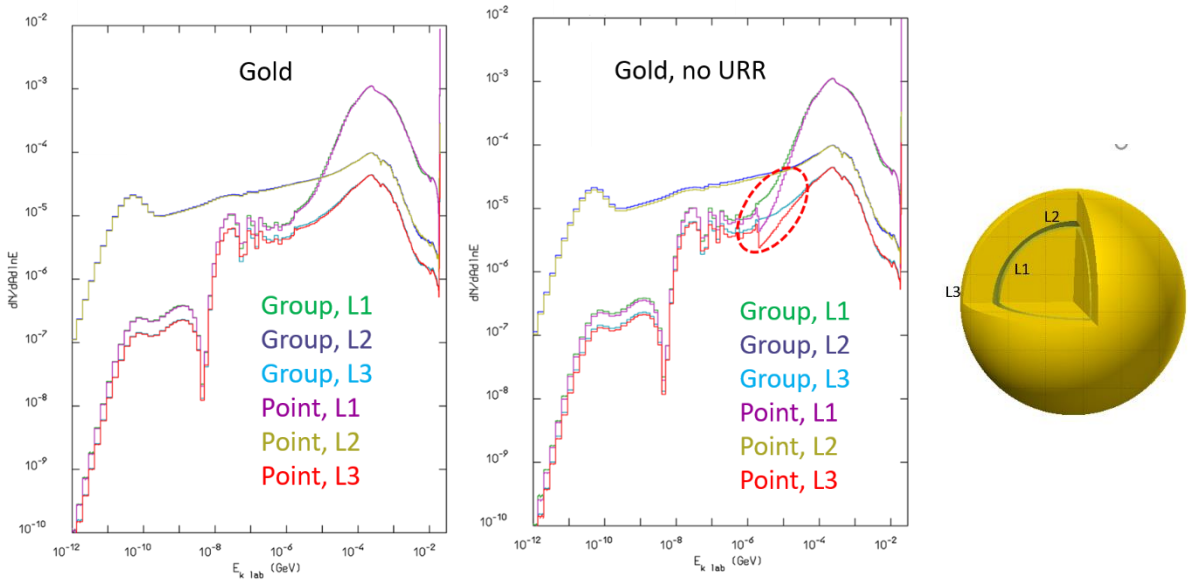

Discrepancy between group-wise and non-URR pointwise is encircled in red. Otherwise, spectra are so similar to be barely distinguishable.
Source: FLUKA collaboration 2021

It is also evident that, as expected, point-wise cross sections allow simulating automatically and correctly the effect of self-shielding (SS): in Figure 2.1 the comparison is with fully SS group-wise cross sections. Intermediate levels of self-shielding can be simulated automatically with point-wise treatment. An example with a realistic neutron spectrum on tantalum, a material with large resonances, is shown in Figure 2.2. The neutron flux is generated by 200 MeV protons impinging on a 0.5 cm thick copper target followed by 3 cm of water. It propagates in a thick and wide solid layer. A 100% tantalum composition allows to cross-check the point-wise treatment versus the fully self-shielded group-wise one. More interesting is the propagation in a carbon matrix doped with 10% of tantalum carbide, a material that is added to ceramics to strengthen them and has important applications in aeronautics. Despite the small tantalum percentage, the effect of resonances is still important, with point-wise spectra sitting in between the SS and not SS group-wise spectra.

The greatest advantage of group-wise transport is speed. Nonetheless, the new pointwise correlated algorithm represents a significant CPU penalty only in worst-case scenarios involving only neutron transport, while CPU times for full shower simulation are marginally affected.

For instance, in the spherical test setup described above, without transport of the electromagnetic component, with transport of charged particle down to 2 MeV, the point-wise algorithm is a factor 1.5 to 5 slower than the group-wise, depending on the material (factor 1.5 on N, 2 on Pb, 4 on Ta, 5 on Fe). This factor can increase if very low thresholds on charged particles are adopted, not because of neutron transport, but because of charged particle transport.

In a more complex setup, for instance the one used to generate the spectra in Figure 2.2, where the neutron spectrum extends above 20 MeV, again without transport of electromagnetic particles, the penalty decreases to 10%-20%. The addition of transport of electromagnetic particles lowers the difference to a few percent.

Figure 2.2. Effect of self-shielding: Point-wise and group-wise simulations in pure Tantalum (left) and in diluted Ta (right)

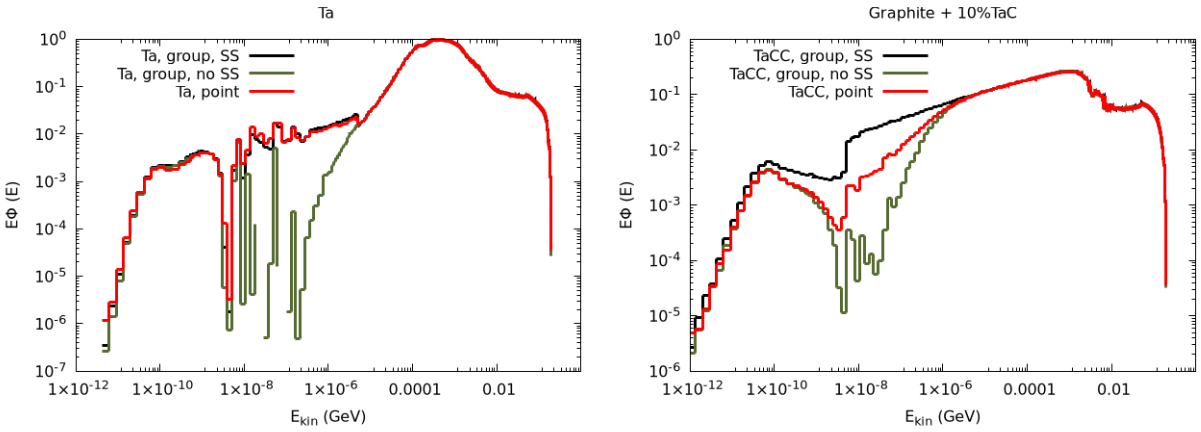

Left: neutron lethargy spectra, after 40 g/cm^2 Ta. Right: after 25 g/cm^2 Graphite + 10% TaC. Point-wise compared with self-shielded (SS) and non-self-shielded group-wise treatment.
Source: FLUKA collaboration 2021

2.4. Event-by-event correlations

Evaluated data files contain uncorrelated and inclusive information. The major consequence for simulations of neutron transport is that energy and momentum are not conserved, neither in single interactions nor even in full "histories". For instance, the sum of photon energies after a neutron capture can exceed the capture Q value. While most shielding applications are insensitive to this aspect, provided energy is conserved on average, applications to particle detector studies can be heavily affected.

Moreover, nuclear recoil spectra are not always available, and are sometimes unreliable, with obvious consequences on the reliability of, for instance, radiation damage calculations.

Pioneering work to include correlations was done in PHITS (Ogawa et al 2014), and correlations are also available in specialized codes for specific applications.

Starting with the FLUKA2021 release, FLUKA provides fully correlated neutron interactions. At each interaction, outgoing products, including the residual nucleus, are sampled ensuring that cross sections and spectra from evaluations are reproduced as much

as possible while conserving energy and momentum. In all cases, extra information or nuclear models are required to supplement the inclusive data sets.

Gamma de-excitation after interactions is always performed with the FLUKA de-excitation algorithm. The gamma cascade proceeds through known levels and branchings according to the RIPL-3 (Capote et al. 2009) database. For isotopes/energies where experimental levels are not available, FLUKA uses a proprietary model (Ferrari et al. 1996), in which the cascade is assumed to be statistical as long as the excitation energy is high enough to allow the definition of a continuous nuclear level density, while for lower energies, discrete levels are assumed to follow a rotational pattern.

For "simple" reactions like (n,el), (n,n'), (n,2n), (n,np), constrained sampling from available spectra is performed. In case of inconsistencies in the data, adjustments are made, with priority always given to the reproduction of the neutron spectrum.

Inconsistencies are indeed present in the evaluations. For instance, there are cases in ENDF/B-VIIIR0 where neutron spectra following (n,2n) interactions are not physical since the integral of the spectrum above one half of the available energy is larger than one half of the total integral.

For neutron capture, the branching ratios of the primary gamma transitions are taken from the Evaluated Nuclear Structure Data File (ENSDF) database (available online at https://www.nndc.bnl.gov/ensdf/), complemented by the FLUKA statistical model (Ferrari et al. 2006) if the data are incomplete. Work is in progress to improve the treatment of incomplete first branching. Correct descriptions of gamma spectra following neutron capture are essential for many applications, such as, for instance, determination of elemental composition by neutron irradiation, or background reduction in dark matter or neutrino experiments. Recently, the DUNE (Abi et al. 2020) collaboration, aiming to build a huge Liquid Argon neutrino detector, is taking into consideration the use of a neutron source in order to calibrate the detector with the energy deposited by capture photons (Maneira 2022). Obviously, an energy-conserving simulation code is essential for this task.

While checking the FLUKA results versus gamma spectra in evaluations, an apparent slip was spotted in the latest ENDF/B-VII and VIII releases, concerning thermal neutron capture in ^{207}Pb. Instead of an almost isolated transition at 7367.8 keV, that in the experimental data exhausts the total capture cross section (Belgya 1991; Martin 2007), a complex spectrum with many lines, not including the 7367.8 keV line, is tabulated. Older ENDF/B versions and the JENDL-5 evaluation contain different gamma spectra.

For more complex reactions like (n,2p), (n,4n), and (n,2nα), the reaction channel is selected according to the ENDF data, the reaction products are calculated with an ad-hoc Monte Carlo based essentially on phase space considerations, similarly to the Fermi Break-up FLUKA model. Clearly, the initial selection is much easier in all cases where all reaction channels are distinguished in the evaluated data. Cases where reactions are grouped in the so called (n,complex) (MT5) are more problematic, needing again support from models or from correlations with residual nuclei production in order to disentangle the various channels. This is a lose-lose approach since this information is available to the evaluators. As Monte Carlo developers, our message to evaluators is to avoid MT5, (n,complex), as far as possible, at least below 20 MeV where the available MT's in the ENDF format cover all possible reaction channels.

Figure 2.3. Comparison between experimental data (Rubchenya 2001), red points, and the old (left) and new (right) versions of the FLUKA fission model, green points, for 60 MeV protons on ^{238}U

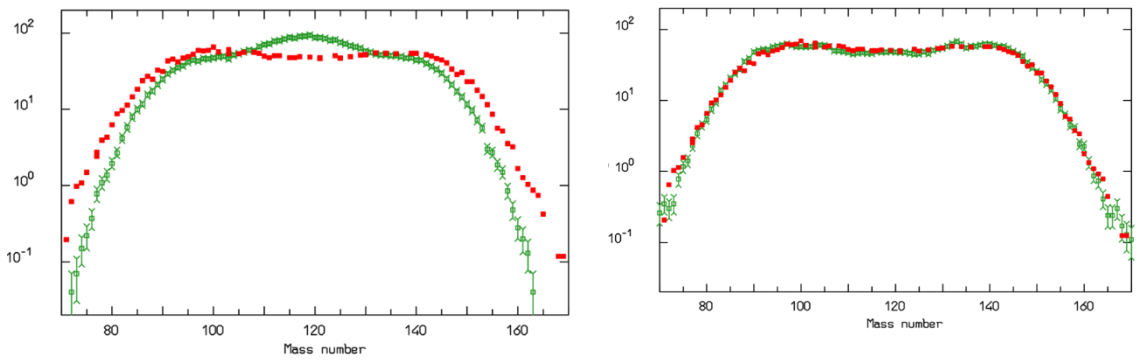

Post-fission, pre-neutron emission, fragment distribution. Distributions in arbitrary units
Source: FLUKA collaboration 2021

Fission is simulated by the FLUKA evaporation model, always forced to end up on fission. This model allows reproducing fission product mass distributions as in evaluated data, while obtaining correlated fission products and neutrons at each event. The fission model has been improved in order to better match the symmetric/asymmetric competition and the shape of the fragment mass distribution. The improvements are particularly visible at higher energies, as shown in Figure 2.3, where old and new results for 60 MeV protons on ^{238}U are shown in comparison with experimental data. The behaviour of the model for low energy neutrons is well illustrated in Figure 2.4. Moreover, an almost perfect agreement with data on prompt neutron multiplicity (see Table 2.1) has been achieved through a careful tune of the Coulomb energy backshift.

Figure 2.4. Comparison between evaluated data (ENDF/B-VIIIR0), red points, and the FLUKA fission model, green points, for 14 MeV n on ^{235}U (left) and Thermal neutrons on ^{239}Pu (right)

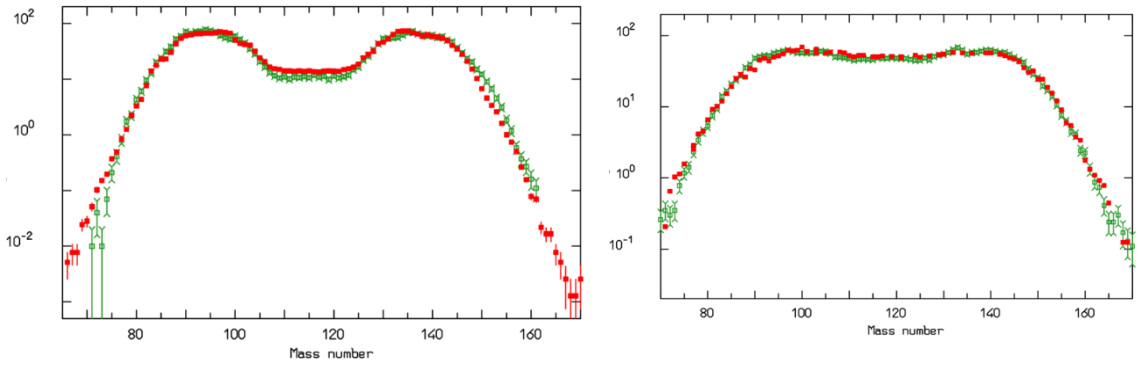

Post-fission, post-neutron emission, fragment distribution. Distributions in arbitrary units
Source: FLUKA collaboration 2021

Table 2.1. Prompt fission neutron average multiplicities

Isotope	Energy	< n prompt exp>	< n prompt FLUKA>	FLUKA/exp
235-U-92	thermal	2.416	2.417	1.000
239-Pu-94	thermal	2.876	2.872	0.999
241-Pu-94	thermal	2.932	2.935	1.001
242-Cm-96	SF	2.528	2.522	0.998
243-Cm-96	thermal	3.433	3.455	1.006
244-Cm-96	SF	2.688	2.532	0.942
245-Cm-96	thermal	3.59	3.544	0.987
252-Cf-98	SF	3.683	3.684	1.000
232-Th-92	8 MeV	3.15	3.15	1.000
238-U-92	5 MeV	3.05	3.01	0.987

Source: data from ENSDF and IAEA, Simulations Fluka collaboration 2022

2.5. Example: Diamond detector

Pillon et al (2017) published results about energy deposition spectra collected with a high resolution diamond detector irradiated with monochromatic neutrons. The 500 micron thick diamond semiconductor device acts at the same time as target and detector. Figure 2.5 shows the comparison between published experimental data and FLUKA simulations. A realistic energy resolution was applied to the Monte Carlo results. The total simulated energy deposition and the contributions from the various particle types are shown. The sub-contributions show no distinctive peaks, while the total energy does, exactly in correspondence of specific reaction channels where the correlated energies of the secondaries sum up to the reaction Q value. In absence of correlated interactions, no peak would be visible.

Figure 2.5. Comparison between experimental data (Pillon et al. 2017), left, and FLUKA fully correlated simulations (right) for energy deposition spectra in a diamond detector exposed to a 20.49 MeV neutron beam

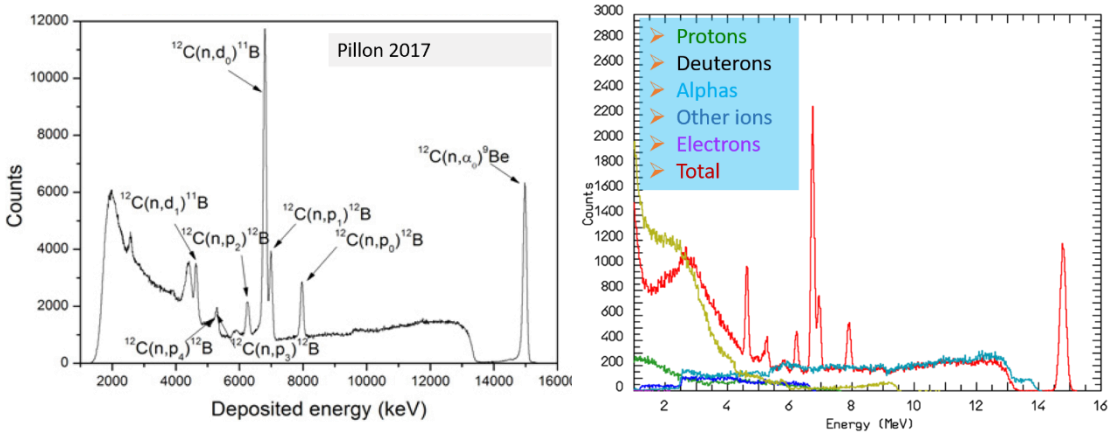

Source: Left: Pillon 2017, right: FLUKA collaboration 2022

2.6. Example: Silicon Carbide detector

Similar considerations arise from the comparison of FLUKA simulations with energy spectra from a SiC diode, having an active layer thickness of 44 microns. The detector was irradiated with 13.031 MeV neutrons, either bare or with a High-Density PolyEthylene (HDPE) converter in front. The experimental paper (Sedlačková et al. 2016) included comparisons with MCNP simulations, where the agreement with data was fair, except for the lack of a peak at the $^{12}C(n,\alpha)$ Q value, ascribed by the authors to a lack of correlations in MCNP. Indeed, FLUKA correlated results show this peak, as well as a very good agreement with data. The contributions from reactions on Si and C are shown in Figure 2.6, as well as the breakup in individual components, all of them concurring in the build-up of the spectrum.

The non-negligible contributions from heavy residuals, which match the low-energy experimental peak, underlines the importance of including them in neutron transport simulations. Besides special detector simulations, reliable calculations of radiation damage cannot be performed without a precise description of low energy heavy fragments.

Figure 2.6. Comparison between experimental data (Sedlačková 2016),left and FLUKA fully correlated simulations (middle and right) for energy deposition spectra in a SiC detector exposed to a 16 MeV neutron beam

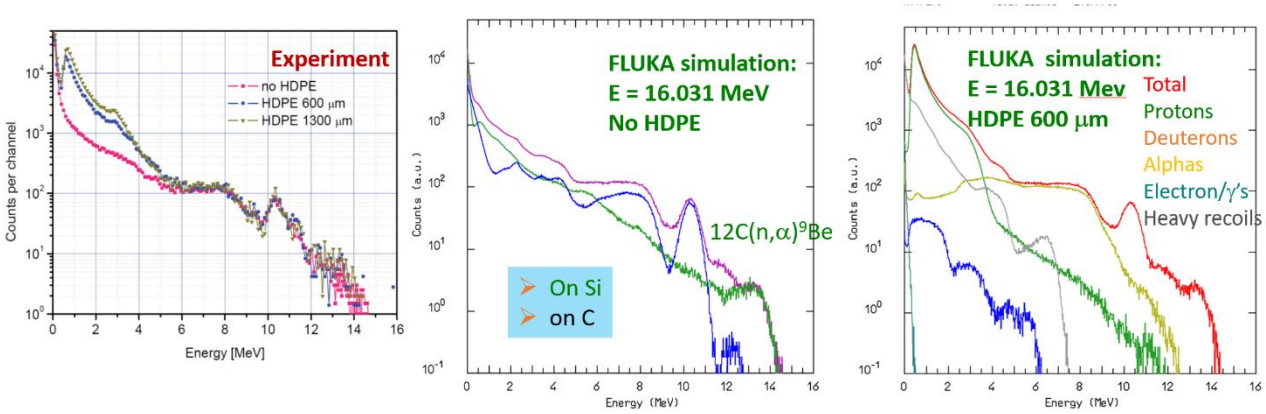

Size of plots has been adjusted to the same vertical scale. Realistic energy resolution convoluted with simulation
Source: Left: Sedlačková 2016, middle and right: FLUKA collaboration 2022

2.7. Summary and Conclusions

Low energy neutron transport in FLUKA is in continuous evolution. Two choices are offered to the user since the FLUKA2021 release. Group-wise treatment benefits from an enlarged isotope database, and from updates to the latest evaluated datasets. On option, group-wise is complemented by a precise point-wise description of the most sensitive targets and reaction channels. The completely new point-wise fully correlated algorithm represent an immense improvement, not only with respect to the old FLUKA2011 versions, but also with respect to most general purpose Monte Carlo codes. All reaction products, including residual nuclei, are generated and transported. Energy and momentum are conserved at each interaction. Consequently, FLUKA can now be used for detailed event by event analysis, as for particle detector simulations. This new algorithm is also important

for all applications requiring a reliable simulation of charged secondary, such as calculations of radiation damage. And, of course, point-wise transport automatically accounts for self-shielding in pure and diluted materials.

Low-energy neutron transport would not be possible without evaluated data sets. All Monte Carlo developers are indebted to evaluators who provide excellent and exhaustive data sets. A few glitches still present in the latest evaluations are brought to their attention, as well as a plea to avoid as much as possible the conglobation of several reaction channels in a single set.

2.8. List of references

Abi, B. et al. (2020) “Deep Underground Neutrino Experiment (DUNE), Far Detector Technical Design Report, Volume II: DUNE Physics” [arXiv:hep-ex/2002.03005].

Böhlen, T.T., et al. (2014), “The FLUKA Code: Developments and Challenges for High Energy and Medical Applications", Nuclear Data Sheets, 120, 211.

Belgya, T. et al. (1991) “Levels of ^{208}Pb from the ^{207}Pb(n,γ) reaction with a guided neutron beam” Phys. Rev. C 57, 2740

Brown, D.A et al. (2018),”ENDF/B-VIII.0: The 8th Major Release of the Nuclear Reaction Data Library with CIELO-project Cross Sections, New Standards and Thermal Scattering Data”, Nuclear Data Sheets,148,1-142, DOI:10.1016/j.nds.2018.02.001.

Capote, R. et al. (2009) “Reference Input Parameter Library (RIPL-3)”, Nuclear Data Sheets 110, 3107-3214

Cuccoli, E., Ferrari, A., Panini, G.C (1991) , “A group library from JEF 1.1 for flux calculations in the LHC machine detectors”, JEF-DOC-340 (91).

Cullen, D.E., (2019) “PREPRO 2019”, IAEA-NDS-229, website http://redcullen1.net/Homepage.new/PREPRO2019/PREPRO19.HTM

Engel, R., et al. (2021) “Neutron production in extensive air showers”, in Proceedings of the International Conference on Cosmic Rays, Proceedings of Science (ICRC2021), 492.

Ferrari, et al. (1996) “Cascade particles, nuclear evaporation, and residual nuclei in high energy hadron-nucleus interactions.”, Z Phys C - Particles and Fields 70, 413. https://doi.org/10.1007/s002880050119

Ferrari, A., Sala, P.R., Fassò, A. and Ranft, J. (2005) `FLUKA: A multi-particle transport code (Program version 2005)", CERN-2005-010, SLAC-R-773, INFN-TC-05-11.

Ferrari, A., for the FLUKA Collaboration (2022), these proceedings.

Iwamoto, O. et al. (2020), "Status of JENDL", EPJ Web of Conferences, 239, 09002_1-6.

Koning, A.J. et al. (2019), "TENDL: Complete Nuclear Data Library for Innovative Nuclear Science and Technology", Nuclear Data Sheets 155, 1.

MacFarlane, R.E and Kahler A.C. (2010), “Methods for Processing ENDF/B-VII with NJOY” Nuclear Data Sheets 111, 2739-2890, http://t2.lanl.gov/codes/

MacFarlane, R.E. et al. (2016), “The NJOY Nuclear Data Processing System,Version 2016, “ LA-UR-17-20093.

Maneira, J. (2022) “Techniques for TPC Calibration: Application to Liquid Ar-TPCs”. Particles 5, 74–83. https://doi.org/10.3390/particles5010007

Martin, M.J. (2007), “Nuclear Data Sheets for A = 208”, Nuclear Data Sheets 108, 1583.

Ogawa, T. et al. (2014), “Development of a reaction ejectile sampling algorithm to recover kinematic correlations from inclusive cross-section data in Monte-Carlo particle transport simulations” Nuclear Instruments and Methods A763, 575.

Pillon, M. et al. (2017), “High-resolution measurements of the exited states (n,p_n), (n,d_n) C-12 cross sections”, EPJ Web of Conferences 146, 11005.

Plompen, A.J.M. et al. (2020) "The joint evaluated fission and fusion nuclear data library, JEFF-3.3", Eur. Phys. J. A56, 181.

Rubchenya, V.A. et al. (2001), “Neutron and fragment yields in proton-induced fission of 238U at intermediate energies”, Nuclear Instruments and Methods A463, 653. https://doi.org/10.1016/S0168-9002(01)00176-0.

Shibata, K. et al. (2011) "JENDL-4.0: A new library for nuclear science and engineering", J. Nucl. Sci. Technol. 48, 1.

Sedlačková, K. et al. (2016), International Journal of Modern Physics: Conference Series 44, 1660226

Sublet, J.-Ch. et al. (2010), “the European activation file EAF 2010 neutron induced cross-section library” *https://scientific-publications.ukaea.uk/papers/the-european-activation-file-eaf-2010-neutron-induced-cross-section-library/*

2.9. List of abbreviations and acronyms

EAF	European Activation File
ENSDF	Evaluated Nuclear Structure Data File
SS	Self-Shielding
URR	Unresolved Resonances Region

3. Recent updates and shielding benchmark of PHITS

Tatsuhiko OGAWA[1*], Yosuke IWAMOTO[1], Shintaro HASHIMOTO[1], Tatsuhiko SATO[1], Norihiro MATSUDA[1], Satoshi KUNIEDA[1], Yurdunaz CELIK[2], Naoya FURUTACHI [3], Koji NIITA[3], Takuya FURUTA[1], Shinichiro ABE[1], Takeshi KAI[1], Yusuke MATSUYA[1,4], Yuho HIRATA[1], Lan YAO[1], Pi-En TSAI[5], Hunter N. RATLIFF[6], Hiroshi IWASE[7], Yasuhito SAKAKI[7], Nobuhiro SHIGYO[8], Lembit SIHVER[9,10]

[1]Nuclear Science and Engineering Center, Japan Atomic Energy Agency, Tokai, Ibaraki, Japan,
[2] Advanced Nuclear Systems Institute, SCK CEN, Belgian Nuclear Research Institute, Boeretang 200, 2400 Mol, Belgium
[3] Department of Software Development, Research Organization for Information Science and Technology, Tokai, Ibaraki, Japan,
[4] Faculty of Health Sciences, Hokkaido University, Sapporo, Hokkaido, Japan
[5] Zap Energy Inc., Seattle, Washington, US,
[6] Western Norway University of Applied Sciences, Inndalsveien 28, 5063 Bergen, Norway,
[7] High Energy Accelerator Research Organization (KEK), 1-1 Oho Tsukuba, Ibaraki, Japan,
[8] Kyushu University, Department of Applied Quantum Physics and Nuclear Engineering, Fukuoka, Japan,
[9] Nuclear Physics Institute of the CAS, Prague, Czech Republic
[10]Atominstitut, Technische Universitat Wien, Stadionallee 2, 1020 Vienna, Austria
[*] ogawa.tatsuhiko@jaea.go.jp

The general-purpose radiation transport code PHITS has been updated in various perspectives such as development of pre/post-processing software, reaction physics models, and cross section data reading modules.

Meanwhile, a benchmark study was carried out to verify the shielding calculation accuracy of PHITS, which relies on such updates. The benchmark illustrated that use of the evaluated cross section data library JENDL-4.0/HE in place of nuclear reaction models makes neutrons deep penetration simulation more accurate.

3.1. Introduction

Radiation transport calculation is one of the key technologies to certify safe and effective use of ionizing radiation. Owing to recent growth of computer performance, Monte-Carlo radiation transport calculation codes, which are often CPU-expensive, became common tools. One of these codes, PHITS (Particle and Heavy Ion Transport code System) has been upgraded to meet the needs from various domains. One of the improvements is development of software which complements PHITS by performing pre-processing, post-processing, and visualization. Such developments facilitate the use of the code and extend the coverage and illustration of the simulated phenomena.

Another trend is development and improvement of nuclear reaction models. Since the reaction mechanisms of nuclear reactions are dependent on the energy range, particle species, and target nuclei, reactions are simulated by a combination of various nuclear reaction models. To achieve higher accuracy and calculation efficiency, these models are continuously upgraded.

However, event-by-event calculation by nuclear reaction models is not a global solution for low-energy neutron transport, which are usually simulated by using evaluated cross section data libraries. In addition, recent nuclear-related technologies such as accelerator-based neutrons sources [Matsuya 2022], transmission material imaging, and non-

destructive material assay based on radiation interrogation require high precision radiation transport calculation. Therefore, in addition to conventional nuclear data for neutrons with energy lower than 20 MeV, cross section data libraries for protons, deuterons, high energy neutrons, and photo-nuclear reactions draw particular interest.

Development of the models and incorporation of nuclear data should be supported by benchmarking with experimental results to verify their accuracies. Recently, a comprehensive shielding benchmark was conducted by Iwamoto et al. [Iwamoto 2022]. The findings in this study are globally useful for shielding calculations because the beam, geometry, and detection configurations well represent the shielding at typical radiation facilities.

In this paper, the results of the shielding benchmark study are reviewed, and these recent upgrades of PHITS are presented.

3.2. Highlights of latest PHITS features

Since PHITS version 3.17 released in October 2019, PHITS has been updated 4 times with the following new features. Among them, 6 underlined features are explained in detail.

- Long random number sequence based on Xorshift64 algorithm [Marsaglia 2003]
- User-defined stopping power
- Cosmic ray source based on PARMA (PHITS-based Analytical Radiation Model) [Sato 2016]
- Mu-pair production
- DNA (DeoxyriboNucleic Acid) damage estimation function [Matsuya 2020]
- Systematic uncertainty analysis function based on ANOVA (ANalysis Of VAriance) [Hashimoto 2019]
- [Repeated Collisions] to improve the statistics of nuclear reactions
- Organic scintillator response calculation based on SCINFUL-QMD [Satoh 2022]
- Automated cross section energy range selector
- Update of burn-up calculation code DCHAIN- PHITS [Ratliff 2020]
- Interactive 3D geometry viewer PHIG-3D
- Interface to read cross sections for deuterons, alphas and photo-nuclear reactions.
- EXFOR (EXchange FORmat) reader
- RT-PHITS (Radiation Therapy package), GUI (Graphical User Interface) for radiation therapy [Furuta 2022]
- Track-structure code KURBUC (Kyushu University RadioBiology Unit Code) and ITSART (Ion Track Structure calculation model for Arbitrary Radiation and Targets) [Matsuya 2021, Ogawa 2021]

DCHAIN- PHITS is a burn-up calculation code coupled to and bundled with PHITS for simulation of buildup and decay of radioactivity. The former version of its code included in the PHITS package was DCHAIN-SP 2001 [Kai 2001]. It allowed calculation of the activation induced by neutrons below 20 MeV by convolution of activation cross sections and neutron track length energy spectra and activation by other particles using nuclear reaction event generators with accounting for the build-up and disintegration. However, the

libraries of nuclear reactions and decay have substantial been update in the last two decades. The internal data, such as conversion coefficients, were taken from databases with available references, which should have been identified for the sake of reproducibility. Moreover, coupling calculations of PHITS and DCHAIN-SP 2001 only accepted region-wise meshes because the material composition required to calculate the activation cross sections had to be uniform in each region. Despite the fact that PHITS calculation results have statistical uncertainty and that the systematic uncertainties of nuclear data libraries are evaluated, DCHAIN-SP 2001 could not calculate the propagation of these uncertainties.

Therefore, the following new features were implemented to the new version of DCHAIN named DCHAIN-PHITS [Ratliff 2020]; (1) modern activation cross sections libraries, such as JENDL(Japanese Evaluated Nuclear Data Library)/AD-2017 [Shibata 2016], JENDL-4.0 [Shibata 2011], ENDF(Evaluated Nuclear Data Library)/B-VIII.0 [Brown 2018], and JEFF(Joint Evaluated Fission and Fusion file)-3.3 [Plompen 2020], and decay data libraries JENDL/DDF-2015 [Katakura 2016], ENDF/B-VIII.0, and ENSDF [Bhat 1992], (2) induced and spontaneous fission yield libraries supplied by the GEF (The GEneral description of Fission observables) code [Schmit 2016] and the ENDF/B-VIII.0, JENDL/FPY-2011 [Katakura2 2016], and JEFF-3.3 libraries, (3) gamma dose coefficients taken from ICRP (International Commission on Radiological Protection) 74 [ICRP 1996] and 116 [ICRP 2021], (4) compatibility with tetra-hedral geometry meshes (that with cartesian grid meshes had been implemented in another project), and (5) uncertainty propagation attributed to fluxes, nuclide yields, activation cross sections and decay data. The advantage of new decay data libraries is illustrated in one of the DCHAIN application studies [Ogawa 2022] , where it can be seen that there is as a good agreement between the fission fragment decay heat time evolutions calculated using DCHAIN and the new decay data libraries and the data taken from literature.

PHIG-3D is an interactive 3D geometry viewer dedicated to PHITS, which was developed based on Gxsview [Ohnishi 2021]. PHITS has also a 2D geometry viewer called the [gshow] function and 3D geometry plotter called [t-3dshow]. They create files containing the data of colors, coordinates and strings, which are subsequently processed by Angel, one of the PHITS subprograms which converts the numerical outputs of PHITS to EPS (Encapsulated PostSript) files, to generate graphical output. They were powerful geometry plotting tools but owing to this processing scheme, users had to run PHITS to change the coordinates of the viewpoint, plot range, light source, etc. These coordinates were defined as numerical data, which users had to optimise by trial-and-error.

Figure 3.1. Geometry of a PHITS input file plotted by PHIG-3D

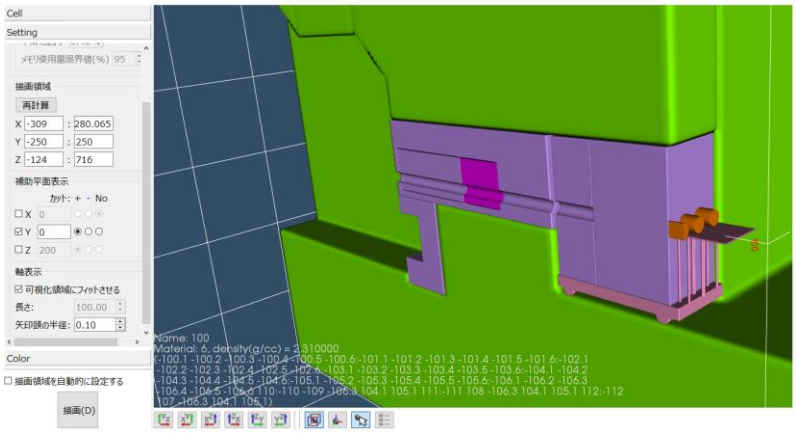

PHIG-3D (Fig. 3.1) is a solution for such laborious geometry plotting. Users can change the viewpoint, and select the regions to be shown/hiden by intuitive mouse/touch pad operations. Users can specify the clipping x,y,z planes, and the plot resolution from the console window. Aside from the above configurations, PHIG-3D is automated. The initial viewpoint and frame width are automatically chosen based on the size of principal cells, for example.

The updated cross section reading modules are compatible with the cross section data for deuteron-induced, alpha-induced, and photo-nuclear reactions. PHITS is capable of using ACE (A Compact ENDF)-formatted cross section data for (1) neutrons below 20 MeV, (2) neutrons above 20 MeV, (3) protons, and (4) electron-gamma cascade. All the other particles are transported based on respective reaction event generators and energy dissipation models. Among such reactions, accurate simulation of deuteron reactions and alpha reactions are challenging owing to their extraordinarily small and large binding energies, respectively. Photo-nuclear reactions have been calculated by reaction models [Noda 2015] based on different theories such as giant-dipole resonance, quasi-deuteron decay and single nucleon resonance, depending on the photon energy. Their calculated results agreed in general with measurement data [Iwamoto 2017] but they had to tune some parameters to cover some specific conditions.

Figure 3.2. Double-differential neutron production cross section of ^{9}Be(d,xn) reactions. The experimental data is from [Saltmarsh 1977].

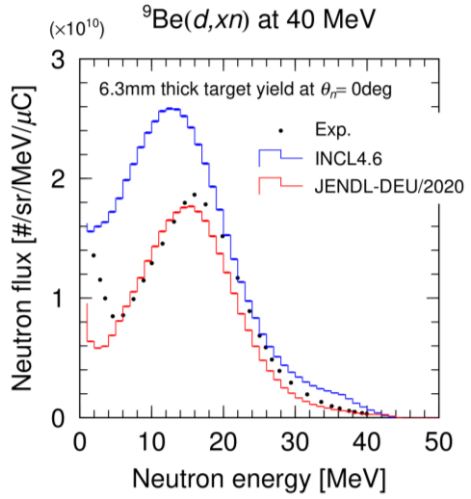

The updated cross section reading module is a solution for accurate simulation of the above-mentioned reactions. It can read deuteron, alpha, photo-nuclear reaction cross sections written in the ACE-format. In addition to the reading module, deuteron-induced reaction cross section data library JENDL-DEU/2020 [Nakayama 2021] is bundled with PHITS distribution package . The reactions of ^{Nat}Li(d,n) and ^{9}Be(d,n) by deuterons of some 10 MeV are those typically used as quasi-monoenergetic neutron sources. INCL [Boudard 2013] model used for these reactions by default in PHITS is not accurate enough to reproduce the shape of outgoing neutron spectrum. In contrast, the simulation using JENDL-DEU/2020 can reproduce the shape of neutron spectra well as illustrated in Figure 3.2. JENDL-5 [Iwamoto 2020] of ACE-format to be released in 2023 will be also bundled to PHITS and read by this interface.

The EXFOR reader is one of the software bundled to PHITS complementary to the cross section reading module update. EXFOR is an open storage of experimental data, where one

can take nuclear reaction measurement data written in a common EXFOR format[1]. EXFOR reader can convert cross section data which are characterised by incident particle species, incident energy, and outgoing particle (as single- or double-differential distribution) to create a [frag data] section to be read by PHITS as a part of input files. The particle production in the condition specified by [frag data] section follows the given data in place of the reaction models or the default cross section data.

RT(Radiation Therapy package)-PHITS [Furuta 2022] is an interface to convert data on radiation transport and that of radiology in a bilateral manner. Radiological data are usually stored in a format called DICOM (Digital Imaging and COmmunications in Medicin), while the result of radiation transport is usually in ASCII (American Standard Code for Information Interchange) text arrays. The data conversion between radiation transport simulation and radiology is crucial for simulation-based dosimetry, which is vital for optimization of treatment and diagnosis and radiation-based imaging.

RT-PHITS offers a function to convert the data from one format to the other. Feeding a CT(Computed Tomography)-image file in DICOM format to RT-PHITS as an input, users receive PHITS input files that replicates the CT scanning in PHITS. The source information can be also created from RT-plan data for carbon ion therapy or PET(Positron Emission Tomography)/SPECT(Single Photon Emission Tomography) images for nuclear medicine [Sato 2021]. When the dose distribution calculated by PHITS is the input, RT-PHITS returns a RT-Dose file in DICOM format, which can be further processed by third-party DICOM processors to analyze or visualise the data. RT-PHITS is associated with a Python-based GUI which allows users to tune auxiliary parameters used in conversion.

Historically, the energy dissipation of charged particles in matter was calculated by a method called condensed-history method and continuous slowing-down approximation, which assume that charged particles deposit their energy in matter with predefined steps of several 10 (g/cm^2) at the expense of spatial resolution. Track structure is a calculation algorithm to calculate reactions on an event-by-event basis to analyze energy deposition at the atomic scale.

A track-structure code ETS(Electron Track Structure)-mode [Matsuya 2020] was implemented into PHITS to perform molecular-scale electrons transport calculation in liquid water. It opened a door towards full Monte-Carlo calculations of energy deposition in cells taking into account every single event of scattered electrons. ETS-mode is a promising model to understand the impact of radiation exposure, but it is dedicated to electrons and positrons. Therefore, the track-structure calculation models for protons and ions, PHITS-KURBUC [Matsuya 2021] and ITSART [Ogawa 2021], were implemented into PHITS. PHITS-KURBUC is a model specialised in transport of protons and carbon ions in liquid water with secondary electron production . The cross sections of all the relevant interactions such as ionization, electronic excitation, molecular excitation, elastic scattering, electron capture and electron stripping as functions of energy and charge state are incorporated to account for these reactions explicitly. ITSART is another track-structure model which is complementary to PHITS-KURBUC. ITSART uses parameterised cross sections of ionization, excitation and elastic interaction to allow users to calculate ionization, excitation and elastic scattering of arbitrary ions in arbitrary matter. ITSART does not have the cross sections of some channels, which could lead to underestimation of stopping power; therefore, ITSART is supplemented by stopping power calculated by ATIMA (ATomic Interaction with Matter, https://web-docs.gsi.de/~weick/atima/) to reproduce the stopping power. Production of secondary electrons, which are further transported by ETS-mode down to 10 eV, and atomic-scale energy deposition calculated

[1] https://www-nds.iaea.org/exfor/

by these track-structure models are key ingredients for studying radiation biology, water radiolysis, radiation-induced material damage, soft error analysis of nano-scale devices, etc.

Owing to the features explained above, PHITS has now a wider range of applicability, higher reliability, and more intuitive usability. Further improvements on the reaction models, transport algorithms, and bundled software are in progress.

3.3. PHITS shielding benchmark

The updates on cross section data discussed in Section 1.2 are key players of shielding calculations because the uncertainty of deep shielding calculation comes from their uncertainties accumulated over the thickness of the shielding. Before being released, the reaction models and cross section data are verified against experimental data, but the inaccuracies which looked trivial could build up and dominate the integral quantities of thick shielding.

In view of this, Iwamoto *et al*. benchmarked PHITS version 2.88 [Iwamoto 2022] against the data taken from the database SINBAD (Shielding Integral Benchmark Archive and Database, https://www.oecd-nea.org/science/wprs/shielding/sinbad/) to evaluate the accuracy of shielding calculation by PHITS. Since the incorporation of EGS5 [Hirayama 2005], the electron-gamma shower algorithm of PHITS has essentially not changed; therefore, Iwamoto focused on hadronic shielding studies. Even when restricted to hadronic shielding, many models complement each other to cover the variety of particle species and a wide energy range. To involve more models and data relevant to shielding, representative entries were selected from SINBAD. Among them, four examples are reviewed in this paper.

(1) Source : 43MeV p + ^{7}Li. Shield : Iron

In this experiment, the quasi-monoenergetic source neutrons were produced by hitting a ^{7}Li target with a 43 MeV proton beam. The neutrons transmitted through the shielding behind the target were measured with NE213 neutron spectrometers [Nakao 1996A 1996B]. Fig. 3.3 shows the comparison of neutron spectra taken from the literature and those calculated by PHITS.

Figure 3.3. Geometry and result of 43 MeV Li(p,xn) source shielding benchmark

Source: < Iwamoto, Y., Sato, T., Hashimoto, S., Ogawa, T., Furuta, T., Abe, S. I., ... & Niita, K. (2017). Benchmark study of the recent version of the PHITS code. Journal of Nuclear Science and Technology, 54(5), 617-635.>

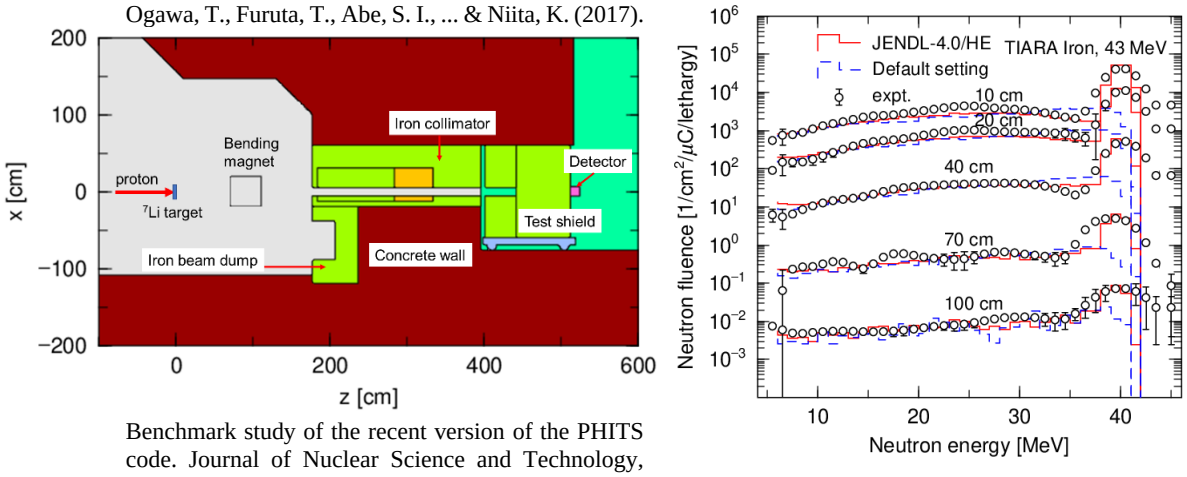

The calculated tails of spectra below 35 MeV agree well with the measurement regardless of the depths, indicating good accuracy of neutron down-scattering. By the default settings, the neutron inelastic reactions in this energy range are simulated by cross sections calculated by the formula of Perlstein-Niita [Niita 2001] and kinematics calculated by INCL (Liège Intranuclear Cascade model) [Boudard 2013]. INCL cannot reproduce the high energy peak at 40 MeV which comes from the (p,xn) reactions in the Li target, because INCL is an event generator which calculates the kinematics of participating particles without any premises on the reaction channels. But this inaccuracy is not crucial for transmission in thick shielding. The high energy peak missing in the spectrum calculated by INCL suggests that it is advisable to use the evaluated nuclear data to simulate quasi-monoenergetic neutrons produced by a proton beam directed to Li and Be targets. The disagreement of the high energy peak is seen even at the depth of 100 cm.

(2) Source : 52MeV p + C. Shield : Water

The advantages of the evaluated nuclear data are symbolically illustrated in the above example (1). A similar calculation with a carbon target [Shin 1979] [Uwamino 1982] shows that the use of evaluated nuclear data is not always the perfect solution.

Fig.3.4 shows the source neutron spectrum of a carbon target irradiated by 52 MeV protons and the neutron spectra measured behind concrete shielding of 60 cm and 101 cm. The source spectra shows that JENDL-4.0/HE [Kunieda 2016] overestimates the high energy edge above 30 MeV whereas INCL+GEM (Generalized Evaporation Model) [Furihata 2000] agrees with the measurement data in the most forward angle. The spectra of neutrons transmitted through shielding inherit the trend in the forward angle. The overestimation of the high energy peak calculated by JENDL-4.0/HE is seen even beyond 101 cm of shielding. The calculation by the default setting is more accurate, but its problem is the connection gap between the reaction model and the evaluated cross section data. The discrete gap at 20 MeV owes to the switching from the combination of INCL and GEM to the JENDL-4.0 cross section data library [Shibata 2011]. The gap was not visible in the case (1), but it is pronounced in this case indicating that the size of the switching gap is situationally dependent. To solve the problems on the source spectrum accuracy and the switching gap, the source neutrons whose spectrum was taken from the measurement data were transported by the combination of JENDL-4.0 and JENDL-4.0/HE. Since these nuclear data libraries are seamlessly joined, this coupled calculation accurately reproduced the neutron spectra shown as the red histogram in the right of Fig.3.4.

Figure 3.4. Result of 52 MeV C(p,xn) source shielding benchmark.

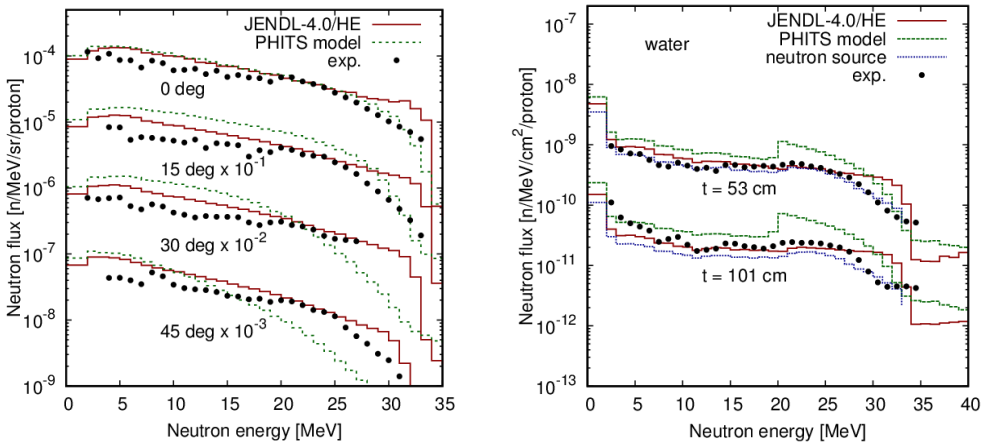

Source: < Iwamoto, Y., Sato, T., Hashimoto, S.,
Ogawa, T., Furuta, T., Abe, S. I., ... & Niita, K. (2017). Benchmark study of the recent version of the PHITS code. Journal of Nuclear Science and Technology, 54(5), 617-635.>

(3) Source: 500MeV p + W. Shield: Concrete

In the energy range below 100 MeV, nuclear reactions are affected by the nuclear structure of target materials and shielding materials. Such effects are blurred at higher energies. Fig.3.5 shows the reaction rates of activation detectors measured in a concrete shield exposed to the neutrons produced by bombarding a tungsten target with 500 MeV protons [Nakao 2004] [Oishi 2005]. In this case, the difference between the calculation by JENDL-4.0/HE and that by default settings is scarcely seen, indicating that the used models are equally accurate in this energy regime. Moreover, JENDL-4.0/HE covers only up to 200 MeV, which means that the source neutrons above 200 MeV are calculated by the default nuclear reaction models.

The reaction rates of bismuth detectors, which are sensitive to the neutrons above 20 MeV, are in good agreement with the measurement data. In contrast, ^{115}In(n,n') sensitive to the neutrons from 1 to 10 MeV and well-known thermal neutron detectors ^{197}Au(n,g) are overestimated throughout the shielding. This indicates that the source low energy component, which is responsible for the reactions at the surface, and the down-scattered neutrons, the main contributors in depth, are both overestimated.

Figure 3.5. Geometry and result of 500 MeV W(p,xn) source shielding benchmark.

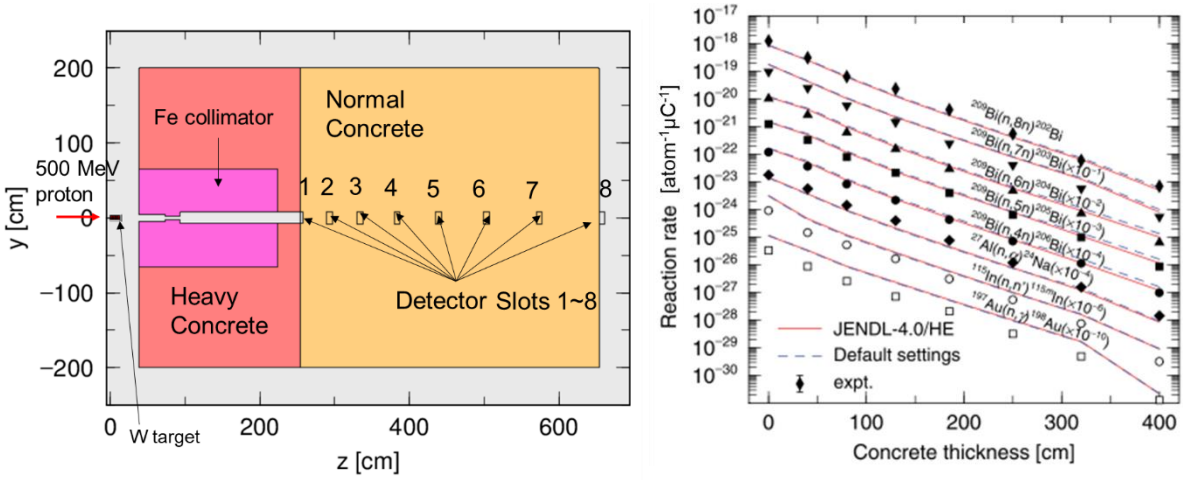

Source: < Iwamoto, Y., Sato, T., Hashimoto, S., Ogawa, T., Furuta, T., Abe, S. I., ... & Niita, K. (2017). Benchmark study of the recent version of the PHITS code. Journal of Nuclear Science and Technology, 54(5), 617-635.>

(4) Source : 800MeV p + Ta. Shield : Composite

The last example [Nunomiya 2001] [Nunomiya 2002] is featured by the geometrical configuration shown in the left of Fig. 3.6. The central axis of the shielding is perpendicular to the beam axis; therefore, the transverse component of the source neutrons is concerned unlike the forward shielding case discussed above.

Fig. 3.6 shows the reaction rates of ^{12}C(n,2n) measured in the additional shielding 500 cm from the target. Unlike the example (3), the calculation by JENDL4.0/HE and that by the default setup are substantially different. This trend is consistent with that in the example 3 in which the ^{115}In(n,n') reaction rate was overestimated. However, such an overestimation trend is not seen in the calculation by JENDL4.0/HE, which agrees well with the measurement data for iron. This example indicates that JENDL4.0/HE is more accurate than the default nuclear reaction models, even if the primary particle energy is higher than its upper limit of 200 MeV. This is probably because the shielding is in the transverse

direction where the source neutrons spectrum is not as hard as that in the forward direction as in the example (3). From the viewpoint of neutron energy range, this example is closer to the example (2).

Figure 3.6. Geometry and result of 800 MeV p(Ta,xn) source shielding benchmark.

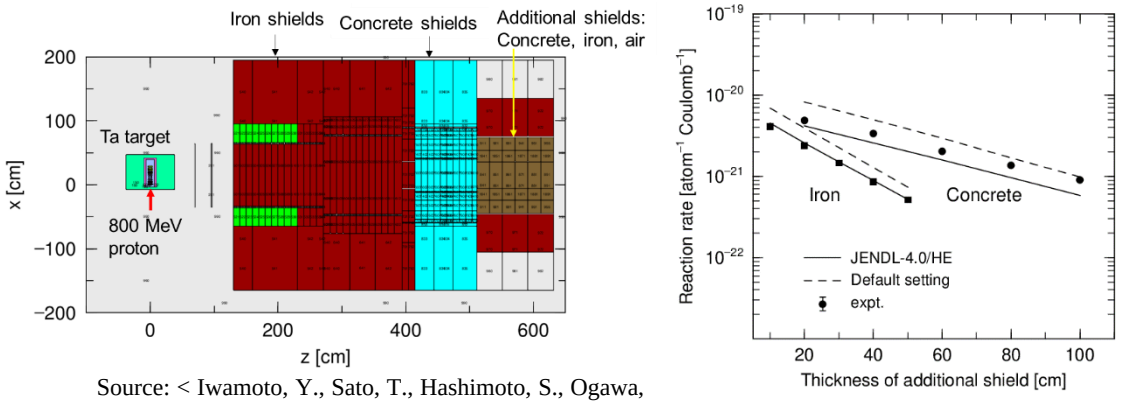

Source: < Iwamoto, Y., Sato, T., Hashimoto, S., Ogawa, T., Furuta, T., Abe, S. I., ... & Niita, K. (2017). Benchmark study of the recent version of the PHITS code. Journal of Nuclear Science and Technology, 54(5), 617-635.>

3.4. Summary and Conclusions

In this paper, a general overview of the latest PHITS developments was presented. In the first half of this paper, some highlights of recent new functions and improved features were introduced. One of the important recent developments is the enhancement of supplementary software. Advanced functions such as interactive geometry viewer, interface for medical physics calculation, and burn up calculations are offered as external software. This provides robust pre/post processing without increasing the executable file size or the memory load. The improvement of these supplementary programs enhances the potential of PHITS as an integrated package.

The core of PHITS, radiation transport and reaction algorithms, are updated continuously to handle physical mechanisms and quantities which PHITS could not previously take into account. The nuclear reaction models are powerful to cover wide energy ranges, various reaction channels or particle species while the evaluated cross section data libraries were mainly used for neutrons below 20 MeV, photons, electrons, and positrons. Now high-energy data libraries for other particles, protons, neutrons, alphas, and photo-nuclear reactions are also being released. Accordingly, the cross section reader module of PHITS was upgraded to read all of these cross sections. High precision and high speed are the most remarkable advantages of the transport calculation based on the evaluated cross section data libraries. By using the evaluated cross section data, PHITS does not have to perform time-consuming nuclear reaction model calculations in the monolithic geometries of shielding calculation.

Under these circumstances, a shielding benchmark of PHITS was performed to evaluate the current state of accuracy. The benchmark studies showed that PHITS can reproduce the shielding benchmark data within a factor of 2 in general. The additional lessons learned are: (1) It is advisable to use the evaluated cross section data libraries to calculate the source neutron spectra which are strongly affected by nuclear structures (e.g. p+Li). (2) Use of evaluated cross section data libraries is encouraged in general for accurate transport in shielding materials. (3) Occasionally, neither nuclear reaction models nor evaluated cross section data libraries are accurate to simulate the source term. In that case, they should be replaced with measurement data.

PHITS and its supplementary software are going to be further upgraded by incorporating new models, revising algorithms, and introducing new reliable data to keep its competitiveness in the field of radiation transport. In the meantime, PHITS verification studies go on to evaluate its reliability by performing shielding benchmarks and comparison with differential data.

3.5. List of references

Bhat, M. R. "Evaluated nuclear structure data file (ENSDF)." Nuclear data for science and technology. Springer, Berlin, Heidelberg, 1992.

Boudard, A., Cugnon, J., David, J. C., Leray, S., & Mancusi, D. (2013). New potentialities of the Liège intranuclear cascade model for reactions induced by nucleons and light charged particles. Physical Review C, 87(1), 014606.

Brown, David A., et al. "ENDF/B-VIII. 0: The 8th major release of the nuclear reaction data library with CIELO-project cross sections, new standards and thermal scattering data." Nuclear Data Sheets 148 (2018): 1-142.

Furihata, S. (2000) Statistical analysis of light fragment production from medium energy proton-induced reactions. Nucl Instrum Meth B. 171, 251–258

Furuta, T., & Sato, T. (2021). Medical application of particle and heavy ion transport code system PHITS. Radiological Physics and Technology, 14(3), 215-225.

Furuta, T., Koba, Y., Hashimoto, S., Chang, W., Yonai, S., Matsumoto, S., ... & Sato, T. (2022). Development of the DICOM-based Monte Carlo dose reconstruction system for a retrospective study on the secondary cancer risk in carbon ion radiotherapy. Physics in Medicine & Biology, 67(14), 145002.

Hashimoto, S., & Sato, T. (2019). Estimation method of systematic uncertainties in Monte Carlo particle transport simulation based on analysis of variance. Journal of Nuclear Science and Technology, 56(4), 345-354.

Hirayama, H., Namito, Y., Bielajew, A.F., Wilderman, S.J. Nelson, W.R. (2005) The EGS5 code system, SLAC-R-730 and KEK Report 2005-8.

Iwamoto, Y., Sato, T., Hashimoto, S., Ogawa, T., Furuta, T., Abe, S. I., ... & Niita, K. Benchmark study of the recent version of the PHITS code. Journal of Nuclear Science and Technology, 54(5), (2017). 617-635.

ICRP, "Conversion Coefficients for use in Radiological Protection against External Radiation". ICRP Publication 74. Ann. ICRP (1996) 26

ICRP, "Conversion Coefficients for Radiological Protection Quantities for External Radiation Exposures". ICRP Publication 116, Ann. ICRP 40 (2010) 2-5

Iwamoto, O, Iwamoto, N., Shibata, K., Ichihara, A., Kunieda, S., Minato, F. and Nakayama, S. (2020) Status of JENDL, EPJ Web of Conferences, 239, 09002_1-6

Iwamoto, Y., Hashimoto, S., Sato, T., Matsuda, N., Kunieda, S., Çelik, Y., ... & Niita, K. (2022). Benchmark study of particle and heavy-ion transport code system using shielding integral benchmark archive and database for accelerator-shielding experiments. Journal of Nuclear Science and Technology, 59(5), 665-675.

Kai, T., Maekawa, F., Kasugai, Y., Takada, H., Ikeda, Y., & Kosako, K. (2001). DCHAIN-SP 2001: High energy particle induced radioactivity calculation code (No. JAERI-DATA/CODE--2001-016). Japan Atomic Energy Research Inst..

Katakura, Jun-ichi, and Futoshi Minato. JENDL decay data file 2015. Nihon Genshiryoku Kenkyū Kaihatsu Kikō, 2016.

Katakura, Jun-ichi, Futoshi Minato, and Kazuya Ohgama. "Revision of the JENDL FP fission yield data." EPJ web of conferences. Vol. 111. EDP Sciences, 2016.

Kunieda, S., Iwamoto, O., Iwamoto, N., Minato, F., Okamoto, T., Sato, T., ... & Murata, T. (2016). Overview of JENDL-4.0/HE and benchmark calculations (No. JAEA-CONF--2016-004).

Marsaglia, G. (2003) Xorshift RNGs. Journal of Statistical Software. 8(14), 1-6.

Matsuya, Y., Kai, T., Yoshii, Y., Yachi, Y., Naijo, S., Date, H., & Sato, T. Modeling of yield estimation for DNA strand breaks based on Monte Carlo simulations of electron track structure in liquid water. Journal of Applied Physics, 126(12), (2019) 124701.

Matsuya, Y., Nakano, T., Kai, T., Shikazono, N., Akamatsu, K., Yoshii, Y., & Sato, T. (2020). A simplified cluster analysis of electron track structure for estimating complex DNA damage yields. International Journal of Molecular Sciences, 21(5), 1701.

Matsuya, Y., Kai, T., Sato, T., Liamsuwan, T., Sasaki, K., & Nikjoo, H. (2021). Verification of KURBUC-based ion track structure mode for proton and carbon ions in the PHITS code. Physics in Medicine & Biology, 66(6), 06NT02.

Matsuya, Y., Kai, T., Sato, T., Liamsuwan, T., Sasaki, K., & Nikjoo, H. Verification of KURBUC-based ion track structure mode for proton and carbon ions in the PHITS code. Physics in Medicine & Biology, 66(6), (2021).06NT02.

Matsuya, Yusuke, et al. "Features of accelerator-based neutron source for boron neutron capture therapy calculated by particle and heavy ion transport code system (PHITS)." AIP Advances 12.2 (2022): 025013.

Nakashima, H., Nakao, N., Tanaka, S. I., Nakamura, T., Shin, K., Tanaka, S., ... & Baba, M. (1996). Transmission Through Shields of Quasi-Monoenergetic Neutrons Generated by 43-and 68-MeV Protons—II: Iron Shielding Experiment and Analysis for Investigating Calculational Method and Cross-Section Data. Nuclear science and engineering, 124(2), 243-257.

Nakao, N., Nakashima, H., Nakamura, T., Tanaka, S. I., Tanaka, S., Shin, K., ... & Nakane, Y. (1996). Transmission Through Shields of Quasi-Monoenergetic Neutrons Generated by 43-and 68-MeV Protons—I: Concrete Shielding Experiment and Calculation for Practical Application. Nuclear science and engineering, 124(2), 228-242.

Nakao, N., Yashima, H., Kawai, M., Oishi, K., Nakashima, H., Sasaki, S. I., ... & Maruhashi, A. (2004). KENS Shielding Experiment (1)-Measurement of Neutron Attenuation through 4m Concrete Shield Using a High Energy Neutron Irradiation Room. Journal of Nuclear Science and Technology, 41(sup4), 22-25.

Nakayama, S., Iwamoto, O., Watanabe, Y., & Ogata, K. (2021). JENDL/DEU-2020: Deuteron nuclear data library for design studies of accelerator-based neutron sources. Journal of Nuclear Science and Technology, 58(7), 805-821.

Niita, Koji, et al. "High-energy particle transport code NMTC/JAM." Nuclear Instruments and Methods in Physics Research Section B: Beam Interactions with Materials and Atoms 184.3 (2001): 406-420.

Noda, S., Hashimoto, S., Sato, T., Fukahori, T., Chiba, S., & Niita, K. (2015). Improvement of photonuclear reaction model below 140 MeV in the PHITS code. Journal of Nuclear Science and Technology, 52(1), 57-62.

Nonomiya, T., Nakao, N., & Wright, P. (2002). Experimental data of deep-penetration neutrons through a concrete and iron shield at the ISIS spallation neutron source facility using an 800-MeV proton beam (No. KEK--2001-24). High Energy Accelerator Research Organization.

Nunomiya, T., Nakao, N., Wright, P., Nakamura, T., Kim, E., Kurosawa, T., ... & Perry, D. R. (2001). Measurement of deep penetration of neutrons produced by 800-MeV proton beam through concrete and iron at ISIS. Nuclear Instruments and Methods in Physics Research Section B: Beam Interactions with Materials and Atoms, 179(1), 89-102.

Ogawa, T., Hirata, Y., Matsuya, Y., & Kai, T. (2021). Development and validation of proton track-structure model applicable to arbitrary materials. Scientific Reports, 11(1), 1-10.

Ogawa, T., Litaize, O., Mancusi, D., Chebboubi, A., & Serot, O. (2022). Post fission time evolution calculation by FIFRELIN coupled with PHITS and DCHAIN. The European Physical Journal A, 58(8), 1-9.

Ohnishi, S. (2021) Gxsview: Geometry and cross section viewer for calculation radiation transport, SoftwareX, 14, 100681

Oishi, K., Nakao, N., Kosako, K., Yamakawa, H., Nakashima, H., Kawai, M., ... & Nakamura, T. (2005). Measurement and analysis of induced activities in concrete irradiated using high-energy neutrons at KENS neutron spallation source facility. Radiation protection dosimetry, 115(1-4), 623-629.

Ratliff, H. N., Matsuda, N., Abe, S. I., Miura, T., Furuta, T., Iwamoto, Y., & Sato, T. (2020). Modernization of the DCHAIN-PHITS activation code with new features and updated data libraries. Nuclear Instruments and Methods in Physics Research Section B: Beam Interactions with Materials and Atoms, 484, 29-41.

Plompen, Arjan JM, et al. "The joint evaluated fission and fusion nuclear data library, JEFF-3.3." The European Physical Journal A 56.7 (2020): 1-108.

Saltmarsh, M. J., et al. "Characteristics of an intense neutron source based on the d+ Be reaction." Nuclear Instruments and Methods 145.1 (1977): 81-90.

Satoh, D., & Sato, T. (2022). Improvements in the particle and heavy-ion transport code system (PHITS) for simulating neutron-response functions and detection efficiencies of a liquid organic scintillator. Journal of Nuclear Science and Technology, 1-14.

Sato T (2016) Analytical Model for Estimating the Zenith Angle Dependence of Terrestrial Cosmic Ray Fluxes. PLOS ONE 11(8): e0160390.

Sato, T., Iwamoto, Y., Hashimoto, S., Ogawa, T., Furuta, T., Abe, S. I., ... & Niita, K. Features of particle and heavy ion transport code system (PHITS) version 3.02. Journal of Nuclear Science and Technology, 55(6), (2018) 684-690.

Sato, T., Furuta, T., Liu, Y., Naka, S., Nagamori, S., Kanai, Y., Watabe, T. (2021) Individual dosimetry system for targeted alpha therapy based on PHITS coupled with microdosimetric kinetic model EJNMMI Phys. 8, 1–16

Schmidt, K-H., et al. "General description of fission observables: GEF model code." Nuclear Data Sheets 131 (2016): 107-221.

Shibata, K., Iwamoto, O., Nakagawa, T., ... & Katakura, J. (2011) JENDL-4.0: a new library for nuclear science and engineering. J Nucl Sci Technol. 48, 1–30.

Shibata, Keiichi, et al. “Activation Cross-section File for Decommissioning of LWRs” JAEA-Conf 2016-004, (2016) 47-52

Shibata, Keiichi, et al. "JENDL-4.0: a new library for nuclear science and engineering." Journal of Nuclear Science and Technology 48.1 (2011): 1-30.

Shin, K., Uwamino, Y., Yoshida, M., Hyodo, T., & Nakamura, T. (1979). Penetration of secondary neutrons and photons from a graphite assembly exposed to 52-MeV protons. Nuclear Science and Engineering, 71(3), 294-300.

Uwamino, Y., Nakamura, T., & Shin, K. (1982). Penetration through shielding materials of secondary neutrons and photons generated by 52-MeV protons. Nuclear Science and Engineering, 80(3), 360-369.

4. Moira: A bridge between Monte Carlo worlds

André Donadon Servelle[1,2*], Vasilis Vlachoudis[1], Gabrielle Hugo[1], Francisco Ogallar Ruiz[1], Chris Theis[1]

[1] European Organization for Nuclear Research (CERN), Geneva, Switzerland
[2] École Polytechnique Fédérale de Lausanne (EPFL), Lausanne, Switzerland
[*]andre.donadon.servelle@cern.ch

In this paper, the development of a Geant4 application enabling simulations with FLUKA input files is presented. The creation of this novel tool, temporarily named Moira, arises from two main motivations: to allow the execution of FLUKA and Geant4 simulations using the same setup with minimal user intervention as well as to set up the scaffolding for the long-term evolution of the FLUKA code, aiming to exploit natural synergies between both Monte Carlo communities.

Consistently with the FLUKA user experience, Moira currently supports combinatorial geometries, scoring, biasing techniques, complex magnetic fields, transport and production cutoffs as a function of the particle's kinetic energy, among other features. It is also fully integrated in the Flair graphical interface.

The level of maturity achieved by Moira so far is detailed, and comparisons of simulation results concerning various real cases are presented. These include studies concerning complex radiation environments, such as the CERN CHARM facility and the LHC.

4.1. Introduction

The Monte Carlo (MC) method is an efficient approach to solving the radiation transport problem, relying on a numerical simulation of an ensemble of particle trajectories emanating from a radiation source and undergoing prescribed interaction mechanisms. The description of these interaction mechanisms differs among MC codes, as is the case between FLUKA (Cerutti et al., 2022; Basttioni et al., 2015; FLUKA.CERN website, 2023) and Geant4 (G4) (Allison et al., 2016; Allison et al., 2006; Agostinelli et al., 2003).

In the next sections, a novel development temporarily named *Moira* is presented. This tool allows running FLUKA input files using the G4 toolkit. It greatly facilitates the use of the latter code in areas where FLUKA has had a predominance, e.g. FLUKA is extensively applied in machine protection studies at the European Organization for Nuclear Research (CERN) involving complex geometries like sections of the Large Hadron Collider (LHC). Making use of Moira, these calculations are now possible to be performed in a systematised way with G4.

Beam loss monitor (BLM) benchmarks, which are common calculations for accelerator machine protection studies, were carried out with Moira for two cases: the CERN CHARM facility and the momentum cleaning region of the LHC (IR3). The Moira simulation results were compared with the FLUKA simulations, and the experimental data. The BLM benchmarks obtained for IR3 are the first achieved for particles transported in complex geometries at TeV energies using the G4 toolkit.

4.2. FLUKA and Geant4

FLUKA and G4 are two frequently used MC codes for particle transport in matter. Both evolved during the last decades to be general-purpose codes, allowing to track photons,

leptons, hadrons, and ions in a wide energy range. Because of their independent histories and user communities, the two programs feature many differences.

4.2.1. General philosophy

Even though FLUKA and G4 were developed for a common purpose, their code structure, which influences the usage, is substantially different.

FLUKA is an integrated application, where many features are already included in the code with a simple access via text commands, providing a relatively easy experience for the user.

Instead, the toolkit structure of G4 allows a higher flexibility to create a simulation application customising any feature desired by the user, from the scoring options to the physics models. Nevertheless, the more flexible approach of G4 comes with the drawback of an important user responsibility in terms of usage.

For instance, while FLUKA activates by default all the relevant physics models, allowing just to turn on or off some processes, in G4 the user has the responsibility of defining all the relevant particles and physics processes that will take part in the simulation. Although there are packages predefined to facilitate the use of the toolkit (denominated *physics lists*), G4 still relies on the user's knowledge to discriminate the "correct" physics models for each situation.

4.2.2. Input file (launch a simulation)

To launch a simulation in FLUKA the user has to provide an ASCII file to the FLUKA executable. The ASCII file includes the information of the geometry, beam parameters, and all the extra features needed for the case, like magnetic fields, biasing techniques, etc. In case the integrated features are not sufficient for the user needs, the *user routines* permit a degree of flexibility to extend these functionalities.

In G4, the user has the following options:

1. Start from scratch and generate the C++ application using the G4 toolkit.
2. Use a predefined application, as the examples provided by the G4 repository, and use it as a baseline to start to construct the rest of the application.
3. Use a predefined application only making use of the User Interface (UI) commands to modify some characteristics of the simulations, e.g. the beam parameters using the general particle source commands. The users can also define their own UI command to extend the functionalities of the simulation.

Finally, to define the geometry there are two persistency options in G4. One is the *Textgeom*: G4 geometry from text file option, where the user can "import the geometry setups based on a plain text description, according to a well defined syntax for identifying the different geometrical entities (solids, volumes, materials and volumes attributes)" (TextGeom, 2023).

Figure 4.1. FLUKA combinatorial geometry description

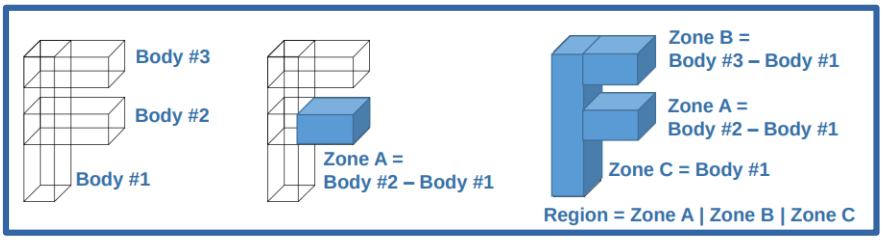

Definition of a volume with the shape of an F. This description is based on the definition of the regions in the simulation geometry through boolean operations of basic second order objects and/or infinite planes and cylinders.

The second option is the *Geometry Description Markup Language* (GDML) description. It is an "application-independent geometry description format based on XML" (Chytracek et al., 2006).

Although the previous description simplifies a bit the picture, it exhibits the main manners to run a simulation with each code, and the difference in terms of user responsibility in each case.

4.2.3. Geometry description

In FLUKA, the geometry description denominated *Combinatorial Geometry (CG) (FLUKA.CERN beginner training slides, 2022),* relies on applying the boolean operations of intersection and union to basic shapes (e.g. spheres, cylinders, etc) denominated *BODIES* to generate more complex shapes (called *ZONES* and *REGIONS*). Fig. 4.1 illustrates this concept creating the F of FLUKA for the simulation geometry.

G4 uses the concept of "Hierarchical Geometry" (Geant4 training, 20??). Here, 3D finite objects (e.g. boxes, spheres, cones, twisted solids, etc) named *solids* are defined as the basic blocks to generate the geometry. Making use of the *solids,* the user defines the *logical volumes,* where the physical properties like materials and fields are selected. Finally, the *logical volumes* are used to define the *physical volumes,* placing the former in a hierarchical description (*with respect to* the local coordinate system of another volume) in the simulation geometry (Fig. 4.2).

Figure 4.2. G4 Hierarchical geometry description

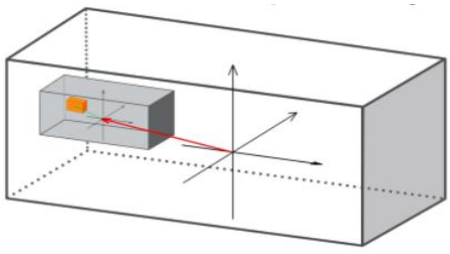

Position and rotation of 3D finite macro objects are defined with respect to the local coordinate system of another volume.

Each geometry description requires a dedicated tracking navigator of the particles in the simulation, making the navigator of each MC code totally incompatible with the other one.

4.2.4. Flair and G4 GUIs

The last point to discuss in this section is the existing Graphical User Interfaces (GUIs) for FLUKA and G4. The latter has many GUIs in the market, but most of them are for relatively

simple simulations (e.g. wisp) (wisp website, 2023), others oriented to particular fields (e.g. GAMOS for medical applications) (Arce et al., 2014), or dedicated to geometry visualisation (Qt UI with OpenGL Graphic viewer, DAWN, HepRep and more) (Ribon, 2014).

On the other side there is Flair (Vlachoudis, 2009), the powerful graphical interface for FLUKA. Flair is a complete integrated working environment for FLUKA. It allows an easy editing of the input files and provides a powerful geometry editor to modify and visualise the simulation geometry. In addition, the user can manage the runs for the simulations and finally, do the post-processing and plotting of results. All these features greatly facilitate the usage of FLUKA.

4.3. Moira, a novel tool for Monte Carlo simulations

Exposing the main differences between FLUKA and G4, this novel tool can be defined:

"Moira is a G4 application that provides a FLUKA experience using the G4 toolkit"

To be a G4-based application implies that Moira profits from existing G4 modules, but also shares the characteristics of FLUKA. Moira is an integrated tool, with a CG description, integrated within Flair. To launch a simulation the user has to provide an ASCII file which is equivalent to the FLUKA input file.

4.3.1. Moira: Motivation

Considering that MC codes are defined, as it is between FLUKA and G4, with different physics models, transport algorithms and cross-section data, it is important to have more than one MC code in order to obtain more robust results. Moira comes into play to remove the difficulties of comparing results between these two codes, making Moira a very powerful inter-comparison tool.

4.3.2. Moira: Status

Input

Currently, running Moira requires two input files:

- A geometry description file with a format based on the aforementioned *Textgeom*.
- A typical macro file, composed of all the UI commands needed for the simulation. Moira allows the use of the default G4 commands, as well as new commands created to mimic the FLUKA features.

Geometry

Moira uses a hybrid geometry where one can combine a standard G4 geometry and the FLUKA one, working at the same time. This is achieved by extending the default G4 geometry, with the introduction of a new *FLUKA Solid*, which encapsulates the full FLUKA geometry as children, using a custom-built external navigator. The *FLUKA regions* appear as standard G4 *physical volumes*. The external navigator is based on the *geoviewer* library of Flair which is able to navigate in a FLUKA described CG, using all the FLUKA features including *LATTICEs*. Special emphasis was paid to minimise the performance penalty and deal with possible numerical precision issues that might arise when complex geometries are used.

The G4 Textgeom persistency format was enhanced in order to allow the description of a FLUKA equivalent combinatorial geometry defined with *BODY*: cutting surfaces, *CELL*:

equivalent to *FLUKA regions* and G4 volumes and *LATTICE*: replication capabilities of FLUKA. Currently, the *FLUKA Solids* can only be described with the use of Textgeom. However, in addition to Textgeom the user can make use of GDML to describe the G4 geometry.

Scoring

A fully custom scoring implementation was included in Moira. It allows continuity with most of the scoring capabilities available in FLUKA.

Among the currently available quantities, the user can score: energy deposition, non-ionizing energy deposition, electromagnetic (EM) energy, particle track lengths, particle count, number of secondary particles and residual nuclei.

A standalone scoring infrastructure was created, with dedicated data containers and histograming capabilities.

Scoring on specific volumes, or through a boundary, is ensured through a touchable identification scheme which supports the G4 replica / parametrized / division volumes, and the a-la-FLUKA lattices.

Single-differential and double-differential scoring are supported.

A mesh scoring implementation has been added. It is available in both cartesian and cylindrical modes (Fig. 4.3). It does not rely on a scoring manager and on parallel worlds, which are the keys to mesh scoring in G4 core code. Instead, it is a fully custom implementation, relying on a different design of the data collection and synchronisation in a multithreaded environment. The granularity of the statistics is run-based (like in FLUKA), instead of event-based (like in G4 core). The implementation prevents the mesh definitions to interfere with the particle tracking: like in FLUKA, the step size is independent from the mesh binning. Additionally, this approach allows a significant reduction of runtime and RAM use: at least one order of magnitude with respect to the core G4 implementation (depending on test cases).

Figure 4.3. Cylindrical mesh scoring with Moira

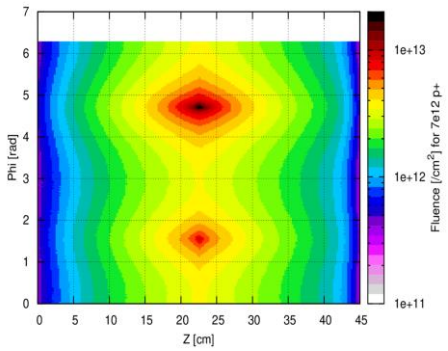

Protons fluence in lead target. 20 GeV proton gun.

Magnetic Fields

The magnetic fields are implemented using the G4 infrastructure. Support for complex magnetic fields is added following the FLUKA capabilities. These are analytical magnetic fields, including dipoles, quadrupoles, sextupoles, octupoles and decapoles, and tabulated 2D/3D fields for numerical interpolation. It is possible also to use symmetries to define these fields, combining them with analytical and interpolated fields. Figure 4.4 shows an example of a LHC superconducting dipole, where such functionality is used.

Figure 4.4. Moira magnetic field maps

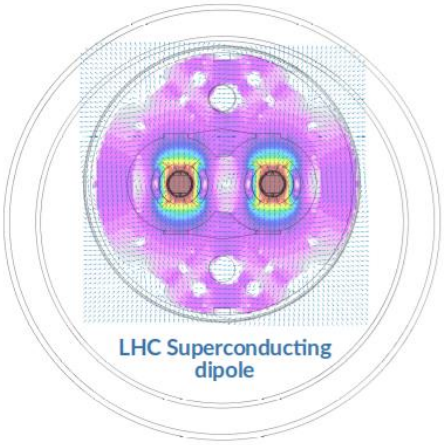

Plot of field strength and direction of the magnetic fields of a superconducting dipole in the LHC. The field was created from a magnetic field map, making use of the symmetries of the field and mixing it with dipolar analytical fields in the beam pipes.

Biasing

Biasing in Moira is directly derived from G4. The following variance reduction techniques were added:

- Region importance and weight window biasing: particles are split or killed as a function of the importance assigned to the regions they traverse.
- Leading particle biasing: particle killing after EM interactions to avoid the geometrical increase of the number of e-, e+ and photons in EM showers. There is also an analog implementation for hadrons (multiplicity tuning).
- Interaction biasing: it permits an artificial reduction of the mean free path of non-elastic nuclear interactions.

Tracking cutoffs

Tracking in Moira is presently fully relying on the G4 implementation.

Particle production cuts can be set by the user, like in any G4 application, with a threshold expressed as a range (distance unit). To ensure continuity of the user experience with FLUKA, the possibility for the user to set a threshold expressed in particle kinetic energy has been added. The latter is made possible by directly calling the G4 implementation, which already provides such functions internally. Similarly, particle transport cuts have been added (Fig. 4.5), also in view of ensuring continuity of the user experience with FLUKA.

4.3.3. 3.2.7 Flair integration

In the previous sections, Flair was presented as a complete integrated working environment for FLUKA. The GUI was extended to integrate Moira. Flair now has the capability of editing Moira input files, visualising and generating the geometry, managing the run, and performing the post-processing and plotting of the results.

Figure 4.5. Transport thresholds in Moira

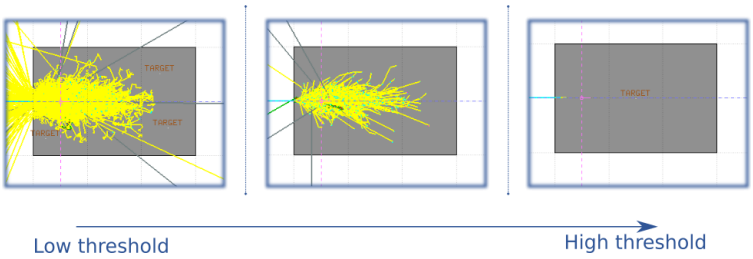

Particle tracks generated by the transport of an electron at 1 GeV for various transport cutoff thresholds.

Flair is able to automatically convert FLUKA input files into Moira input format. This is of great practical utility for the user, allowing to run both FLUKA and Moira calculations from a single input file.

4.4. First validations using Moira: BLM benchmarks

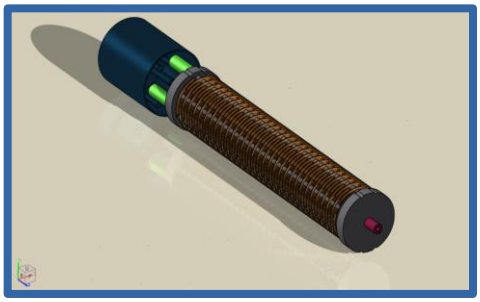

The BLM system of the LHC is composed of a series of ionisation chambers utilised for accelerator machine protection purposes. The LHC relies on approximately 4000 BLMs, located in critical loss locations. The purpose of these detectors is to convert particle shower information into electrical signals. The measured dose rates are compared against predefined thresholds, defining the cases where the beam should be extracted to avoid too high levels of irradiation of the equipment and a potential damage (Holtzer et al., 2012). In the following sections, a comparison between the results of FLUKA, Moira simulations and measurements of the dose absorbed in the BLMs is discussed.

4.4.1. CHARM facility

The CERN High Energy Accelerator Mixed-Field (CHARM) facility (Mekki et al., 2016; Prelipcean et al., 2022) is a flexible irradiation infrastructure, dedicated to testing electronics and systems in a well characterised mixed-radiation field. The facility is unique due to its possibility to replicate in a controlled way environments like space, the atmosphere, or accelerator complexes.

CHARM facility description

Fig. 4.6 shows the layout of the main features in the CHARM facility.

The 24 GeV/c protons delivered from the Proton Synchrotron (PS) accelerator at CERN impinge on one of the three possible targets:

Copper (cp), Aluminium (al) or Aluminium with holes (alh). These materials were chosen due to their different density (here decreasing), with a direct effect on the radiation generated. The target is composed of a 50 cm long cylinder with 8 cm diameter. The other important factor that contributes to the radiation generated in the area is the configuration. There are four movable blocks, whose dimensions are 20 x 214 x 350 cm^3.

Figure 4.6. Top view of the CHARM test area.

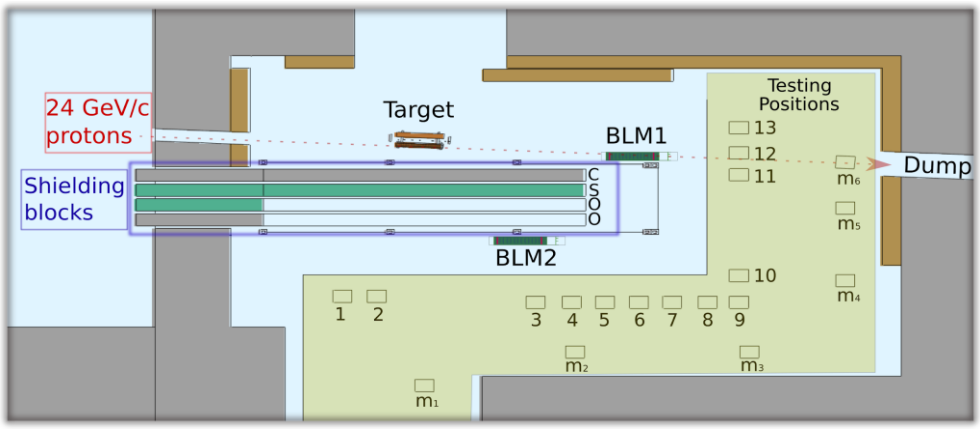

Top view of the CHARM facility. The shielding configuration illustrates the CSOO case. BLMs are positioned one metre above beam height.

These blocks are placed between the target and some test locations, and can be chosen in different combinations. The outer ones are made of concrete (C) and the inner ones of stainless steel (S). For instance, the configuration observed in Figure 4.6 will be specified as CSOO, where O expresses that the 3rd and 4th blocks are not used. The figure also shows the testing positions and the two BLMs used for the benchmarks presented.

CHARM facility results

Figure 4.7 shows the BLM1 and BLM2 benchmarks for various shielding configurations. The physics list selected for Moira was the default one (FTFP_BERT_HP), recommended for high energy physics studies (physics lists guide, 2023).

BLM1 shows a relatively constant dose for the different shielding cases. Indeed, it is in a position where the shielding impact is almost negligible. A potential incidence of backscattering due to the blocks could explain the little increase in the dose of the cases with shielding. The reduction of dose depending on the material is explained by the reduced density: lower density is translated into lower radiation field intensity, which means lower dose in the BLM. The same explanation applies for the BLM2, where the reduction due to the shielding block is substantial.

Comparing results, the ratios for the different configurations in BLM1 between FLUKA and G4 express a constant overestimation of FLUKA with respect to G4 of ~20-30%. The G4 results exhibit a similar behaviour to FLUKA and Data, never exceeding the 50% percent difference between Moira-Data and Moira-FLUKA (except the alCSOO case). The BLM2-cpCSSC indicates a peculiar result. As the data shows, this is the case of the copper target with the lowest dose, which is reasonable considering the presence of the full shielding. This is not replicated by the results of FLUKA and Moira. They obtain a higher dose compared to other cases with less shielding. Further investigation is currently ongoing to understand the cause of these values.

4.4.2. LHC Momentum cleaning region (IR3)

The Momentum cleaning region is one of the 8 long straight sections of the LHC. It is a part of the collimation system in charge of intercepting off-momentum particles, rendering this area as the third most radiated of the accelerator (Kaltchev et al., 1998).

Figure 4.7. BLMs dose result

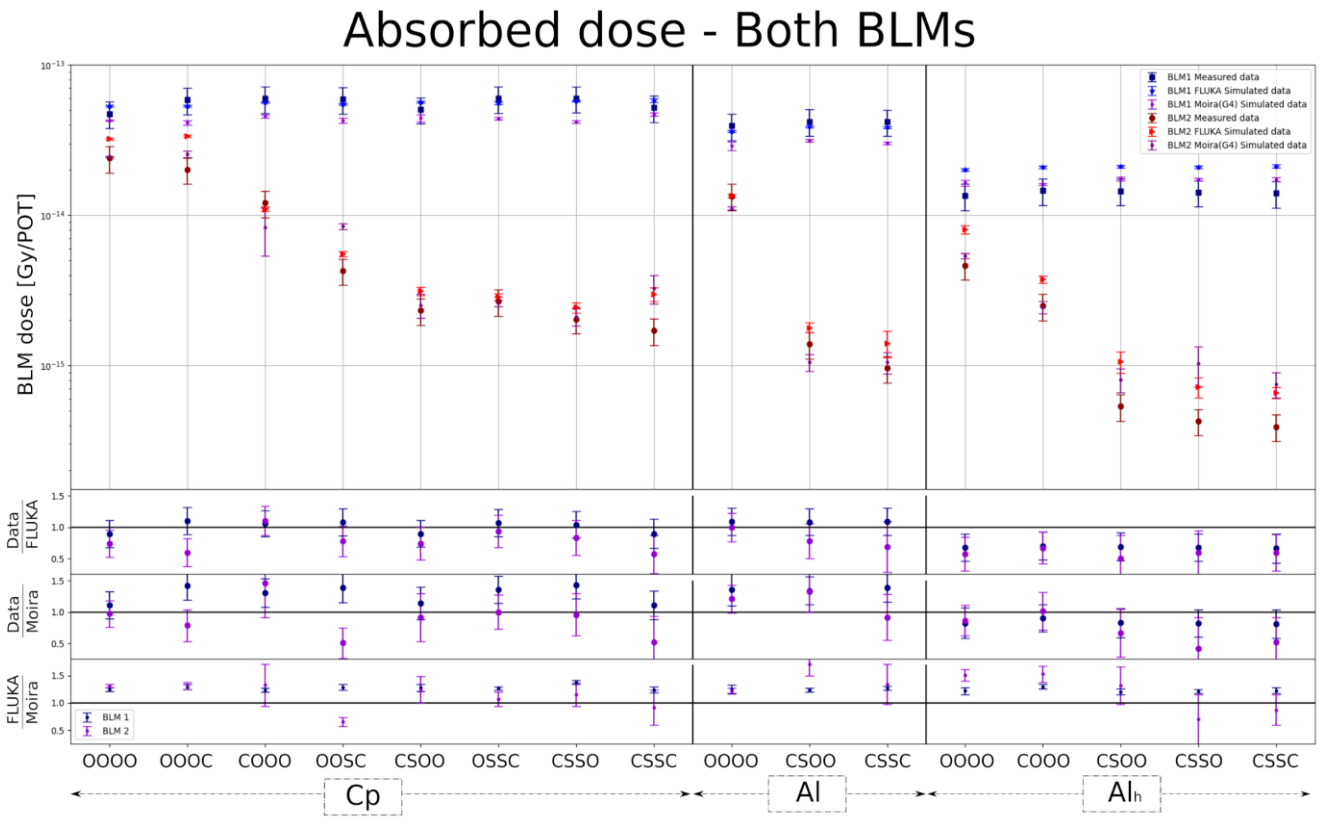

IR3 description

For this study 60 metres of the IR3 section upstream the centre of the section is used. Fig. 4.8 exhibits the main components of the geometry. The protons at ~6.5 TeV are transported from the collimator, and their trajectory is affected by the warm dipole and quadrupole magnets. 11 BLMs positioned in critical locations (next to the mentioned collimator and magnets) measure the radiation generated by the particle shower of the transported protons. The BLM dose per proton was calculated with Moira (G4) and FLUKA, and the results are compared with measurements from 2018.

Figure 4.8. IR3 section layout

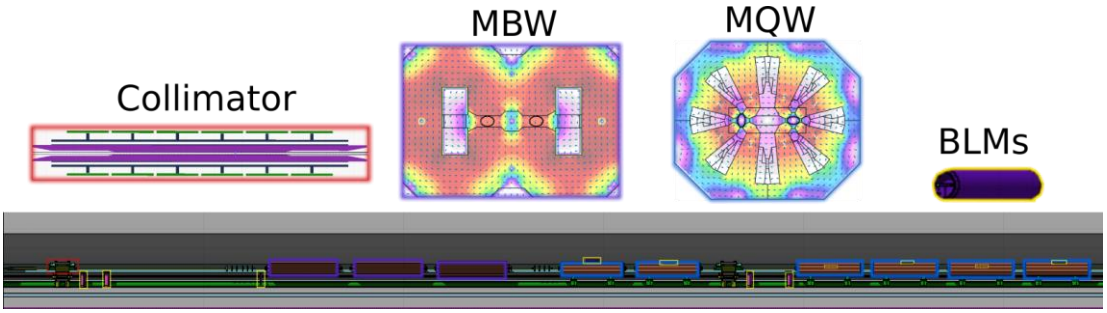

Layout of the first 60 m in IR3 LSS used for the study. The collimator from where the protons at 6.5 TeV are transported, as well as the warm magnets and the beam loss monitors are shown.

IR3 results

The first plot in Fig. 4.9 shows the aforementioned results, the comparison of the BLM dose per primary obtained with FLUKA, Moira (G4) using the default physics list recommended for high energy physics (FTFP_BERT_HP), and measurements from 2018. The two other plots in Fig. 4.9 represent the ratios Data/G4 and FLUKA/G4 for various physics lists which are also suitable for high energy physics calculations.

The dose on the first three BLMs exhibits a good agreement with differences below the 20% and even 10% for the various physics lists. More pronounced discrepancies exist for the downstream BLMs. The ratio with the measured data shows a mismatch for all the BLMs up to a factor of 2.5 to 3.5. Between FLUKA and G4, the disagreement reaches a factor of 2.2 when using the FTFP_BERT_HP physics list. All other physics lists are below a factor 2 in the 11 BLMs. It is noticeable that the worst cases are observed for the last 8 BLMs which are located downstream of the magnets. Therefore, it requires further investigation to understand if a potential inaccuracy in the field map definition could generate these differences.

4.5. Summary and Conclusions

In this paper the concept and status of a novel tool for MC simulations temporarily called *Moira* was presented. Two machine protection studies were carried out with this development. The BLM benchmarks obtained from Moira showed a discrepancy below 50% between Moira-FLUKA and Moira-Data for the CHARM study for all the BLMs, and a maximum discrepancy of a factor of 3.5 in Moira-Data in IR3 and a factor of 2 for Moira-FLUKA for most of the physics lists utilised. The results obtained are quite promising showing the robust implementation of the geometry tracking, scoring, and biasing in Moira. Moreover, they can be considered as the first trials using Moira for these complex geometries at TeV energies. Further investigation is required to validate the good behaviour of the magnetic field maps for IR3 and future studies with Moira.

Figure 4.9. IR3 section results

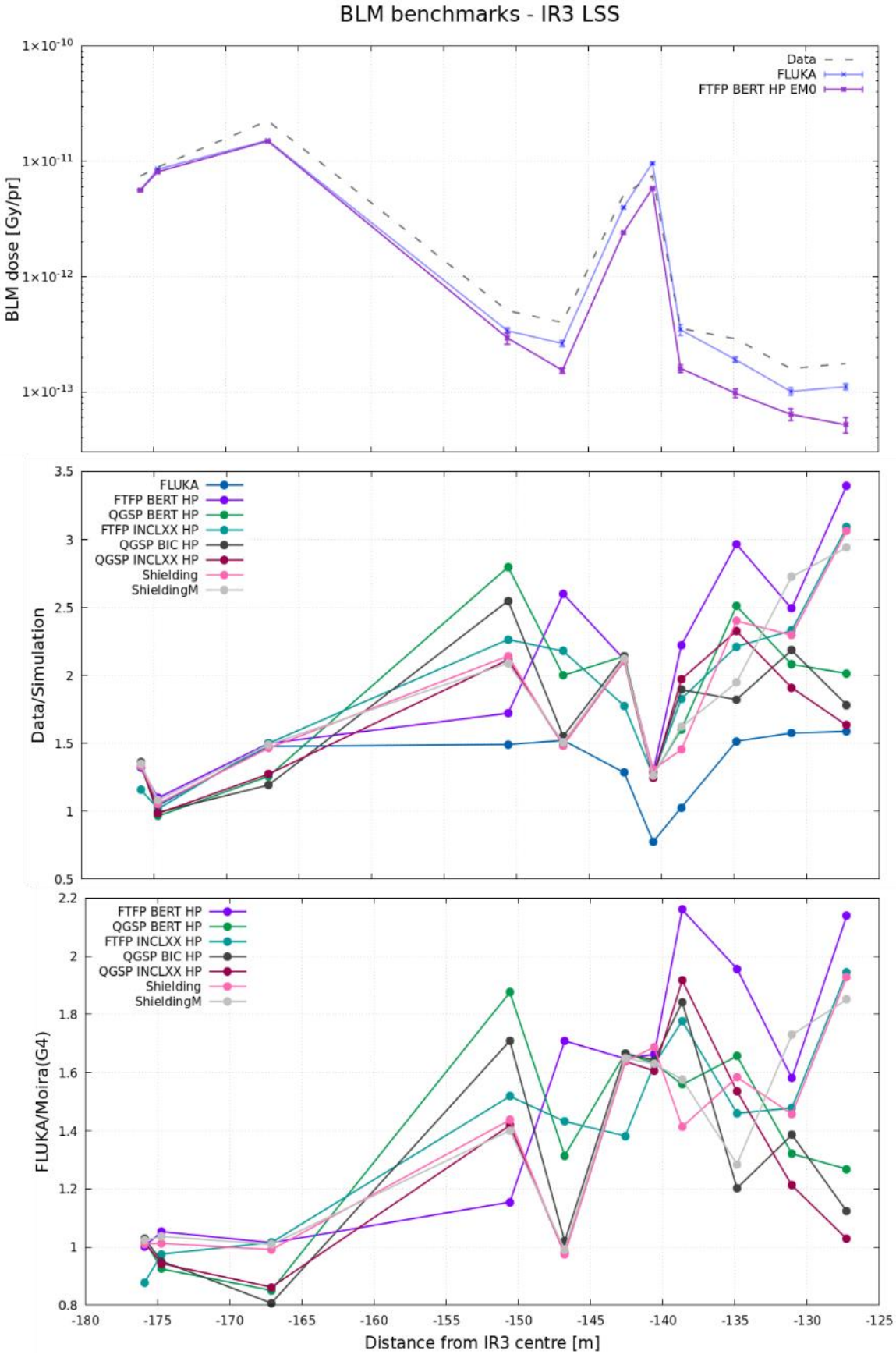

4.6. References

F. Cerutti et al. (2022), “New Capabilities of the FLUKA Multi-Purpose Code”, Frontiers in Physics 9, 788253.

G. Basttioni et al. (2015), “Overview of the FLUKA code”, Annals of Nuclear Energy 82 10 – 18.

https://fluka.cern (Accessed: 30.05.2023).

J. Allison et al. (2016), “Recent Developments in Geant4”, Nucl. Instrum. Meth. A 835 186 - 225.

J. Allison et al. (2006), “Geant4 Developments and Applications”, IEEE Trans. Nucl. Sci. 53 270 - 278.

Geant4 – A Simulation Toolkit, S. Agostinelli et al., Nucl. Instrum. Meth. A 506 (2003) 250 - 303.

https://gitlab.cern.ch/geant4/geant4/-/tree/master/examples/extended/persistency/P03 (Accessed: 30.05.2023).

R. Chytracek et al. (2006), “Geometry Description Markup Language for Physics Simulation and Analysis Applications”, IEEE Trans. Nucl. Sci., 53 2892 - 2896.

https://indico.cern.ch/event/1123370/contributions/4715938/attachments/2444705/4188972/04_Geometry_Basic_2022_ULB.pdf (Accessed: 30.05.2023).

http://geant4.in2p3.fr/IMG/pdf_Lecture-Geometry.pdf (Accessed: 30.05.2023).

http://geant4-resources.com/Geant4GUI/G4GUI.html (Accessed: 30.05.2023).

Pedro Arce et al. (2014), “GAMOS: A framework to do GEANT4 simulations in different physics fields with an user-friendly interface”, Nucl. Instrum. Meth. A 735 304 - 313.

https://indico.cern.ch/event/294651/sessions/55918/attachments/552022/760637/Visualisation.pdf (Accessed: 30.05.2023).

V. Vlachoudis (2009), “Flair: A powerful but user friendly graphical interface for FLUKA”, M&C.

E. V. Holtzer et al (2012), “Beam Loss Monitoring for LHC Machine Protection”, Physics Procedia 37 2055 - 2062.

J. Mekki et al. (2016), “CHARM: A Mixed Field Facility at CERN for Radiation Tests in Ground, Atmospheric, Space and Accelerator Representative Environments”, IEEE Trans. Nucl. Sci. 63.4 2106 - 2114.

D. Prelipcean et.al. (2022), “Benchmark Between Measured and Simulated Radiation Level Data at the Mixed-Field CHARM Facility at CERN”, IEEE Trans. Nucl. Sci., 69 1557 - 1564.

http://geant4.in2p3.fr/IMG/pdf_PhysicsLists.pdf (Accessed: 30.05.2023).

D. Kaltchev et al. (1998), “Momentum Cleaning in the CERN LHC”, 6th European Particle Accelerator Conference 353 - 355.

4.7. Acknowledgment

Thanks to Daniel Prelipcean for providing the CHARM input file, the FLUKA results and participating in the post-processing/plotting.

Thanks to Andreas Waets for providing the IR3 input file and FLUKA results.

Thanks to Kacper Bilko for the BLMs data in CHARM and IR3.

4.8. List of abbreviations and acronyms

MC: Monte Carlo.

G4: Geant4.

LHC: Large Hadron Collider.

LSS: Long Straight Section.

CHARM: CERN High Energy Accelerator Mixed-Field.

PS: Proton Synchrotron.

BLM: Beam Loss Monitors.

5. Neutronics Calculations with the Unstructured Mesh Model of the ORNL's Second Target Station

Lukas Zavorka*, Kristel Ghoos, and Igor Remec
Oak Ridge National Laboratory, Oak Ridge, TN, USA
*zavorkal@ornl.gov

The Second Target Station (STS) at the Oak Ridge National Laboratory's Spallation Neutron Source is designed to become the highest peak-brightness source of cold neutrons in the world. The current conceptual design of STS consists of a rotating tungsten spallation target driven by a short-pulsed, 1.3-GeV, 700-kW proton beam; and two coupled pure parahydrogen neutron moderators surrounded with water premoderator and a beryllium reflector. To advance the STS design efficiently and cope with a large volume of supporting neutronics calculations, we employ the most efficient computational tools available. A key among these tools is the Unstructured Mesh (UM) geometry capability of the radiation transport code MCNP6.2. The UM geometry capability allows us to automatically convert the computer aided design (CAD) engineering models into high-fidelity models for neutronics calculations, reduce the time necessary to generate the models, and deliver results for the subsequent thermal and structural stress analyses with high spatial resolution.

In this paper we review a couple of applications of the UM geometry capability within the scope of the STS conceptual design. We focus on building hybrid UM/constructive solid geometry (CSG) models to calculate energy deposition and radiation damage in terms of displacement per atom (dpa) in the target, moderators, core vessel (CV), and CV shielding. We demonstrate the application of the FW-CADIS variance reduction technique to provide well-converged heating results in the distant regions of the CV shielding. We also introduce an automated optimization workflow based on UM geometries and modern Dakota optimizer. With the limited space available, this paper serves more like an overview of the UM geometry capability within the STS; however, it does not intend to provide full details about the individual calculations, as can be found elsewhere, e.g. (Zavorka et al., 2023; Ghoos et al., 2023a; Ghoos et al., 2023b; Zavorka & Remec, 2022; Zavorka & Remec, 2021).

5.1. Introduction

The Second Target Station (STS) (ORNL, 2020; Remec et al., 2018) at the Oak Ridge National Laboratory's (ORNL) Spallation Neutron Source (SNS) is designed to become the highest peak-brightness source of cold neutrons in the world. After its completion, the STS will operate as a rotating solid tungsten target driven by a short-pulsed (<1 μs) proton beam with the energy of 1.3 GeV, the beam power of 700 kW, and the 15 Hz repetition rate. Spallation reactions will release neutrons from the target. Neutrons born with a broad energy spectrum will be slowed down and moderated to cold energies in one of the two neutron moderators. The coupled moderators use parahydrogen at 20 K and they are surrounded with a light water premoderator and a beryllium reflector. The cold neutrons will travel tens of meters from the moderators through the beamlines to a fleet of eventually 22 novel instruments designed for different neutron scattering experiments (Qian et al., 2022; Sala et al., 2022; Borgstahl et al., 2022; Garlea et al., 2022; Do et al., 2022; Mamontov et al., 2022; Liu et al., 2022; An et al., 2022). The instruments will benefit from high peak brightness, which means high neutron flux per unit solid angle in a small area and short time. At STS, high peak brightness is primarily achieved by the use of low-

dimensional moderators (Morishima et al., 2002; Batkov et al., 2013; Mezei et al., 2014; Andersen et al., 2018; Zanini et al., 2019; Zanini et al., 2020, Zhao et al., 2013, Gallmeier et al., 2016; Gallmeier et al., 2022) with small emission surfaces (square 3 cm x 3 cm and circular 3 cm in diameter) and a short distance between the high-density spallation target and moderators (1.1 cm).

STS is a high-power accelerator facility with a high instantaneous energy (50 J/cm^3/pulse) deposited locally in the target by the pulsed high-energy proton beam. After each pulse, a large number of neutrons, photons, and a variety of other neutral and charged particles will be generated via spallation in the target. Especially the high-energy neutral particles can penetrate long distances (several meters) through the radiation shielding around the target while simultaneously depositing portions of their energy as they slow down to low energies by interacting with atoms and nuclei. The extremely fast spallation reactions (10^{-22}–10^{-18} s) also generate a wide range of unstable spallation residuals that can have both very short and very long decay times (> 10^6 years). As these residuals decay, they generate additional decay heat and gamma rays that need to be removed and shielded, respectively. This is to illustrate that the physics processes at STS span many orders of magnitude on the scales of energy, time, and distance, and they can be challenging to evaluate.

In order to design STS reliably and in compliance with radiation safety regulations, a wide spectrum of supporting radiation transport (neutronics) calculations is necessary. These calculations include but are not limited to instantaneous energy deposition in the target, instantaneous energy deposition in the neutron moderators and surrounding components, such as core vessel (CV) and CV shielding, activation and decay heat generation in the target and other components, displacement-per-atom (dpa) to determine radiation damage of the components and predict their lifetime, prompt and delayed radiation shielding calculations, and many others. Some of these calculations can be done with the simplified geometry models, either fully extended or local models, while other calculations require high-fidelity models. The complexity and duration of the calculations vary extensively, together with a constantly evolving design of the STS components, driven by the results of the previous calculations.

To perform the neutronics calculations in a timely manner, we employ the most efficient computational tools that are currently available. The most important among these tools is the Unstructured Mesh (UM) geometry capability of the radiation transport code MCNP6.2 (Werner et al., 2017; Martz et al., 2017). The UM geometry capability allows us to efficiently convert the computer aided design (CAD) engineering models directly into the high-fidelity models for neutronics calculations. The automated CAD to MCNP model conversion greatly reduces the time necessary to build the neutronics models, which is of great importance when the design of a component evolves rapidly. MCNP results from the UM models can have higher fidelity and spatial resolution in comparison with the traditional rectangular mesh tallies. The results can be imported for the subsequent thermal and structural stress analyses much more conveniently. Moreover, the same engineering CAD model can be used both for neutronics and thermal analyses. We found the UM geometry capability indispensable when calculating energy deposition and radiation damage in various components, as well as when determining the neutronics performance of the moderators and radiation dose rate levels throughout the facility.

Importantly, the automated CAD to MCNP model conversion opens the door to the development of a fully automated multi-parameter optimization workflow not only for neutronics (such as maximizing the neutronics output of a moderator) but also for the coupled neutronics–structural stress (multi-physics) optimization problems (such as simultaneously maximizing neutron production and minimizing structural stress in the target). We have developed such an automated optimization workflow (Zavorka et al.,

2023) controlled by a modern optimizer Dakota (Adams et al., 2021). The workflow was used to optimize the neutronics performance of the moderators (Ghoos et al., 2023a) and to optimize several target concepts (Ghoos et al., 2023b). Without any doubt, the workflow has significantly advanced the entire STS engineering design process.

In this paper, we first present a method for building a suitable model for neutronics calculations with MCNP of the two key STS components—target and moderators. Then we present results of the energy deposition calculations in these components. Afterwards we move to the surrounding core vessel (CV) and CV shielding, where an application of the variance reduction (VR) technique FW-CADIS with UM is necessary because of the increasing distance from the target. We present results on energy deposition and radiation damage in the CV. We conclude by introducing a novel automated optimization workflow.

5.2. Hybrid UM/CSG Models for MCNP

The prime advantage of using UM models for neutronics calculations is that the model can be automatically converted from the existing engineering CAD models without the need to separately build a constructive solid geometry (CSG) model, which is a traditional approach in MCNP. Building a detailed CSG model manually can be time-consuming and usually requires a significant user experience to proceed efficiently. Moreover, manual conversion of the complicated objects is prone to errors. On the other hand, it is relatively simple to build traditional CSG models for large and trivial objects, such as bulk shielding blocks. Such simple CSG models result in efficient radiation transport in MCNP and require low computer memory in comparison with the detailed UM models. The detailed UM models require more memory, because they are typically composed of a large number of smaller UM cells, and as a result, radiation transport in MCNP can be slower. Fortunately, MCNP works efficiently with hybrid UM/CSG models, as discussed recently by Alwin et al., 2019, Zavorka & Remec, 2022 and Zavorka & Remec, 2021.

The essence of building the hybrid UM/CSG models is that large, trivial, and less important objects are built manually as traditional CSG, and non-trivial detailed objects of great importance are automatically converted from CAD into UM. Both model categories are then combined in one single MCNP input deck. In a properly balanced hybrid model, the time necessary to build the model is minimal, and the execution time and computer memory requirements are optimal. As with many other disciplines and ways of discoveries, finding such an optimal balance can take some time and user experience; however, the benefits outweigh the potential difficulties involved.

For the STS project, one of the hybrid UM/CSG models was composed such that the spallation target and neutron moderators are built as high-fidelity UM models and the surrounding radiation shielding is built as CSG. The model was used to calculate energy deposition and dpa rates in the target and moderators. Another similar model was composed with a portion of the surrounding shielding also built as UM to calculate energy deposition and radiation damage in the shielding. These models are discussed in the next section.

Last point before we proceed to the next section is to describe how we convert the CAD models into the detailed UM models for neutronics calculations. We use Attila4MC (Attila4MC, 2020) to generate the UM models and to pre-generate an MCNP input deck, which needs to be afterwards populated with the surrounding CSG objects if necessary. Attila4MC allows the user to specify UM quality parameters, such as the maximum edge length of a mesh, curvature refinement, to identify local mesh refinements, and a range of other parameters. It also assigns materials and densities to the individual components. Attila4MC can be executed either from a command line or using its graphical user interface.

However, Attila4MC is not only the mesh generator. One of its crucial features is the ability to calculate deterministic weight windows for efficient variance reduction (VR) in MCNP using CADIS or FW-CADIS methods (Wagner et al., 1998; Wagner et al., 2014). We typically generate weight windows for any MCNP calculation that requires well converged results at a distance of one meter from the target or larger. At these distances, it is difficult to obtain converged results without the VR within a reasonable computing time. We show an example of the weight windows in the next section as well.

5.3. Hybrid UM/CSG Model of the Second Target Station

The solid CAD model of the rotating spallation target and two moderators is shown in Figure 5.1 and Figure 5.2. The current target design consists of 21 individual segments cooled with light water. The cylindrical moderator is located above the target and the tube moderator is located below the target. The former is designed to provide maximum peak brightness to up to 16 neutron instruments while the latter will deliver maximum time integrated brightness to up to six instruments. Both moderators are pure parahydrogen at 20 K in aluminium vessels separated by a vacuum gap from a light water premoderator and a beryllium reflector. The gap between the target and moderators is 1.1 cm wide.

To calculate energy deposition in the target after the proton pulse, we generated a hybrid UM/CSG model shown in Figure 5.3. It consists of the target and moderators converted into UM (see also Figure 5.1) and the surrounding steel shielding built as CSG. Energy deposition was tallied only in the UM portion of the model and the results were stored in the MCNP UM elemental edit output file. The file contains data about energy deposition in every single mesh element. The file was processed with an in-house post-processing script and the results were imported for the subsequent thermal and structural stress analyses, to guide the design of the efficient cooling, and to determine the lifetime of the components. Maximum volumetric energy deposition and radiation damage in the target is 50 J/cm^3/pulse and 0.9 dpa/year, respectively, assuming the 5000-hour operation per year. Figure 5.4 shows energy deposition in the target and moderators, with the UM displayed in the target nose region. Relative errors are below 5%.

Figure 5.1. Solid CAD and UM model of the target and moderators

Solid CAD model (left) of the target and moderators converted into the detailed UM (right).

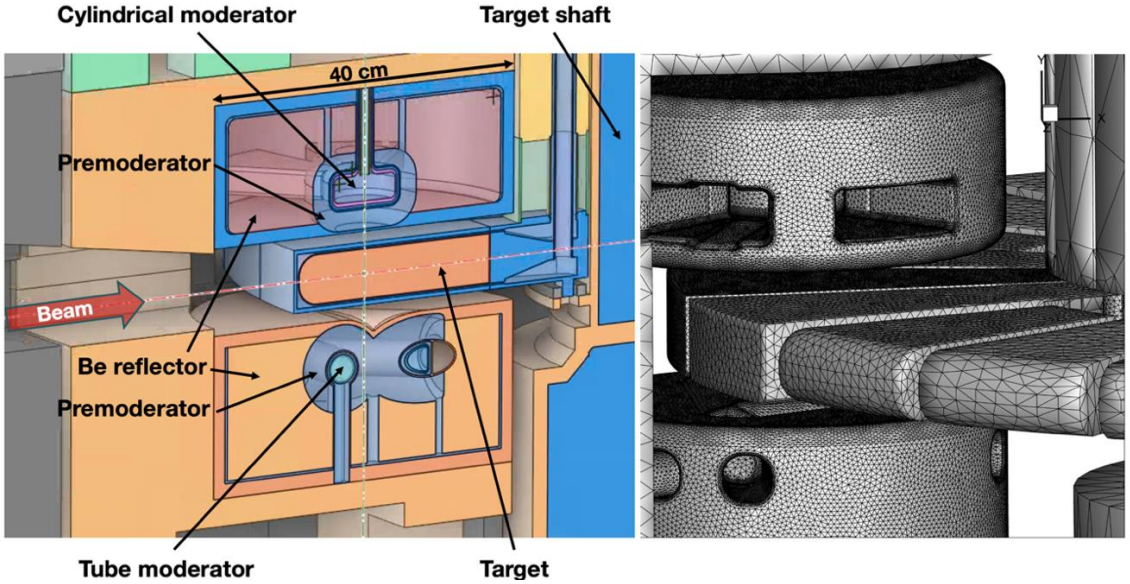

Figure 5.2. Horizontal view of the moderators

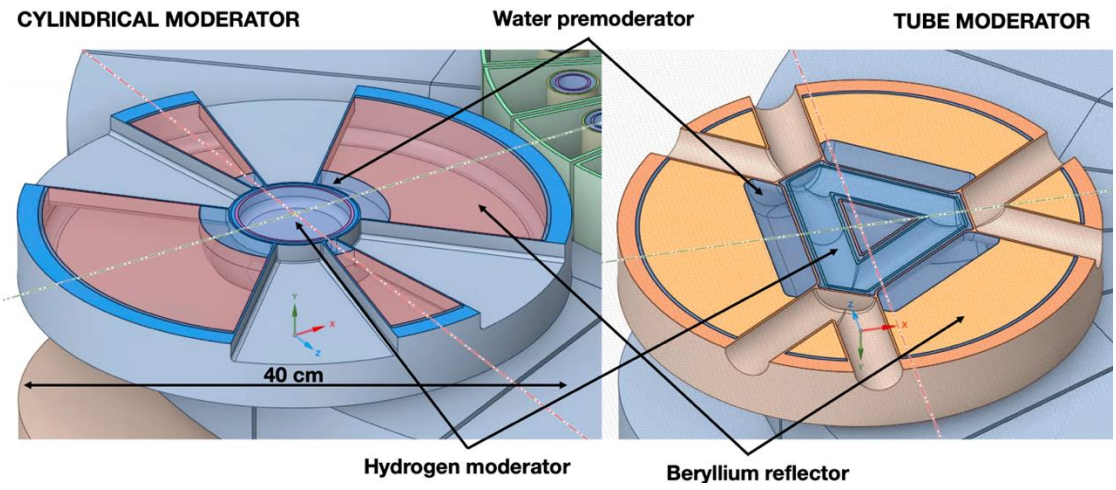

Figure 5.3. Hybrid UM/CSG model of the target and moderators

Elevation plot of the hybrid UM/CSG model. Cylindrical moderator (UM1), target (UM2), and tube moderator (UM3) are built as UM, and the surrounding steel radiation shielding is built as CSG.

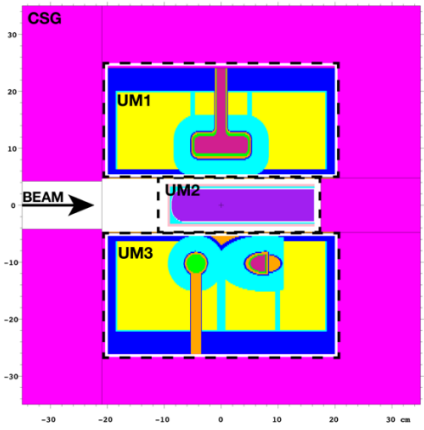

Figure 5.4. Energy deposition in the target and moderators

A detailed view of energy deposition in the target nose with the displayed UM (left). Horizontal cut through the energy deposition profile in the three target segments (centre) and the vertical cut through the target and moderators (right). The 60-cm^2 proton beam impinges on the target along the *x* axis from the left.

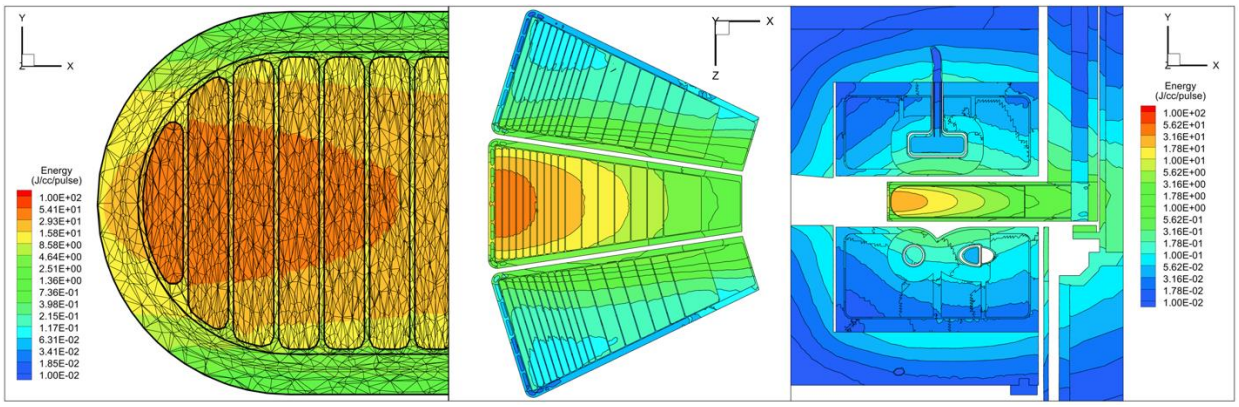

Another task was to calculate energy deposition and radiation damage in the stainless steel (SS316L) core vessel (CV) and CV shielding that surrounds the target. For this particular calculation, yet another hybrid UM/CSG model was built. The model uses a coarser mesh for the target and a relatively fine mesh for the CV shielding. In this case, the UM was built only for the portion of the shielding where the heating results were required, and CSG was used for more distant, uncooled regions of the shielding. Such a hybrid model arrangement leads to a faster MCNP calculation in comparison with a fully extended UM model.

Because the CV shielding extends well beyond one meter from the spallation target, it was necessary to calculate weight windows to achieve good convergence of the results. The deterministic energy-dependent weight windows for neutrons and photons were calculated with the FW-CADIS method implemented in Attila4MC, in which both forward and adjoint solutions of the transport equation are calculated. An example of the lower bounds of the weight windows for the 1 MeV neutrons is presented in Figure 5.5. The red horseshoe marks a downstream portion of the CV and a tally region where the good convergence of the results is required.

Figure 5.6 shows the energy deposition in the same portion of the CV (marked again with the red horseshoe), as well as the relative errors as a contribution from neutrons and photons that stay well below 10%. The errors are higher outside of the tally region.

Figure 5.5. Weight windows for a downstream portion of the core vessel

Horizontal view of the CV shielding (left). 2D (centre) and 3D (right) plots of the weight windows for the 1 MeV neutrons. The red horseshoe marks the downstream portion of the CV where the results are required.

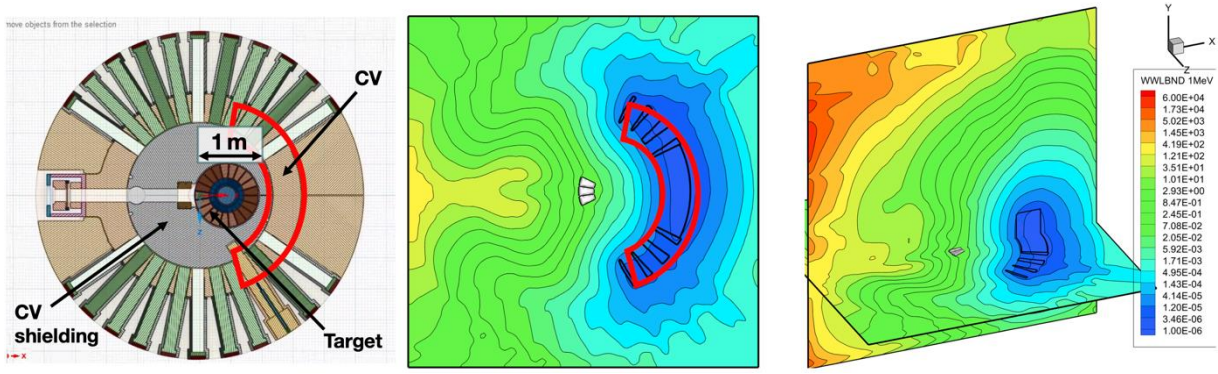

Figure 5.6. Energy deposition in the downstream portion of the core vessel

Energy deposition in the downstream portion of CV (left) with errors for neutrons (centre) and photons (right)

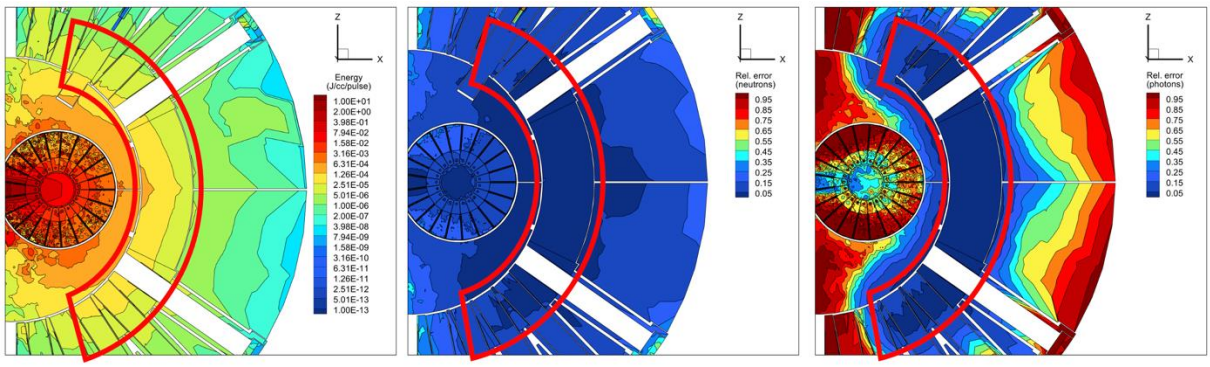

Figure 5.7. DPA rate in a portion of the core vessel

3D view of the dpa rate in an upstream portion of the CV (left). Horizontal view of the dpa rates in the CV and CV shielding at the level of the cylindrical moderator (centre) and the tube moderator (right).

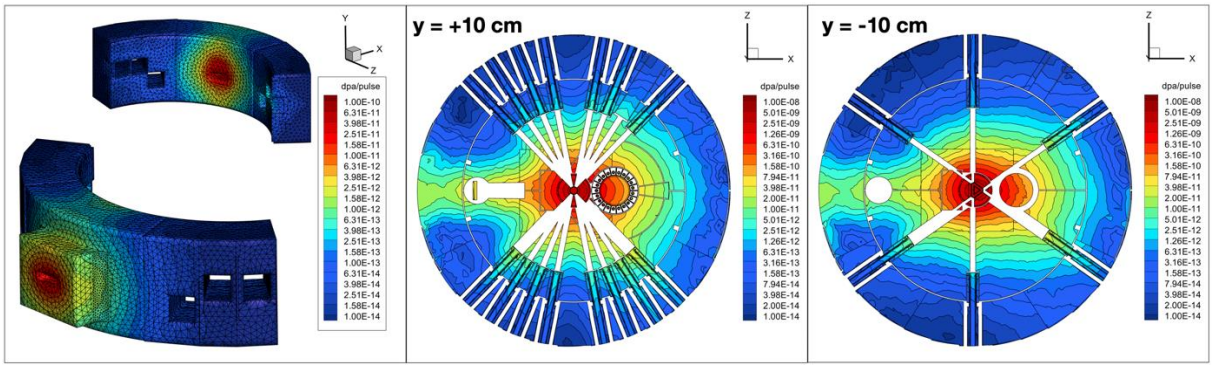

In a similar fashion, as shown in Figure 5.7, we calculated radiation damage in terms of dpa in the key regions of the CV shielding using the neutron- and proton flux-to-dpa cross sections for SS316L (Lu et al., 2006a; Lu et al., 2006b; Lu et al., 2017).

5.4. Automated optimization workflow

Finally, we discuss the UM-based fully automated optimization workflow that was developed to help design major STS components, including the target and moderators. The schematic of the workflow is shown in Figure 5.8. As an input, the workflow utilizes the detailed solid CAD engineering models parametrized either in Creo Parametric (Creo, 2022) or SolidWorks (Solidworks, 2023). The advantage is that the model parametrization is accomplished in CAD rather that in traditional MCNP CSG format using the mcnp_ pstudy (Brown et al., 2004) tool. The legacy CSG parametrization with mcnp_pstudy could potentially require significant model simplifications, and building a reliably parametrized model over a wide range of parameters might have been challenging. The next advantage is that the same CAD model can be used for the subsequent engineering analyses that follow the neutronics analysis.

When the solid CAD model is regenerated with the new set of geometry parameters, it is imported into SpaceClaim (Spaceclaim, 2022) for further processing. The processing includes filling the void vessels with liquids, which is more convenient to do in SpaceClaim rather than in Creo, fixing potential model interferences, and finalizing the geometry. Then the model is imported in Attila4MC to generate the high-fidelity UM model for neutronics. Mesh generation is fully automatic with the predefined mesh parameters. An MCNP input deck is generated and supplemented with additional components, such as the surrounding shielding built as traditional CSG. In this modular way, it is possible to build the UM exclusively for a component that is subjected to optimization. For example, if the optimized component is the cylindrical moderator, as shown in Figure 5.3, the mesh is regenerated only for the moderator in the UM1 region, and all other components remain the same from the previous optimization iterations. This approach significantly minimizes the mesh generation time.

Then the final MCNP input deck and the geometry file are passed to MCNP, and the neutronics calculation is executed. The results, such as the peak brightness and time-integrated brightness, are extracted from the MCNP mctal output file, or from the UM elemental edit outputs if the energy deposition was tallied.

Figure 5.8. Schematic of the automated optimization workflow

Schematic of the UM-based automated optimization workflow controlled by Dakota. One single iteration starts with the new parametric model in CREO (top left) and continues clockwise.

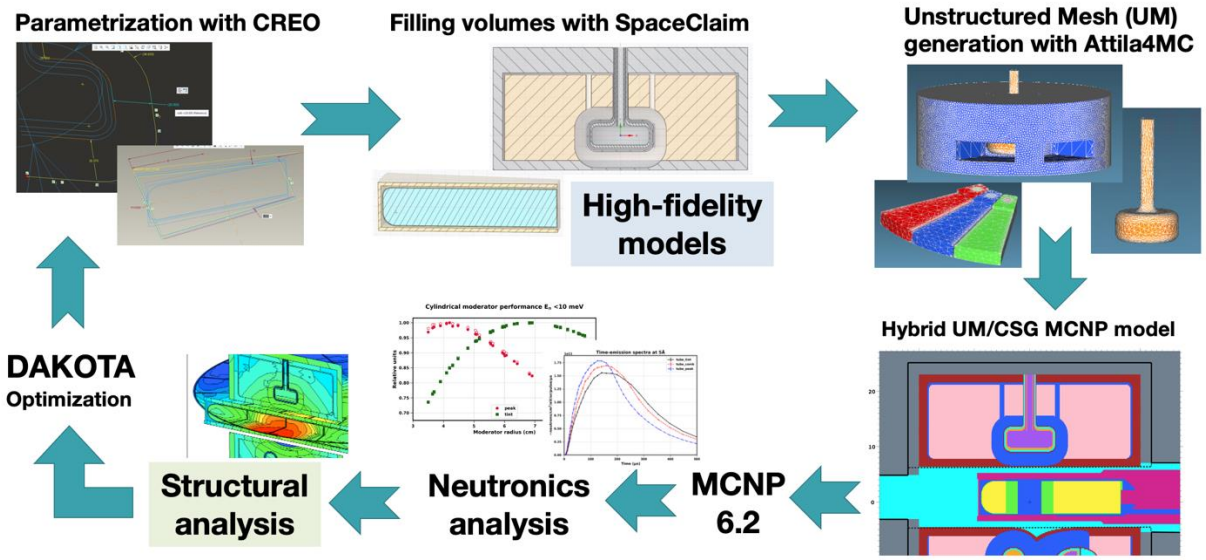

The workflow can be launched in one of the two following modes: the first mode is a pure neutronics optimization, in which the brightness is passed directly to the Dakota optimizer. The second mode also includes the structural stress optimization in a coupled neutronics-structural stress (multi-physics) optimization, in which additional UM-based engineering analyses (Ghoos et al., 2023b; Tipton et al., 2023) are executed. The two modes are controlled by Dakota, which offers both parameter study and a range of modern optimization methods for efficient convergence of a problem.

The workflow is fully automated and does not require any user interference except for building the initial parametrized model and setting the parameter ranges. All the software tools can be executed from the command line, and the file transfer in between the tools is controlled by the customized Windows .bat and Linux .bash scripts.

The workflow was recently used to optimize the neutronics performance of the moderators (Zavorka et al., 2023; Ghoos et al., 2023a) with the nine geometry parameters, and to optimize the neutronics output and structural stress of several target designs (Ghoos et al., 2023b; Tipton et al., 2023) with up to 16 geometry- and incident proton beam parameters. The workflow allowed us to explore an unprecedented amount of design options in a short time and turned out to be an indispensable tool in developing the STS design and in advancing the project towards successful completion.

5.5. Summary and Conclusions

In this paper we reviewed several applications of the UM geometry capability of MCNP6.2 for the radiation transport calculations in support of the STS project at ORNL. The use of UM advances the neutronics analyses in many ways. Most importantly, the engineering solid CAD models can be automatically converted into UM for neutronics calculations without the need to manually build the traditional CSG models. Next, the high-fidelity UM models can contain significant level of details from the original CAD model. Moreover, the neutronics results, such as energy deposition, can have high spatial resolution and can be directly imported from the MCNP elemental edit outputs into the subsequent structural

stress and thermal analyses, which is not possible with the traditional rectangular MCNP mesh tallies without a significant amount of postprocessing. Finally, the UM geometry capability opened the door to the development of the fully automated neutronics and coupled neutronics-structural stress multi-physics multi-parameter optimization workflow that will continue to be used in the future to optimize various components of the STS.

We demonstrated the use of UM with the hybrid UM/CSG model to calculate energy deposition and radiation damage in the spallation target and moderators. The same quantities were determined in the core vessel and its shielding around the target. The deterministic weight windows were calculated on UM and they were applied to achieve good convergence of the results farther away from the target. We introduced the fully automated optimization workflow that we used to optimize neutronics performance of the moderators and optimize neutronics output and structural stress of several target design concepts.

The UM geometry capability of MCNP6.2 together with our fully automated optimization workflow has the potential for use at other nuclear and accelerator facilities to significantly advance their engineering design process and to explore many more design options in the blink of an eye.

5.6. List of references

Adams, B. et. al. (2021), “Dakota, A Multilevel Parallel Object-Oriented Framework for Design Optimization, Parameter Estimation, Uncertainty Quantification, and Sensitivity Analysis: Version s14 User’s Manual”, Sandia Technical Report SAND2021-5822.

Alwin, J., J. Spencer and G. Failla (2019), “Criticality Accident Alarm System Analysis Using MCNP6.2 Constructive Solid Geometry/Unstructured Mesh Hybrid”, Los Alamos National Laboratory, LA-UR-19-24892.

An, K., A. D. Stoica, T. Huegle, J. Y. Y. Lin and V. Graves (2022), “MENUS—materials engineering by neutron scattering”, Review of Scientific Instruments 93 (5), 053911.

Andersen, K. H., M. Bertelsen, L. Zanini, E. B. Klinkby, T. Schonfeldt, P. M. Bentley and J. Saroun (2018), “Optimization of moderators and beam extraction at the ESS”, Journal of Applied Crystallography 51 (2), 264–281.

Attila4MC (2020), “Attila4MC 10.2 Overview of Core Functions”, Silver Fir Software, Inc., Gig Harbor, WA, USA, SFSW-UR-2020-OCF102.

Batkov, K., A. Takibayev, L. Zanini and F. Mezei (2013), “Unperturbed moderator brightness in pulsed neutron sources”, Nuclear Instruments and Methods in Physics Research Section A: Accelerators, Spectrometers, Detectors and Associated Equipment 729, 500–505.

Borgstahl, G. E. O., W. B. O’Dell, M. Egli, J. F. Kern, A. Kovalevsky, J. Y. Y. Lin, D. Myles, M. A. Wilson, W. Zhang, P. Zwart and L. Coates (2022), “EWALD: A macromolecular diffractometer for the second target station”, Review of Scientific Instruments 93 (6), 064103.

Brown, F., J. Sweezy and R. Hayes (2004), “Monte Carlo parameter studies and uncertainty analyses with MCNP5”, Los Alamos National Laboratory, LA-UR-04-0499.

Creo (2022), https://www.ptc.com/en/products/creo

Do, C., R. Ashkar, C. Boone, W.-R. Chen, G. Ehlers, P. Falus, A. Faraone, J. S. Gardner, V. Graves, T. Huegle, R. Katsumata, D. Kent, J. Y. Y. Lin, B. McHargue, B. Olsen, Y.

Wang and D. Wilson (2022) “Expanse: A time-of-flight expanded angle neutron spin echo spectrometer at the second target station of the spallation neutron source”, Review of Scientific Instruments 93 (7), 075107.

Gallmeier, F. X., W. Lu, B. W. Riemer, J. K. Zhao, K. W. Herwig and J. L. Robertson (2016), “Conceptual moderator studies for the spallation neutron source short-pulse second target station”, Review of Scientific Instruments 87 (6), 063304.

Gallmeier, F. X. and I. Remec (2022), “A liquid hydrogen tube moderator arrangement for SNS second target station”, Review of Scientific Instruments 93 (8), 083301.

Garlea, V. O., S. Calder, T. Huegle, J. Y. Y. Lin, F. Islam, A. Stoica, V. B. Graves, B. Frandsen and S. D. Wilson (2022), “Verdi: Versatile diffractometer with wide-angle polarization analysis for magnetic structure studies in powders and single crystals”, Review of Scientific Instruments 93 (6), 065103.

Ghoos, K. et al., (2023a), “Optimization of the moderators for the Second Target Station with Dakota”, submitted for publication in Nuclear Instruments and Methods in Physics Research Section A.

Ghoos, K. et al. (2023b), “Designing the Second Target Station with an Advanced Multiphysics Optimization Workflow”, Proc. of the M&C 2023 - The International Conference on Mathematics and Computational Methods Applied to Nuclear Science and Engineering, Niagara Falls, Ontario, Canada, August 13–17.

Liu, Y., H. Cao, S. Rosenkranz, M. Frost, T. Huegle, J. Y. Y. Lin, P. Torres, A. Stoica and B. C. Chakoumakos (2022), “Pioneer, a high-resolution single-crystal polarized neutron diffractometer”, Review of Scientific Instruments 93 (7), 073901.

Lu, W., M. S. Wechsler and Y. Dai (2006a), “The NCSU Radiation Damage Database; Proton-Induced Damage Energy and Application to Radiation Damage at SINQ”, J. Nucl. Mater., 356, 280-286.

Lu, W., M. S. Wechsler, P. D. Ferguson and E. J. Pitcher (2006b), “Spallation Radiation Damage Calculations and Database: Cross-Section Discrepancies between the Codes”, J. ASTM Inter., Vol. 3, No. 7, 212-219.

Lu, W. and M. S. Wechsler, (2017), “The Radiation Damage Database: Section on Helium Cross Section”, J. Nucl. Mater., 361, 282–288.

Mamontov, E., C. Boone, M. J. Frost, K. W. Herwig, T. Huegle, J. Y. Y. Lin, B. McCormick, W. McHargue, A. D. Stoica, P. Torres and W. Turner (2022), “A concept of a broadband inverted geometry spectrometer for the second target station at the spallation neutron source”, Review of Scientific Instruments 93 (4), 045101.

Martz R. (2017), “The MCNP6 Book on Unstructured Mesh Geometry: User’s Guide for MCNP 6.2”, Los Alamos National Laboratory, LA-UR-17-22442.

Mezei, F., L. Zanini, A. Takibayev, K. Batkov, E. Klinkby, E. Pitcher and T. Schonfeldt (2014), “Unperturbed moderator brightness in pulsed neutron sources”, Journal of Neutron Research 17, 101–105.

Morishima, N. and Y. Matsuo (2002), “Cold neutron production in liquid para- and normal-h2 moderators”, Nuclear Instrum. and Methods in Physics Research Section A: Accelerators, Spectrometers, Detectors and Associated Equipment 490 (1), 308–315.

ORNL (2020), “Spallation Neutron Source, Second Target Station, Conceptual Design Report, Vol. 1: Overview, Technical and Experiment Systems”, Oak Ridge National Laboratory, S01010000-TR0001.

Qian, S., W. Heller, W.-R. Chen, A. Christianson, C. Do, Y. Wang, J. Y. Y. Lin, T. Huegle, C. Jiang, C. Boone, C. Hart and V. Graves (2022), "Centaur, the small-and wide-angle neutron scattering diffractometer-spectrometer for the second target station of the Spallation Neutron Source", Review of Scientific Instruments 93 (7), 075104.

Remec, I., Gallmeier, F. and Rennich, M. (2018), "Neutronics analyses for the ORNLs spallation neutron source second target station", IOP Conf. Series: Journal of Physics: Conf. Series 1021, 012084.

Sala, G., M. Mourigal, C. Boone, N. P. Butch, A. D. Christianson, O. Delaire, A. J. DeSantis, C. L. Hart, R. P. Hermann, T. Huegle, D. N. Kent, J. Y. Y. Lin, M. D. Lumsden, M. E. Manley, D. G. Quirinale, M. B. Stone and Y. Z, Chess (2022), "The future direct geometry spectrometer at the Second Target Station", Review of Scientific Instruments 93 (6), 065109.

Solidworks (2023), https://www.solidworks.com/

Spaceclaim (2022), https://www.ansys.com/products/3d-design/ansys-spaceclaim

Tipton, J. et al. (2023), "Spallation Target Fatigue Lifetime: Uncertainty Quantification & Optimization", at the 15th International Workshop on Spallation Materials Technology, Santa Fe, NM, March 5-9.

Wagner, J. and A. Haghighat (1998), "Automated Variance Reduction of Monte Carlo Shielding Calculations Using the Discrete Ordinates Adjoint Function", Nuclear Science and Technology, 128 (2).

Wagner, J., D. Pepolow, and S. Mosher (2014), "FW-CADIS Method for Global and Regional Variance Reduction of Monte Carlo Radiation Transport Calculations", Nuclear Science and Technology, 176 (1).

Werner, C. (editor) et al. (2017), "MCNP User's Manual, Code Version 6.2," LA-UR-17-29981, Los Alamos National Laboratory.

Zanini, L., K. Andersen, K. Batkov, E. Klinkby, F. Mezei, T. Schonfeldt and A. Takibayev (2019), "Design of the cold and thermal neutron moderators for the European spallation source", Nuclear Instruments and Methods in Physics Research Section A: Accelerators, Spectrometers, Detectors and Associated Equipment 925, 33–52.

Zanini, L., E. Klinkby, F. Mezei and A. Takibaye (2020), "Low-dimensional moderators at ESS and compact neutron sources", EPJ Web of Conferences 23, 04006.

Zavorka, L., K. Ghoos, J. Risner, and I. Remec (2023), "An unstructured mesh based neutronics optimization workflow", submitted for publication in Nuclear Instruments and Methods in Physics Research Section A.

Zavorka, L. and Remec, I. (2022), "Shielding Calculations with the Unstructured Mesh Model of the ORNL's Second Target", Proc. of the ICRS 14/RPSD 2022 Sept 25-29, 462.

Zavorka, L. and Remec, I. (2021), "Neutron Dose Rate Calculation with the MCNP6 Hybrid Geometry Model of the Second Target Station", Transactions of the American Nuclear Society, 124, 680.

Zhao, J. K., K. W. Herwig, J. L. Robertson, F. X. Gallmeier and B. W. Riemer, (2013), "Instrument performance study on the short and long pulse options of the second spallation neutron source target station", Review of Scientific Instruments 84 (10), 105104.

List of abbreviations and acronyms

CAD	Computer Aided Design
CADIS	Consistent Adjoint Driven Importance Sampling
CSG	Constructive Solid Geometry
CV	Core Vessel
FW-CADIS	Forward-Weighted CADIS
ORNL	Oak Ridge National Laboratory
SNS	Spallation Neutron Source
STS	Second Target Station
UM	Unstructured Mesh
VR	Variance Reduction

Acknowledgements

This manuscript has been authored by UT-Battelle LLC under Contract No. DE-AC05-00OR22725 with the US Department of Energy (DOE). The US government retains and the publisher, by accepting the article for publication, acknowledges that the US government retains a nonexclusive, paid-up, irrevocable, worldwide license to publish or reproduce the published form of this manuscript, or allow others to do so, for US government purposes. DOE will provide public access to these results of federally sponsored research in accordance with the DOE Public Access Plan (http://energy.gov/downloads/doe-public-access-plan).

6. Advanced Monte-Carlo method for prompt and residual radiation calculations in light-ion accelerators

F. Ogando[1*], P. Sauvan[1], V. López[1]
[1]Universidad Nacional de Educación a Distancia (UNED), Spain
[*]fogando@ind.uned.es

Ion accelerators may produce intense secondary radiation fields from intended or unintended nuclear interactions of the accelerated particles with their environment. Besides interactions in the target or beam dump, some of the accelerated particles are unavoidably lost to the beam pipe and some other collided to scrapers and collimators resulting in intense neutron and gamma fields. These fields pose a risk for workers and public during operation, and also result in material activation, which may difficult the hands-on maintenance of the device. The proper calculation and transport of prompt and residual sources of radiation is critical for the licensing of equipment and experimental setups.

Here is presented a new advanced tool for radiation field calculation. This tool is based on the MCNP6 code, which is one of the most used tools for radiation transport.

The srcUNED-Ac is a user-defined source module, where secondary particle sources in typical simple geometries (pipes, scrapers, target) can be easily defined with an arbitrary number of double differential neutron and (prompt or residual) gamma spectra. It is a tool intended for making quick flexible calculations for estimating doses when accelerated particles are fully contained in the beam pipe.

6.1. Introduction

Ion accelerators are normally a source of secondary particles from induced nuclear reactions, among other neutrons and gamma photons, which may result in a radiological risk for the workers and public in the environment where they are located. These nuclear reactions may also result in the production of radioactive material through an activation process, creating so a radiation source even after the shutdown of the accelerator. Nuclear analyses are required in order to devise appropriate shielding measures to fulfil the legal requirements of doses. Due to the affordable availability of computational power, Monte Carlo codes are now widely spread to produce the radiation field calculations necessary for the nuclear analyses. These codes provide high flexibility and are adaptable to multiple physical processes involved in the radiation-matter interactions.

MCNP (Werner, 2017) is one of the best radiation transport codes used for computing neutron fields. It has been adopted as the reference code of the most complex neutronic facility in the world, the ITER fusion reactor, currently under construction in France.

The MCNP code has builtin capability (SDEF card) of defining radiation sources with good flexibility, in spatial are energy interdependencies. Even while the MCNP code is capable of transporting also charged particles, this builtin capability is however not flexible enough to reproduce the complexity of radiation sources, that may be produced in a particle accelerator.

Accelerated particles are found to have diverse energy values in different zones of the accelerator. This difference in energy results in diverse double-differential emission spectra for secondary particles, especially neutrons and gamma photons. The MCNP code can

reproduce a double-differential spectrum using its built-in capability, but not a wide variety of them each corresponding to different particle energies or interacting materials.

Having its developers foreseen such situation, the MCNP code has the possibility to be compiled with a so-called source subroutine, in which more complex source distributions may be defined, and this serves the basis of the srcUNED-Ac module.

The srcUNED-Ac module is a set of FORTRAN subroutines and programs, designed to provide the MCNP code the required capabilities to reproduce the secondary radiation sources, that may be found in a particle accelerator. These secondary particles can be externally defined in a configuration file, which allows the user to run different configurations without having to recompile the source subroutine for every case.

Section number 1.2 describes de internal operation and configuration files of the modules, and section 1.3 shows some basic comparisons with particle emission from detailed transport runs with charged particles.

6.2. Mode of operation of scrUNED-Ac

The srcUNED-Ac module is valid for reproducing radiation sources from particle-matter interaction, both prompt and residual from activated materials. The module may be configured for multiple double-differential spectra, corresponding to prompt or residual radiation. The module works under the main assumption, that charged particle range in matter is negligible. This assumption is limiting for medium to high energy beams, where beam losses could travel across the beam pipe into the surrounding air. In the case of accelerated particles being effectively retained inside the beam pipe, the transport of charged particles only considers the slow-down process, with little movement of the particles.

The source module has been developed to provide a flexible tool for addressing the existence of different spectra of secondary particles, but all of them being created in interacting surfaces, which must be defined with the beam pipe shape and dimensions. This approximation neglects the actual range of accelerated particles inside matter, but in the case of low energy ions, this is a realistic approximation. The module does not transport the charged particles at all, but only launches the secondary source particles on the defined surfaces, with the given beam line orientation and with double-differential spectra, which must be precompiled into small data files.

The source module has been developed to be compiled into MCNP v6.2, and the neutronic input files must be defined without any SDEF cards, so that MCNP makes use of the compiled source subroutine.

The srcUNED-Ac module is configurable through an input file (which must be named “acSource.inp” in the work directory) works with three main sets of parameters. Any of the following cards may appear once or more times in the input file. The cards take additional parameters, that are here omitted for the sake of simplicity.

- SPECTRUM: These cards, as many as necessary, define the double differential distributions of source particles. These data are contained in ASCII data files, which must be built with auxiliary tools, provided along the module. Currently these data can be converted from PTRAC files obtained with MCNP for prompt radiation, or with the results from ACAB calculations for residual radiation.
- LINE: this card represents coordinate transformations but representing only the direction of the accelerator line and an origin point. That is, the transformation is not defined in the perpendicular directions of the accelerator line, since rotational

symmetry is assumed. This is not the case of pyramid distributions, which are treated specifically.

- SOURCE-TY: this card defines a piece of radiation source, which has a specific spectrum, over a given line transformation. This surface is the interaction region of charged particles for the specific source. There may be as many source definitions as needed, and any of them is assigned to a defined line coordinate and particle spectrum. Sources are normally defined along the longitudinal coordinate and may be defined in such a way that particle coordinates are different in both ends. This would correspond to accelerating cavities, where the charged particle energy is different on each end of the device. The source intensity is defined in unit of charged particle deposition power, either by unit length of in absolute magnitude.
    - TY: Two character representing the shape of the source. Currently "CN = cone", "CY = Cylinder", "PL = Perpendicular plane", "TP = truncated pyramid".
- OTHER CARDS: There are other simple cards, that allow to fine configuration of the module.
    - DIRS: Its string argument contains the name of the directory, where the spectrum files are placed.
    - BIASFACTOR: single real value (X) representing for tuning a built-in variance reduction technique. Normally particles are emitted for every source with probability proportional to its intensity and equal weights. This X value forces source sampling with probability proportional to its intensity raised to the power of X. Particle weights are automatically adjusted for every source, to keep the physical meaning of the calculation. Values of X between 0 and 1 result in certain homogenization of the actual source emission among different sources (for example, a value of zero forces equal Monte Carlo emission rate for every source). This option helps to achieve good source sampling in weak sources, that could be nonetheless important at least locally.

Following sample file represents three particle sources, placed on three different axes, forming 45º angles with the closest one. In each of the axes there is a pyramidal, conical and planar source, respectively. The position of a set of these source particles is represented in Figure 6.1, where the three different shapes are visible at different orientations.

Figure 6.1. Sample representation of three particle sources with different shapes

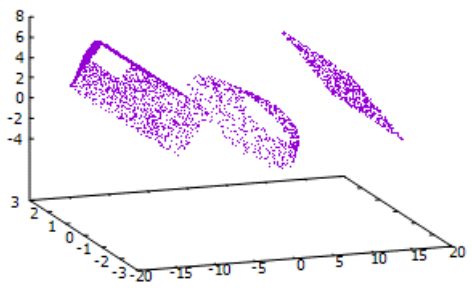

The input file resulting in this distribution is the following, where an arbitrary sample spectrum file has been used (the particle directions or energies are not represented):

```
DIR srcs
```

```
IPT 1
# BIASFACTOR 0.3
#
SPECTRUM  1 n-Nb-8_3-50o.src

# HEBT, DIPOLES, Accel
LINE 1      0  0  0   1     0
LINE 2     10  0  0   0.7 0 0.7
LINE 3    -10  0  0  -0.7 0 0.7
#      TY NL  SPs  Loss     X extent     R0  R1
SOURCE CN 1   1 R   1.0 R   0.0 4.0     3.0 1.5
#      TY NL  SPs  Loss     X extent     Yext Zext
SOURCE PL 2   1 R   1.0 R   4.0 4.0      5.0   2.0
#      TY NL  SPs  Loss     X extent     Yext0 Zext0   Yext1 Zext1
SOURCE TP 3   1 R   3.0 R   4.0 10.0     3.0 3.0       1.0 1.0
```

The results from MCNP6 still need to be normalized to the actual intensity of all considered sources in the input file. In order to facilitate this task to the analyst, every MCNP run using this module will contain the following or similar lines in the corresponding ***outp***.

```
==============================
srcUNED-Accelerators v2.0
COMBINED SOURCE  0.58196E+14
MAX SOURCE WGT 0.26055E+01
MIN SOURCE WGT 0.91514E-03
==============================
```

Where the following information is detailed:

- Version of the source module used in the run.
- Combined intensity of all sources detailed in the input file, calculated by adding up all the values contained in the file.
- Minimum and maximum values of the source particle weight, which differs from number one, in the case of using the BIASFACTOR variance reduction technique.

The so called “combined source” must be used as a scaling value for the results, while the other figures are provided to know the disparity of source weights used in the calculations, which may be problematic, among others, when using weight windows variance reduction. This disparity of weight is only produced in the case of using a BIASFACTOR different than one, function that must be used with care. The use of a radiation source of variable weight may have undesired performance effects with other variance reduction techniques like the weight windows.

There are, however, cases where the sources with different weights are produced in different regions of space with limited interactions among them, and in this case it proves to be a very valuable tool for improving the statistics in the presence of sources with heterogeneous intensity.

6.3. Construction of double differential spectra

In order to run srcUNED, several double-differential spectra must be precompiled into separate files (also called SRC files). The SRC files have text format, and may be edited manually, also including comments for better description of the contained data. These files are later defined in the input file and used in the sampling of source particles. Python scripts have been created to perform this task, following this procedure:

- For prompt radiation:

  - A MCNP/MCUNED case is run, where a small object with the desired material is irradiated with a monoenergetic unidirectional beam at the chosen energy. The object must be large enough to stop all incident particles.
  - PTRAC file is built from the secondary particles created in the run.
  - Dedicated script "makePromptSource.py" builds the file from secondary particle tracks.

- For decay radiation:
  - A MCNP/MCUNED case is run, where a small object with the desired material is irradiated with a monoenergetic point source at the chosen energy. The object must be large enough to stop all incident particles.
  - The flux of incident particles is measured inside the object, with energy resolution structure compatible with EAF data libraries (normally Vitamin-J or Vitamin-J+).
  - A computation of the isotopic evolution is performed with ACAB code.
  - A dedicated script builds the file from most relevant radioisotopes, either with line

Probability distributions inside the SRC files may be continuous or discrete, as in the case of decay radiation, whose energy distribution is considered discrete in the emission lines.

SRC files may be interpolated in the code for the case of regions with different incident particle energy at both ends of its domain. In this case, the interpolation procedure is computed using the secondary particle source at both ends (combining incident particle loss and secondary particle yield), using an exponential interpolation, which sets a random number, that determines which SRC file to use at any point.

6.4. Validation cases

In order to perform validation cases, some test run have been performed, and their results compared with MCNP 6.2, which is capable of handling deuteron transport. These comparisons can be performed only for prompt radiation fields, since MCNP is not capable of automatically producing and transporting residual doses. For these cases, the fourth version of D1SUNED (Sauvan, 2020) will be used, which can perform this kind of calculations.

The selected tests are only focused on the production of source particles and not in transported magnitudes, since transport is handled by MCNP algorithms in any case.

TENDL-2015 has been used for deuteron interaction with matter in calculations of prompt fluxes and doses.

6.4.1. Prompt radiation, point source

A small sphere of niobium is irradiated with a collimated and thin beam of 40 MeV deuterons with a total power deposition of 1 W. Two magnitudes are computed separately:

- Neutron flux averaged on a spherical surface of 1 m radius, centered in the origin (Tally F12).
- Ambient Dose Equivalent (according to ICRP-74), averaged on a spherical surface of 1 m radius, centered in the origin (Tally F22).

Figure 6.2. Example of point source with tally surface and plan segmentators

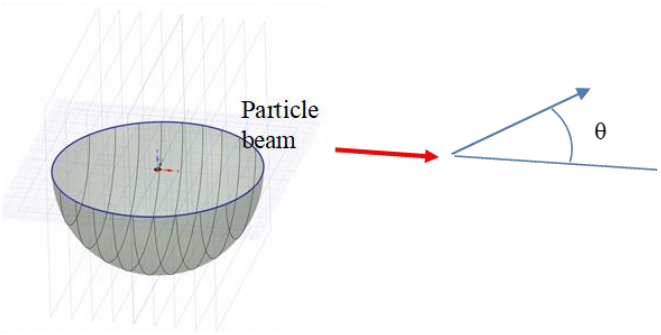

Both tallies F12 and F22 have been segmented by 19 parallel planes in a similar way as the system depicted in previous Figure (which is an approximated representation). Considering the small size of the source in comparison to the tally surface, these plane segmentations produce groups with different cosine of neutron emission, with respect to the beam direction.

The idea after computing both total flux and ADE dose rate is that they are both integrated values of the flux energy distribution, with different weighing factors (in total flux this factor is just unity).

Following table shows a comparison of results between the two methods: pure MCNP6 and srcUNED-Ac. The table shows the unnormalized (Tally) and normalized (Real Tally – RT) values of the tallies. The runs have been carried out until the tally F12 total statistical error was 1%, requiring the following number of histories and computation time (figure of merit is also included).

- MCNP6: NPS = $8 \cdot 10^6$; Cpu time = 388 minutes; FOM(Tally F12) = 27.
- srcUNED-Ac: NPS = $3 \cdot 10^5$; Cpu time = 0.1 minutes; FOM(Tally F12) = 526506.

Figure 6.3. Results for the point-prompt validation test of srcUNED-Ac

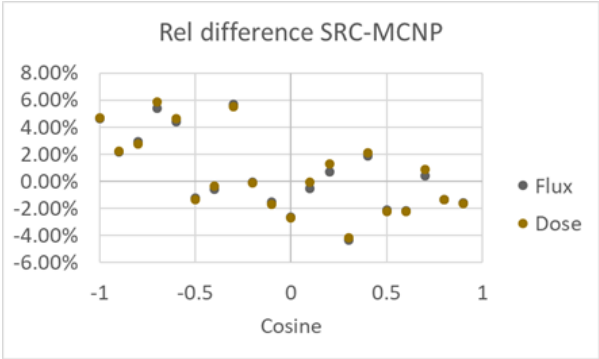

Almost all of the bin results lay within the expected variability of the statistical errors. However, some larger errors (4%) take place because of the difference between a smooth (MCNP6) and a piece-wise constant (srcUNED-Ac) angular distribution of emitted neutrons. The similar error values in flux and dose tallies suggest that energy distribution is considered properly, since these magnitudes are built with different weighing of the particle energy spectrum.

It is most notable the increase of the Figure of Merit, which is more than four orders of magnitude larger with srcUNED-Ac, due to the direct calculation of neutrons without charged particles. This extreme value FOM is due to the fact, that no neutron interactions with matter are considered here. In a more realistic case, the expect FOM ratio would be lower.

6.4.2. Prompt radiation. Continuously varying deuteron energy

Previous sample test considered deuterons with a unique energy, while the scrUNED-Ac module may consider continuously variating deuteron energy. This feature is interesting for accelerating modules with internal loses. This test makes use of the energy interpolation procedure described in Section 6.3, and which is used whenever the double differential spectra at both ends of a region are different.

The following system is devised in order to test the capability of considering heterogeneous deuteron energy. Deuterons are emitted inside a hollow beam pipe with 10 cm radius, in such a way that they collide with the pipe in parallel direction to the beam line. The pipe is 1 m long, and emitted radiation is measured in a concentric cylinder of 30 cm radius, and with longitudinal resolution.

Figure 6.4. Sample test with cylindrical source with increasing deuteron energy

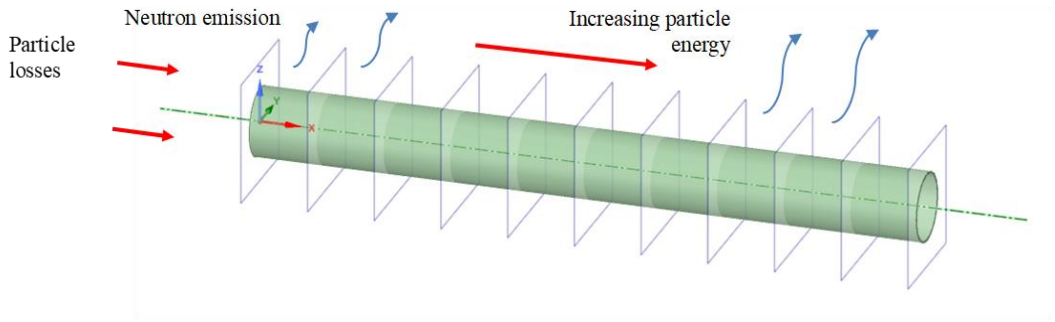

Similar to the first test, both neutron flux (Tally 12) and ADE doses (Tally 22) are measured in the concentric measure cylinder (not represented in figure), with longitudinal resolution as defined by 10 intersecting planes perpendicular to the cylinder axis. The measured values receive contribution from all source sectors.

The assumption on the energy variation will be a steady increase, linear with energy, from E_0 at the left side to E_1 at the right side. Deuteron power loss by unit length is considered homogeneous, and therefore the actual deuteron source is decreasing along the cylinder with the law 1/E.

Following table shows a comparison of results between the two methods: pure MCNP6 and srcUNED-Ac. The table shows the unnormalized (Tally) and normalized (Real Tally – RT) values of the tallies. The runs have been carried out until the tally F12 total statistical error was 1%, requiring the following number of histories and computation time (figure of merit is also included).

- MCNP6: NPS = $5 \cdot 10^6$; Cpu time = 1708 minutes; FOM(Tally F12) = 4.7.
- srcUNED-Ac: NPS = 10^5; Cpu time = 0.17 minutes; FOM(Tally F12) = 206044.

Almost all of the bin results lay within the expected variability of the statistical errors. The similar error values in flux and dose tallies suggest that energy distribution is considered

properly, since these magnitudes are built with different weighing of the particle energy spectrum.

Figure 6.5. Results for the line-prompt validation test of srcUNED-Ac

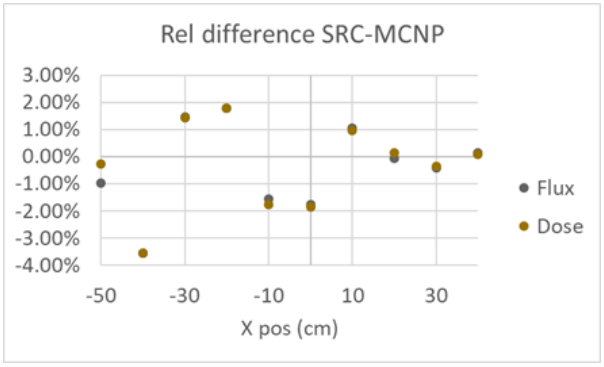

It is most notable the increase of the Figure of Merit, which is more than four orders of magnitude larger with srcUNED-Ac, due to the direct calculation of neutrons without charged particles. This extreme value FOM is due to the fact, that no neutron interactions with matter are considered here. In a more realistic case, the expect FOM ratio would be lower.

6.4.3. Decay radiation. Simple case

In order to test the capabilities of creating and transporting residual radiation from activated materials, the MCNP6 cannot be used for this purpose, since it lacks this capability. The D1SUNEDv4 code is used, instead, which is an enhancement of the MCNP6 with capability of computing residual doses with the D1S algorithm. This code (Sauvan et al., 2020[1]), developed at UNED by the group authoring this report, is not open source, nor freely available. It is, however, an evolution of the D1SUNED-v3.1.4, used by ITER-IO as reference code for residual dose calculations.

A simple case, similar to the system used in Section 6.4.1, has been used for the calculation. A small sphere is irradiated with deuterons, and the resulting radiation fluxes are calculated. In this case copper is used instead of niobium, due to the scarcity of available D1S nuclear data for the recent D1SUNED-v4 code. The resulting flux will be computed with energy resolution, to test the quality of the precompiled data.

Despite the chosen methodology, be it D1SUNED or srcUNED-Ac, an activation case must be run with ACAB, in order to determine the nuclear reactions most relevant to residual doses. These doses are then selected for calculation, automatically in the case of srcUNED-Ac.

- In the case of D1SUNED, these reactions must be manually included by the analyst into its configuration files, and appropriate nuclear data must be prepared for these isotopes. This process may be especially tedious for high energy incident particles, where many nuclear reactions are relevant to the residual dose emission.
- In the case of srcUNED-Ac, the output of ACAB is used to automatically produce an SRC file, which is ready for use. No further nuclear data is needed (only the standard photoatomic data, as provided in the MCPLIB84 library).

In all cases considered here, the irradiation scenario consists of 30 years of irradiation plus 1 day and 1 week of cooling times. Nuclear data for deuteron induced nuclear reactions is taken from EAF-2007 activation file.

First considered case consists of 1 W of 5 MeV deuterons hitting a small sphere of pure copper. The nuclear reactions relevant to residual doses are the ones producing Zn65 and Cu64 radioisotopes. Due to the low energy of deuterons, only few reactions are relevant to the production of radioisotopes, as shown in following table. The reaction rate is computed per unit volume and here must be considered qualitatively for comparative purposes.

Table 6.1. Nuclear reactions relevant to residual gamma emission for 5MeV deuterons on copper

REAC RATE (s^{-1})	FATHER	REACTION	DAUGHTER	CODE
2.43E+04	CU 63	(D,P)	CU 64	103
7.03E+02	CU 65	(D,2N)	CU 64	160
2.98E+01	CU 63	(D,G)	ZN 65	102

The production of these radioisotopes results in a radiation source, with the spectrum represented in previous table. Three plots have been compared:

- Manual creation of a point SDEF source, then used in MCNP6.
- Use of MCNP6 with srcUNED-Ac.
- Use of D1SUNED-v4.

The runs have been carried out until the total statistical error of the flux tally was 1%, requiring the following number of histories and computation time (figure of merit is also included).

- D1SUNED: NPS = 10^7; Cpu time = 435 minutes; FOM(Tally F12) = 25.
- srcUNED-Ac: NPS = $3 \cdot 10^5$; Cpu time = 0.03 minutes; FOM(Tally F12) = $6 \cdot 10^6$.

Figure 6.6. Results for the point-decay validation test of srcUNED-Ac (5 MeV, 1 week cooling)

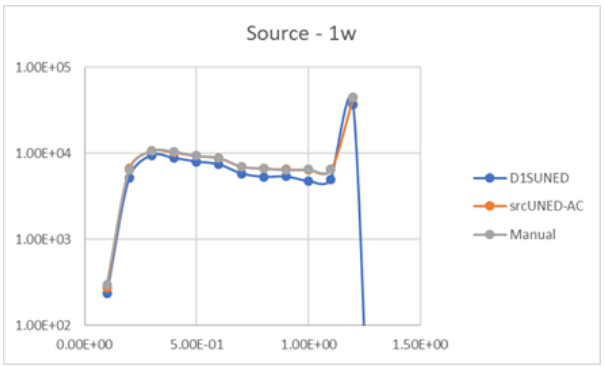

Y-axis: Photon flux per unit energy (a.u.)
X-axis: Photon energy in MeV

Some differences are found between D1SUNED and srcUNED-Ac, while the latter is almost coincident with the manual approximation. This discrepancy is still under investigation.

Table 6.2. Nuclear reactions relevant to residual gamma emission for 40MeV deuterons on copper

REAC RATE (s^{-1})	FATHER	REACTION	DAUGHTER	CODE
2.94E+06	CU 65	(D,2N)	ZN 65	160
2.80E+06	CU 65	(D,2NP)	CU 64	320
8.97E+05	CU 63	(D,P)	CU 64	103
6.85E+05	CU 63	(D,3N)	ZN 62	170
2.86E+05	CU 65	(D,DN)	CU 64	320
2.58E+05	CU 63	(D,2NPA)M1	CO 58M1	1591
2.06E+05	CU 63	(D,2NPA)	CO 58	1590
1.13E+05	CU 65	(D,T)	CU 64	1050
6.12E+04	CU 63	(D,PA)	CO 60	1120
3.05E+04	CU 65	(D,2NPA)	CO 60	1590
2.52E+04	CU 63	(D,DNA)M1	CO 58M1	1581
2.22E+04	CU 63	(D,DNA)	CO 58	1580
2.02E+03	CU-63	(D,G)	ZN 65	102

A more energetic case of 40 MeV deuterons into a small sphere of pure copper. Previous Table 6.2. Nuclear reactions relevant to residual gamma emission for 40MeV deuterons on copper

shows the most relevant nuclear reactions contributing to semi-infinite contact doses, for the cases of 40 MeV deuterons onto pure copper. Only most important reactions leading to isotopes contributing to at least 1% are listed. The reaction rate is computed for an arbitrary irradiated sphere and must be considered qualitatively for comparative purposes. Only two parent nuclides produce 13 such relevant reactions.

There is no available nuclear data for D1SUNED-v4 in order to consider all these reactions. The resulting source using srcUNED-Ac is represented in Figure 6.7.

Figure 6.7. Results for the point-decay test of srcUNED-Ac (40 MeV, 1 week cooling)

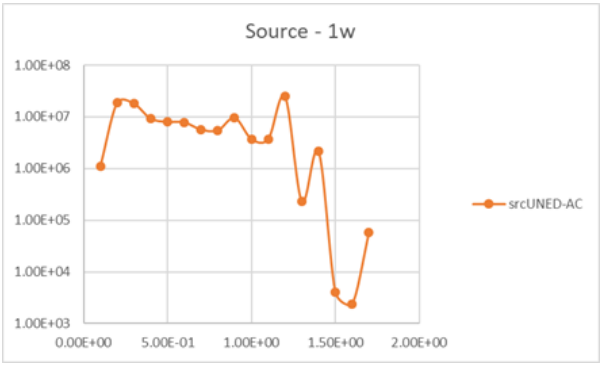

Y-axis: Photon flux per unit energy (a.u.)
X-axis: Photon energy in MeV

6.5. Conclusions

The srcUNED-Ac is an MCNP source module, which extends its capabilities to multiple double differential spectra, which is very useful for accelerator applications.

The comparison between pure MCNP6 and srcUNED-Ac shows a very good match between the two methods. The differences found in the tests have values up to few percent, and this even in extreme cases with no diffusion of secondary particles. These mismatches come from the fact, that srcUNED-Ac considers piecewise constant probability distributions for angle and energy, which are normally much coarser than the typical ACE library used by MCNP6.

On the contrary, the continuous variation of secondary particle yield in scrUNED-Ac is an improvement to the piece-wise constant SDEF distributions in MCNP6, which cannot consider a 1/E spatial incident particle distribution which would correspond to homogeneous power loss.

Regarding dose from decay radiation, the new method is consistent with the manual construction of SDEF source into MCNP6, but still shows some discrepancies with the D1SUNED-v4, which will become the reference code for calculation of residual doses from charged particles.

The best advantage of the srcUNED-Ac module in comparison to other simulations codes is the much better performance, and also the flexibility of source definition, both far beyond the capabilities of MCNP or even the evolved D1SUNED codes.

6.6. Acknowledgements

This work has been partially funded by Spanish Ministery of Science and Innovation (PID2019-106775RB-I00) and the research program of ETS Ingenieros Industriales UNED 2022-ETSII-UNED-14.

6.7. List of references

P. Sauvan, R. Juárez, G. Pedroche, J. Alguacil, J.P. Catalán, F. Ogando, J. Sanz, “D1SUNED system for the determination of decay photon related quantities”, Fus Eng Des 151 111399 (2020).

C.J. Werner (editor), "MCNP Users Manual - Code Version 6.2", LA-UR-17-29981 (2017).

6.8. List of abbreviations and acronyms

MCNP	Monte Carlo n-particle
D1S	Direct one-step
TENDL	Talys Evaluated Nuclear Data Library

7. Composite Models in the MARS15 Code

Igor Tropin
Fermilab
Corresponding Author(s): tropin@fnal.gov

Studies of the physical phenomena resulting from interactions of intense high-energy beams with matter require – in some cases - the use of models complementary to those used in the MARS15 Monte Carlo code.

An example of such a kind is heating of a target and other accelerator and experiment components by the beam pulses followed by relaxation of the temperature field between the pulses. Solution implies calculation of radiation field characteristics in mesh cells, generated by third-party mesh generators which can produce non-liner meshes of arbitrary shaped cells. Page 4 SATIF-15 / Book of Abstracts Another example can be a study of impact of beam losses in accelerator on formation of doses to personnel, machine components and environment. In that case, the beam physics models are usually used to generate a source term to feed the particle transport and interaction codes such as MARS15. In general case establishing interaction between models requires implementation of the data transfer and data representation modules. Function of data transfer module is implementation of data flow between models. Data representation module is aimed to convert information obtained from source to representation usable by the receiver. As an example, this module can perform mapping of phase coordinates received from one model to phase space of the model used in receiver.

The approaches and tools used to integrate MARS15 with a third-party simulation software are described in this presentation. The results obtained with these techniques for the Fermilab Long Baseline Neutrino Facility (LBNF/DUNE) and the Delivery Ring are presented.

8. The On-the-fly Global Variance Reduction Technique and its application for IFMIF-DONES shielding analyses

Yuefeng Qiu[1], Yu Zheng[2], Yuan Hu[3], Arkady Serikov[1]
[1] Karlsruhe Institute of Technology
[2] Institute of Plasma Physics, Hefei Institutes of Physical Science, Chinese Academy of Sciences
[3] State Key Laboratory of Nuclear Physics and Technology, School of Physics, Peking University
Corresponding Author(s): yuefeng.qiu@kit.edu

IFMIF-DONES facility is a deuterium-lithium (d+Li) neutron source driven by a deuteron accelerator (40 MeV and 125 mA) striking at the liquid Li target, and producing neutrons through stripping reactions to provide irradiation data for the construction of a DEMO fusion power plant. The shielding analyses of the accelerator and target demand efficient variance reduction (VR) technique, in particular the global radiation distributions. Due to the complicated particle-material interactions in the accelerator facilities with streaming paths, there are often issues raised during the generation and utilization of the weight-window mesh (WWM). The common methodology such as the deterministic-based FW-CADIS method is widely used, yet still not straightforward to handle the complex source modelling and particle streaming.

An "on-the-fly" global variance reduction technique will be presented. It is based on iterations of flux map and WWM, generating and improving the WWM on-the-fly along with the particle transport simulation. Since it is a Monte Carlo (MC) based method, no extra step is needed for geometry and source modelling and WWM generation. One common issue caused by the streaming path is that, a particle history could be extremely long due to the over-splitting of particle tracks, since the high flux gradient around the streaming path will cause the high gradient of WW. A novel dynamic WW upper bound method has been proposed to limit the splitting by increasing the WW upper bound once sufficient particles have been scored for specific mesh cells. This method has been implemented in the MC transport code MCNP and OpenMC. This method has been tested with computational benchmarks, with promising speed-up achieved compared with the analogue run and FW-CADIS WWM simulation. Similar speed-up have been observed in the application to the IFMIF-DONES shielding calculation, with neutron flux maps being produced over the 3~6 m thick concrete shielding